論文 / 著書情報
Article / Book Information

題目(和文)	
Title(English)	Constitutive Modeling of Granular Materials Subjected to Internal Erosion
著者(和文)	WangGang
Author(English)	Gang Wang
出典(和文)	学位:博士(学術), 学位授与機関:東京工業大学, 報告番号:甲第12015号, 授与年月日:2021年3月26日, 学位の種別:課程博士, 審査員:髙橋 章浩,北詰 昌樹,竹村 次朗,笠間 清伸,千々和 伸浩
Citation(English)	Degree:Doctor (Academic), Conferring organization: Tokyo Institute of Technology, Report number:甲第12015号, Conferred date:2021/3/26, Degree Type:Course doctor, Examiner:,,,,
学位種別(和文)	博士論文
Type(English)	Doctoral Thesis

Constitutive Modeling of Granular Materials Subjected to Internal Erosion

Wang Gang

DISSERTATION

Submitted in partial fulfillment of the requirements for the degree of

DOCTOR OF PHILOSOPHY

at

TOKYO INSTITUTE OF TECHNOLOGY

2021

ABSTRACT

Internal erosion occurs when fines are detached under hydraulic force. More fines are washed out with the void growth. The soils become looser and soil strength decreases, which subsequently causes the failure of earthen structures. The objective of this dissertation is to develop a constitutive model of granular materials considering deterioration induced by internal erosion.

To quantify the seepage-induced internal erosion process, several series of seepage tests are investigated. The effects of the initial conditions (i.e., initial fines content, confining pressure, flow direction) on the erosion mechanism are elaborated. It is found that the post-erosion grading curves shift downward in the fines fraction for all seepage tests; soils with higher confining pressure and smaller initial fines content have less loss of fines. When downward or upward seepage flow is applied to soils, the heterogeneity of both fines and voids exists along the seepage direction. A predictive equation of the final fines content considering confining pressure, initial fines content, and flow velocity is proposed. At the same time, a hyperbolic tangent function is employed to estimate the erosion-induced volumetric strain based on the experimental observations. The Post-erosion void ratio is estimated by considering the cumulative fines loss and erosion-induced volumetric strain.

The mechanical behavior of internally eroded soils under the drained and undrained triaxial shearing is largely dependent on the erosion phenomena (suffusion and suffosion), the fines content, and the intergranular void ratio. When suffosion occurs, the drained strength of the eroded soils is smaller than that of the uneroded soils, while the undrained strength of the eroded soils is larger than that of the uneroded soils. This contradiction may be related to the stress state and associated particle rearrangement. When suffusion occurs, the undrained strength of the eroded soils is smaller than that of the uneroded soils when the intergranular void ratio is relatively low. The subloading Cam-clay model can capture the basic features of the original soils under the drained triaxial shearing condition. Thus, the subloading Cam-

clay model is selected to predict the mechanical behavior of the soils with suffosion under the drained condition. From the simulation of the drained triaxial tests on the eroded soils, evolutions of key parameters (the slope of normal compression line and initial stress ratio) with suffosion are quantified.

The over-consolidation ratio is found to increase with the loss of fines for the eroded loose soils, which indicates that erosion makes the loose soils highly structured condition. This implies that the normal yield surface for loose soils is expected to expand after erosion. However, both peak strength and deviatoric stress at the critical state under the drained condition are smaller for the eroded dense soils, and the volume change characteristic becomes more contractive. This means that the normal yield surface for dense soils is expected to shrink after erosion. Based on these, the subloading Cam-clay model incorporated with the similarity ratio for eroded soils is modified. The determination method of erosion-related model parameters is proposed through experimental results and back analysis of the experimental results.

The modified subloading Cam-clay model can predict the mechanical behavior of the eroded dense soils with different cumulative fines losses under the same confining pressure obtained through both the experiments and the DEM simulation. Both predictive equations for the seepage-induced erosion and the modified subloading Cam-clay model are employed to simulate the seepage and drained triaxial tests of the loose soils with different initial fines contents under the same confining pressure (two-step calculation). This study on the constitutive model considering internal erosion offers some important insights into the design of the earthen structures subjected to seepage flow.

ACKNOWLEDGEMENTS

The whole Ph.D. time seems to be a big challenge for me, which I have never met before. During this process, I have encountered many kind persons. Firstly, I want to thank my positive and energetic supervisor, Prof. Akihiro Takahashi. Whenever I encounter difficulties in research, he always gives me valuable advice. He has a rigorous attitude to research, which affects my attitude to research gradually.

Secondly, I would like to express my gratitude to Prof. Masaki Kitazume, Assoc. Prof. Jiro Takemura, Assoc. Prof. Kiyonobu Kasama, and Assoc. Prof. Nobuhiro Chijiwa, who spend time serving on my committee. Their comments and advice are helpful and constructive, which inspires me a lot in the future study.

It is lucky to be a member of the Takahashi lab. I have made many life-long friends, Jenisha, Saha, and Kumar. We always inspire and encourage each other, especially during the COVID-19 epidemic. I also want to thank the friends I met on campus, Dr. Horikoshi, Mr. Li Yang, Mr. Max, Mr. Xiao Tengxiang, Mr. Hu Lihang, Mr. Wang Yuankai, and Mr. Zhang Tao. I am grateful to Chef Yin Jianzhong in Kouraku Ryo for his consistent encouragement.

I want to express my appreciation to Prof. Qiao Shifan of Central South University, who takes care of my life and study in the last year of the Ph.D. time. The friends in Changsha City always bring me happiness and hope when I feel depressed.

Thanks for the support from my parents. My father, a painter, usually works harder than me, from whom I have learned a lot. Each week, my mother calls me and encourages me. I also want to thank my two older sisters. They have taken good care of my parents for almost twelve years when I am not at home. Finally, I want to express my respect to my grandfather, who cared about my study even he was in very bad condition.

[This page intentionally left blank]

TABLE of CONTENTS

[This page intentionally left blank]

LIST of FIGURES

LIST of TABLES

NOTATIONS

a : material parameter that estimates the eroded fines content;

a_0 : material parameter that estimates the final density of fines;

a_1 : material parameter that determines the final fines content;

a_2 : material parameter that estimates the deviatoric stress at the critical state;

a_3 : material parameter that describes the angle of shearing resistance at the critical state;

a_4 : material parameter that describes the slope of the normal compression line;

a_e : material parameter that determines the reference critical void ratio;

A_1 : material parameter in deciding the maximum shear modulus;

A_2 : threshold value in deciding the erosion-induced volumetric strain;

b : material parameter that estimates the eroded fines content;

b_0 : material parameter that estimates the final density of fines;

b_1 : fitting parameter that determines the final fines content;

b_2 : material parameter that estimates the deviatoric stress at the critical state;

b_3 : material parameter that describes the angle of shearing resistance at the critical state;

b_4 : material parameter that describes the slope of the normal compression line;

b_p : material parameter that indicates the participation of fines in stress transmission;

B_s : constitutive parameter that estimates the grading state index;

c : material parameter that estimates the eroded fines content;

c_0 : material parameter that estimates the final density of fines;

c_1 : material parameter that determines the final fines content;

C_c: : curvature coefficient;

C_p : model parameter ($C_p = \frac{\lambda-\kappa}{1+e_0}$);

C_u : uniformity coefficient;

d : dilatancy;

d_0 : material parameter that describes erosion rate;

d_1 : fitting parameter that determines the final fines content;

d_{10} : effective grain size (mm);

d_{50} : median grain size (mm);

d_{Xf} : grain size when the fines pass X% of the total mass of the fines;

d_X : grain size when X% of mass passing is finer in the grading curve;

d_{85SA} : grain size of 85% passing base soils calculated based on the surface area;

$d\varepsilon_q^p$: plastic shear strain increment;

$d\varepsilon_v^p$: plastic volumetric strain increment;

D : material constant ($D = \frac{C_p}{M}$);

D_{Xc} : grain size when the coarse particles pass X% of the total mass of the coarse particles;

D_{c35} : void size of 35% passing the filters;

e : void ratio;

e_0 : initial void ratio;

e_1 : material parameter that estimates the current fines content;

e_2 : material parameter that estimates the current fines content;

e^* : equivalent void ratio ($e^* = \frac{e+(1-b)FC}{1-(1-b)FC}$);

e_{bs} : initial void ratio before shearing that includes the initial void ratio of the uneroded soils and post-erosion void ratio of the eroded soils;

e_c : void ratio after consolidation;

e_{cr0} : reference critical void ratio;

e_{er} : post-erosion void ratio;

$e_{hc,cr0}$: initial critical void ratio for the pure coarse particles;

$e_{hf,cr0}$: initial critical void ratio for the pure fines;

e_{H1} : void ratio calculated based on the hypothesis (1);

e_{ini} : initial void ratio before consolidation;

e_{max} : maximum void ratio;

e_{min} : minimum void ratio;

e_s : intergranular void ratio ($e_s = \frac{e_c+FC}{1-FC}$);

FC : fines content (mass ratio of current fines to current total soils);

FC_0 : initial fines content (mass ratio of initial fines to initial total soils);

FC_∞ : final fines content;

FC_{er} : eroded fines content;

FC_{th} : threshold fines content;

G : shear modulus;

G_0 : material constant that decides the shear modulus;

G_{max} : maximum shear modulus;

h_0 : material parameter that decides the degrading rate of the structure formed by the erosion;

i : hydraulic gradient;

i_c : critical hydraulic gradient;

I_G : grading state index ($I_G = \frac{lnR_D}{2B_s}$);

k : hydraulic conductivity;

K : bulk modulus;

l : material parameter that decides the smoothness of the erosion-induced volumetric strain-cumulative fines loss curve;

m_e : material parameter that determines the reference critical void ratio;

m_R : material parameter that determines the degradation rate of the over-consolidation property;

p : mean effective stress or confining pressure;

p^* : mean effective stress on the normal yield surface;

p^a : pore air pressure;

p^w : pore water pressure;

p_0 : reference pressure or atmospheric pressure, taken as 98kPa;

p_c : pre-consolidation pressure;

p_{er} : mean effective stress on the normal yield surface of the eroded soils;

p_{nor} : normalized confining pressure;

p_N : intersection point of normal yield surface and mean effective stress;

$p_{N,er}$: intersection point of the normal yield surface for the eroded soils and mean effective stress;

p_{ref} : reference confining pressure (kPa);

p_s : intersection point of subloading yield surface and mean effective stress;

q : deviatoric stress;

q^* : deviatoric stress on the normal yield surface;

q_{er} : deviatoric stress on the normal yield surface of the eroded soils;

r : radius of the hole in the hole erosion tests;

R : similarity ratio or stress ratio that corresponds to the size ratio of subloading surface to normal yield surface $(R = \frac{p_S}{p_N})$;

R_0 : initial stress ratio;

R_{er} : similarity ratio, the size ratio of the normal yield surface for the eroded soils to the normal yield surface for the uneroded soils;

R_D : grading ratio of the maximum grain size to the minimum grain size;

t : seepage time;

u : displacement of the soil skeleton;

v : flow velocity;

v^* : lowest flow velocity;

v_{nor} : normalized flow velocity;

v_{ref} : reference velocity (m/s);

V_{s0} : initial volume of the solid;

V_{V0} : initial volume of the voids;

α : reduction factor;

α_0 : material parameter that describes the initial stress parameter;

β_0 : material parameter that describes the initial stress parameter;

γ : nondimensional parameter that estimates the current density of fines;

γ' : buoyant gravity density;

γ_w : water gravity density;

δ_{ij} : Kronecker symbol;

ΔFC : cumulative fines loss (mass ratio of eroded fines to initial total soils);

Δh : hydraulic head difference across the length of the hole;

$\Delta p_{N,0}$: initial stress parameter that represents the change in the size of the normal yield surface by erosion;

ΔV : volume change;

ΔV_s : volume change induced by the loss of fines;

ΔV_V : volume change induced by the decrease of voids;

ΔZ : length of the hole in the hole erosion tests;

ε_1 : axial strain;

ε_3 : radial strain;

ε_q^p : plastic shear strain;

ε_q : shear strain ($\varepsilon_q = \frac{2}{3}(\varepsilon_1 - \varepsilon_3)$);

ε_v^p : plastic volumetric strain;

ε_v : volumetric strain ($\varepsilon_v = \varepsilon_1 + 2\varepsilon_3$);

ε_v^{er} : erosion-induced volumetric strain;

$\varepsilon_{v\max}^{er}$: maximum erosion-induced volumetric strain;

υ : Poisson's ratio;

ξ : material parameter that determines the reference critical void ratio;

ρ_{f0} : initial density of fines;

ρ_f : current density of fines;

$\rho_{f\infty}^*$: final density of fines;

σ_1 : axial stress;

σ_3 : radial stress;

σ_{ij} : total stress;

$\sigma_{ij}{}^{(1)}$: partial stress of the solid part;

$\sigma_{ij}{}^{(2)}$: partial stress of the fluid part;

η_d : dynamic viscosity;

κ : slope of swelling line in *e*-ln *p* space;

λ : slope of normal compression line in *e*-ln *p* space ($\lambda = \frac{e_1 - e_2}{\ln(p_2/p_1)}$);

Λ : plastic multiplier;

M : slope of the critical state line in *p*-*q* space;

τ : hydraulic shear stress;

φ : angle of shearing resistance at critical state;

ϕ : porosity;

ϕ_{er} : erosion-induced porosity;

Ψ : state parameter;

CSD : constriction (void) size distribution;

NCL : normal compression line;

OCR : over-consolidation ratio;

SL : swelling line.

CHAPTER 1

INTRODUCTION

1.1 Introduction

Internal erosion happens under the seepage flow, which includes concentrated leak erosion, backward erosion, contact erosion, and suffusion (Richards and Reddy, 2012). Concentrated leak erosion occurs at the low seepage velocity but the large hydraulic gradient. Generally, a crack is formed before the initiation of the concentrated leak erosion. When the hydraulic gradient is large enough and the geometric condition is satisfied, the concentrated leak erosion can form the piping.

Backward erosion often occurs in the non-cohesive soils, which is usually categorized into backward erosion piping and global backward erosion. Backward erosion piping always initiates from the downstream side of the embankment dam (Fell and Fry, 2013). The pipe is always vertical in the global backward erosion. Piping was previously termed as natural tunneling, tunneling erosion, and soil piping, which could be usually found in the bedrock of the dryland (Jones, 1981). The initiation and progression of backward erosion can be classified into four steps. Figure 1.1 shows the progression of the backward erosion in the foundation. Firstly, a certain concentrated leakage or crack is formed at the toe of the embankment. Gradually, the backward erosion initiates. Then, the fines are gradually detached or washed out subjected to the seepage flow. Furthermore, the pipe is formed after a large number of fines are washed out. Finally, a breach appears, which can lead to the collapse of the embankment dam or the levee (Fell and Fry, 2013).

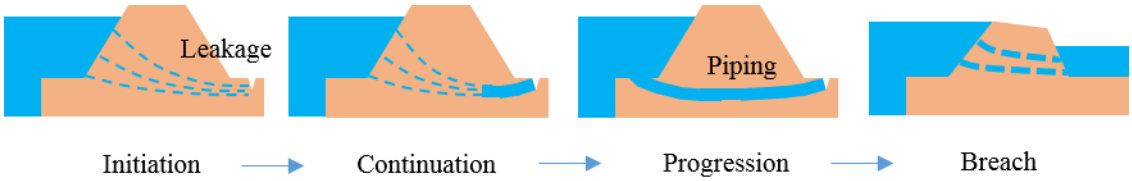

Figure 1.1 Schematic of initiation and progression of back erosion (after Fell and Fry, 2013)

When the erosion occurs in the contact between the gravel and the fines, contact erosion happens. Suffusion, firstly introduced by Pavlov (1989), happens when particles migrate through the soil skeleton under seepage flow (Wan and Fell, 2008). Fannin and Slangen (2014) subdivided the instability phenomena caused by seepage flow into suffosion and suffusion (Fig. 1.2). Suffosion indicates the phenomenon in which collapse of soil structure happens after the loss of fines while suffusion is the phenomenon where the soil structure and volume remain unchanged with the gradual loss of fines under the seepage flow (soil structure in this study mainly refers to the soil skeleton, which bears the most stress). Goldin and Rasskazov (1992) found that cumulative fines loss of 3% could have no impact on the stability of soils. Other researchers suggested that the influence of the loss of fines on the soil structure could be ignored when the cumulative fines loss was smaller than 5% (Wan and Fell, 2008). Therefore, the threshold cumulative fines loss can set to 3% to 5%, below which the soil structure does not change (suffusion).

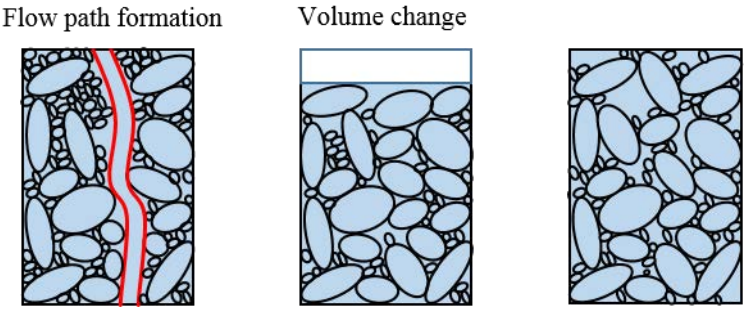

(a) Piping (b) Suffosion (c) Suffusion

Figure 1.2 Schematic of different modes of internal erosion

The erosion can cause damage to both the natural deposits and the earthen structures. For instance, it was found that water can cause serious damage to pavements. Through the cracks, road shoulders, and the subgrade, water could enter the base. If the drainage system does not work well, the internal erosion can occur after a long time, which accounts for more than 90% of the pavement problems (Chapuis *et al.*, 1996; Cedergren, 1997). Piping failure accounts for most of the large embankment dam failures. Depending on the location of the piping, the piping in the embankment dam can be classified into three forms, piping through

the embankment, piping through the foundation, and piping from the embankment into the foundation (Foster, 2000). Two sinkholes appeared in WAC Bennett Dam due to the transportation of fines toward downstream after many years (Muir Wood and Maeda, 2008). Wilson *et al*. (2018) noted that levee and dam failures occurred due to continuing soil erosion by the subsurface flow. When the crushed zones within dams or river embankments are inadequately sealed, the erosion path can be formed through these structures from the downward filters, impervious cores to the upward filters. The continuing dropping of the construction materials on the overlying part of dams or river embankments caused by the seepage flow can cause the settlement of the dam or river embankment surface (Razavi et al., 2020).

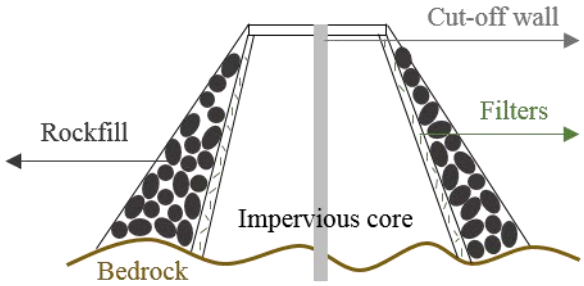

Figure 1.3 Schematic of the cut-off wall in the embankment

Some measures can be taken during the construction to avoid the internal erosion in the dams: (1) keep the homogeneity of the construction materials; (2) set the transitional zones between the fine and coarse materials (Flores-Berrones et al., 2011). At the same time, other remediation options can be adopted to prevent internal erosion, mainly filters and barriers (Koelewijn and Bridle, 2017). Filters system, the first line of defense against the continuation of internal erosion in the dams, can be employed where large hydraulic gradient is developed (Caldeira, 2019). Cut-off wall (e.g., sheet pile wall, diaphragm wall, and soil mixing wall) and grout curtain can be driven into the dam or river embankments, which increase the length of the seepage flow or block the seepage path and reduce the risk of internal erosion (Fig. 1.3, Odenwald and Ratz, 2012; Thongthamchart and Brohmsubha, 2014).

As mentioned above, there are several types of internal erosion. However, in this dissertation, the term “internal erosion” is mainly used to describe either suffosion or suffusion type of erosion.

To fully understand the collapse mechanism, many experimental investigations have been conducted to study the mechanism of the internal erosion process and the mechanical behavior of the internally eroded soils. However, the research on the quantification of the erosion process and the constitutive model of the internally eroded soils is quite limited. Therefore, this dissertation concentrates on the quantification of the seepage-induced erosion process, the variation of the erosion-related model parameters, and the modification of the constitutive model considering the effect of internal erosion.

1.2 Purpose and scope of this study

The hydraulic force or seeping water can cause the loss of fines and rearrange the soil structure, which causes the variation of the mechanical behavior of the eroded soils. With the prolonged loss of fines, hazards like sinkholes and piping are likely to happen. Therefore, the comprehensive understanding of the evolution of fines under different seepage conditions and the subsequent change in the mechanical behavior of the eroded soils is of great importance for the design of the earthen structures in the geotechnical field.

The objectives of this dissertation are as follows:

(1) To quantify seepage-induced erosion process of soils.

(2) To identify and quantify key parameters that govern the eroded soil behavior based on deformation characteristics of the eroded soils.

(3) To propose the modified subloading Cam-clay model that can describe the mechanical behavior of the eroded soils.

(4) To confirm the capability of the proposed models through both the seepage tests and drained triaxial tests.

To achieve these objectives, the following work has been done:

(1) The hydro-mechanical behavior of the soils subjected to the seepage flow has been investigated. Several seepage tests that take the effects of the hydraulic gradient, the initial fines content, and the confining pressure into consideration are studied.

(2) The predictive equation of the fines content after the erosion as a function of the flow velocity, the initial fines content, the confining pressure, and elapsed time is proposed. At the same time, the erosion-induced volumetric strain and post-erosion void ratio are estimated considering internal erosion.

(3) The subloading Cam-clay model is employed to predict the mechanical behavior of the soils with suffosion. The slope of the normal compression line (λ), angle of shearing resistance at the critical state (φ), and initial stress ratio (R_0) are identified as the key parameters, whose relations with the suffosion parameters (void ratio before shearing, final fines content) are established.

(4) Considering the variation of the normal yield surface induced by erosion, the subloading Cam-clay model is modified by incorporating with the similarity ratio for the eroded soils.

(5) Two-step calculation based on the predictive equations in the seepage test part and the modified subloading Cam-clay model is conducted to predict the change of soil properties and mechanical behavior of the eroded soils.

1.3 Layout of the dissertation

This dissertation contains seven chapters. Chapter 1 is the current chapter, which describes the background of this research. Besides, the objectives of this study and the work that has been done are introduced in sequent.

Chapter 2 mainly focuses on the internal erosion related literature review, which can be divided into four aspects. The initiation of internal erosion is discussed firstly. Then, the

variation of the soils under seepage tests, and the numerical simulations on the seepage progress are introduced. Besides, the triaxial tests on the internally eroded soils till now are shown to fully understand the effect of loss of fines on the soil behavior. Finally, the study on the modification of the constitutive model of the internally eroded soils is described.

Chapter 3 mainly quantifies the effects of internal erosion on soil properties. The seepage tests under different conditions are recalled firstly. With the experimental observations on these seepage tests, the evolution law expressing the fines content after the erosion considering the hydraulic gradient, the initial fines content, and the confining pressure is proposed. And erosion-induced volumetric strain and post-erosion void ratio are estimated.

Chapter 4 firstly introduces the effects of erosion phenomena (suffusion and suffosion) and the intergranular void ratio on the mechanical behavior of both loose and dense soils. The subloading Cam-clay model is employed to predict the mechanical behavior of the original soils. After confirming the good predictability of the subloading Cam-clay model, it is used to predict the mechanical behavior of the soils with suffosion. In the end, the key parameters governing the mechanical behavior of the eroded soils are identified and the evolution laws of the key parameters with the suffosion-related parameters are proposed.

Chapter 5 mainly describes the modification of the subloading Cam-clay model considering the effect of internal erosion. The determination method of the erosion-related model parameters is also presented.

Chapter 6 shows the performance of the modified subloading Cam-clay model through the simulation of the drained triaxial tests on eroded soils from both the laboratory and DEM approaches. The predictability of the predictive equations for the seepage stage and the modified subloading Cam-clay model for the shearing stage is confirmed through the seepage and drained triaxial shearing tests.

The conclusions of this study are summarized in Chapter 7. Some recommendations are also given in this chapter.

CHAPTER 2

LITERATURE REVIEW ON INTERNAL EROSION

2.1 Introduction

This chapter gives a brief review of the relevant academic literature on internal erosion related study. Section 2.2 summarizes three criteria for the initiation of internal erosion. The internal erosion process from both laboratory experiments and numerical simulations is described in Section 2.3. At the same time, it also introduces evolution laws that express the effect of erosion on the hydro-mechanical behavior of soils. In Section 2.4, the mechanical behavior of the internally eroded soils obtained from laboratory experiments and DEM approaches are discussed. Section 2.5 mainly focuses on the previous study of the constitutive models considering the effect of internal erosion.

2.2 Review of the initiation of internal erosion

This section mainly focuses on the literature review on the initiation of internal erosion. Although the dissertation mainly focuses on the evolution of the erosion-induced material properties and the constitutive models considering the effect of internal erosion, it is still necessary to understand the required conditions that can cause internal erosion. Generally, the stability of the soil structure depends on the following factors: (1) the particle size distribution (PSD) of the soils, (2) the disturbing forces on the soils, and (3) the relative density of the soils (Kenny and Lau, 1985). Also, some other factors affect the stability of the soil structure, such as the confining pressure, the thickness of the filter, and so on. In this section, the effect of the grain size on soil stability is firstly discussed. Then, the hydraulic force that could cause erosion is presented. Finally, the stress criterion obtained from the microscopic approach is described.

2.2.1 Grading criterion

Kenny and Lau (1985) concluded three conditions for the soils that exhibit the propensity of the unstable grading: (1) the primary structure, supporting or transferring the most stress, exists in the soils, (2) some fines do not transfer any stress inside the voids formed by the primary structure, and (3) the voids are large enough for the fines to move through.

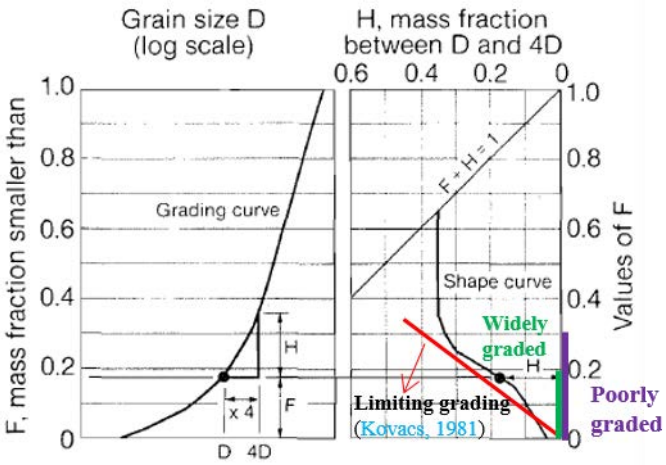

Figure 2.1 Determination of stable and unstable gradings (after Kenny and Lau, 1985)

Kenny *et al*. (1985) found that the fines of diameter D can pass through the voids inside the primary structure formed by particles of diameter 4D and larger. The F indicates the mass ratio of the particles smaller than D to the total soils while the H is the mass ratio of the particles whose diameter is between D and 4D to the total soils, as shown in the left diagram of Fig. 2.1. It can be obtained from previous research that the range of F for widely graded soils is 0 ~ 0.2 and that for the poorly graded soils is 0 ~ 0.3 (soils with the uniformity coefficient larger than five are widely graded; soils with uniformity coefficient smaller than five are poorly graded). The boundary (limiting grading line) between unstable and stable soils was suggested by Kovacs (1981). When the shape curve is in the upper right of the limiting grading line, the soils can be regarded as unstable soils (right diagram of Fig. 2.1). Besides the method depending on the shape curve, other criteria evaluating the potential of stability were also proposed. The fines continue to migrate through the coarse particles under the seepage flow, which could induce the collapse of the earthen structures. Therefore,

Terzaghi and Perk (1948) proposed the concept of the filter for the design of dams (Fig. 2.2). The criteria of the filter were $D_{15c}/d_{85f} \leqslant 4$, $D_{15c}/d_{15f} \geqslant 4$, which were based on the laboratory tests and practical experience (Fig. 2.3). D_{15c} (grain size when the coarse particles pass the 15% of the total mass of the coarse particles) is related to the distance between the randomly coarse particles, which can be selected as the good indicator representing the void size inside the filter (Vanmarcke and Honjo, 1985). d_{85f} (grain size when the fines pass 85% of the total mass of the fines) is the size that all fines can stay stable and the filter can retain the fines of this size (Honjo and Veneziano, 1989). Honjo and Veneziano (1989) modified the filter criteria proposed by Terzaghi by adding another grain size ratio (d_{95}/d_{75}). When the self-healing index (d_{95}/d_{75}) is less than seven, the non-cohesive base soils are considered to be stable.

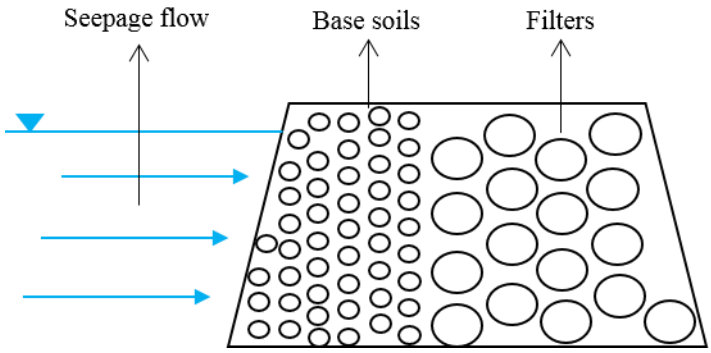

Figure 2.2 Schematic diagram of the filter

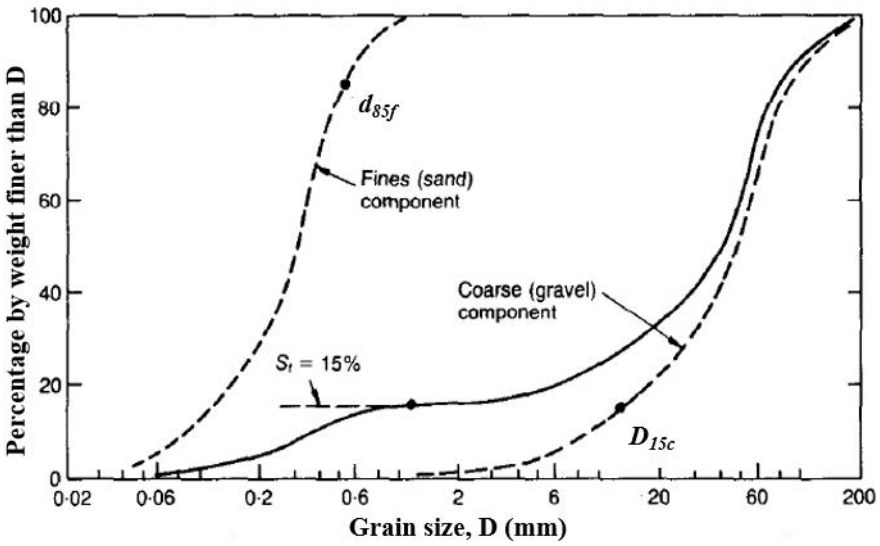

Figure 2.3 The determination of d_{85f} and D_{15c} in the particle size distribution (PSD) (after Kenny and Lau, 1985)

The use of the particle size distribution could cause errors in the widely graded soils, as the large particles with the larger mass and fewer numbers were over-represented. It is difficult for a few large particles to contact each other and form large voids. Considering the ineffectiveness of the sole use of the criterion D_{15c}/d_{85f} on the evaluation of the filter, the concept of the constriction (void) size distribution (CSD) was proposed by Locke *et al.* (2001). Indraratna *et al*. (2007) proposed the method of determining the filter constriction size distribution for the soils with a certain relative density and particle size distribution, which could be calculated based on mass, number, or surface area (Fig. 2.4). The number of coarse particles is small and the surface area of these coarse particles is large, which indicates that the contacts between the coarse particles and others are quite important. Therefore, the filter constriction size distribution calculated based on the surface area was recommended (Humes, 1996). The criterion, D_{c35}/d_{85SA} ＜1, was proposed for the evaluation of the filter effectiveness. The D_{c35} is the constriction (void) size of 35% passing the filters while the d_{85SA} is the grain size of 85% passing base soils calculated based on the surface area. The experimental evidence showed that the criterion (D_{c35}/d_{85SA}) could separate the ineffective filters successfully, and also avoided being conservative compared with the criteria proposed by Terzaghi and Perk (1948).

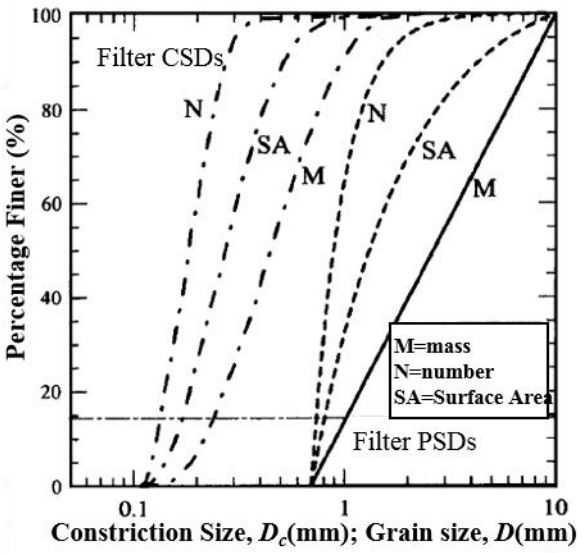

Figure 2.4 Calculated constriction size distributions and particle size distributions by mass, number, and surface area (after Indraratna *et al.*, 2007)

Wan and Fell (2008) also thought the presently employed evaluation criteria for assessing the potential of internal stability were conservative. They modified the Burenkova method incorporated with the grain size ratios (d_{90}/d_{60} and d_{20}/d_5) to obtain the probability contours, which assessed the stability of widely graded soils successfully and failed to evaluate the stability of the gap-graded soils. They found that soils with a flat slope in the fines fraction and steep slope in the coarse fraction were more likely to be unstable. Finally, they suggested that the evaluation of the internal stability of the gap-graded soils should depend on the slope of the fines fraction instead of the grain size ratio (d_{20}/d_5).

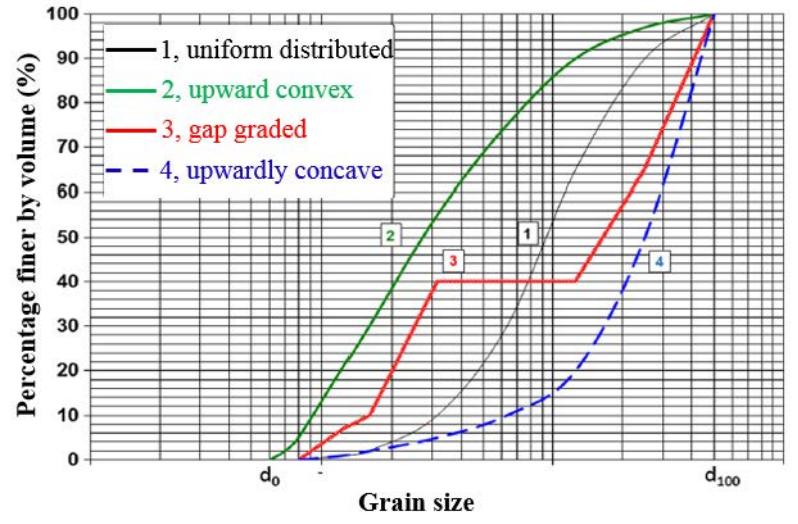

Figure 2.5 Four types of grading curves (after Marot *et al.*, 2016)

Marot *et al.* (2016) assessed the stability of the soils directly from the grading curves. There are four types of grading curves: uniformly distributed, upwardly convex, gap-graded, and upwardly concave respectively (Fig. 2.5). For Curve 1, the total soils including fines and coarse particles are well distributed, showing a typical grading curve of stable soils. When it comes to Curve 2, the soils are mostly constituted by fines. Only a few coarse particles float inside the fines. Therefore, soils under this situation are also considered to be stable. A certain range of particles is missing in the gap-graded soils (Curve 3), which causes larger voids for small particles to migrate under hydraulic force. In this case, the soils are regraded to be unstable. The slope of the fines fraction is flat and that of the coarse fraction is steep

in Curve 4. It seems that the grain size of the coarse particles is well distributed, which forms the primary structure. The number of fines is small compared with that of the coarse particles. The voids formed by the primary structure are large enough for fines to move through. Thus, the soils with the grading shape of upwardly concave (Curve 4) are unstable.

2.2.2 Hydraulic criterion

Hydraulic loading is another necessary factor to induce internal erosion, which can be mainly divided into three categories, the hydraulic gradient, the seepage velocity, and the hydraulic shear stress respectively (Marot *et al.*, 2016). Terzaghi (1925) proposed the theoretic equation of the critical upward hydraulic gradient for the occurrence of piping:

$$i_c = \frac{\gamma'}{\gamma_w} \tag{2.1}$$

where i_c is the critical hydraulic gradient, γ' is the buoyant gravity density, γ_w is the water gravity density. The critical hydraulic gradient of the stable soils under upward flow is one, which means that effective stress equals zero. However, the critical hydraulic gradient of the unstable soils is usually one-fifth to one-third of that of the stable soils. It is also found that the critical hydraulic gradient of soils under the horizontal flow is smaller than that under upward flow. The development of the initiation of piping was shown in Fig. 2.6.

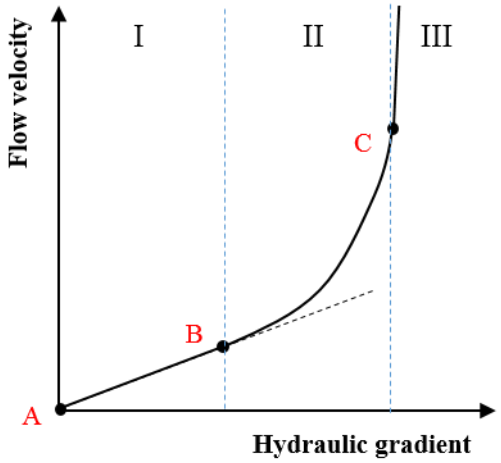

Figure 2.6 Three phases of the initiation of the piping

The whole process can be divided into three phases. In phase I, the permeability is constant. Some small movement of fines occurs at Point B. With the increase of the flow velocity, the permeability increases. The piping is gradually formed from Point B to Point C, during which fines move at many positions and then the slight piping appears at the downstream side. From Point C, strong piping happens (Skempton and Brogan, 1994).

The discrepancy between the critical hydraulic gradients from experimental results and theoretical calculation existed (Wan and Fell, 2008). Skempton and Brogan (1994) proposed a reduction factor α $(\alpha < 1)$, which was used to describe that the load-carry structure mainly consisted of coarse particles that exist in the specimen. The fines can either fill the voids or take part in the stress transmission. When a large number of fines did not take part in the stress transmission, the critical hydraulic gradient decreases. The equation of the critical hydraulic gradient considering the reduction factor α is shown as below:

$$i_c = \alpha \frac{\gamma'}{\gamma_w} \tag{2.2}$$

In the hole erosion tests, the voids of the specimen were assumed as a parallel hole with the radius *r* (Reddi *et al.*, 2000). When the horizontal seepage flow was applied to the specimen, the hydraulic force was replaced by the hydraulic shear stress that occurred on the hole surface. The equation of the hydraulic shear stress was expressed as follow (Hillel, 1980):

$$\tau = \left(\frac{\Delta h \gamma_w}{\Delta Z}\right)\frac{r}{2} \tag{2.3}$$

where ΔZ is the length of the hole, Δh is the hydraulic head difference across the length of the hole. Reddi *et al.* (2000) also proposed the formulation of the relation between the radius *r* and other soils parameters:

$$r = \sqrt{\frac{8k\eta_d}{\phi\gamma_w}} \tag{2.4}$$

where k is the permeability coefficient, ϕ is the porosity, η_d is the dynamic viscosity.

Finally, hydraulic shear stress can be shown as:

$$\tau = \left(\frac{\Delta h}{\Delta Z}\right)\sqrt{\frac{2k\eta_d\gamma_w}{\phi}} \tag{2.5}$$

The upward critical gradient for the soils with high porosity was much lower than that with low porosity from several laboratory tests (Wan and Fell, 2008; Richards and Reddy, 2012). Tomlinson and Vaid (2000) found that confining pressure affected the critical hydraulic gradient. As some clogging was formed by the arch under the seepage flow, the confining pressure could push out the clogging. In this case, the confining pressure was regarded as the destabilizing force. Under the higher confining pressure, the erosion could be triggered by a lower hydraulic gradient. The increasing rate of hydraulic gradient could also affect the onset of internal erosion. During the migration or clogging of the fines, the large increase rate of the hydraulic gradient could cause the fines to continue to be washed out, avoiding the formation of the new filter (Kohler, 1993).

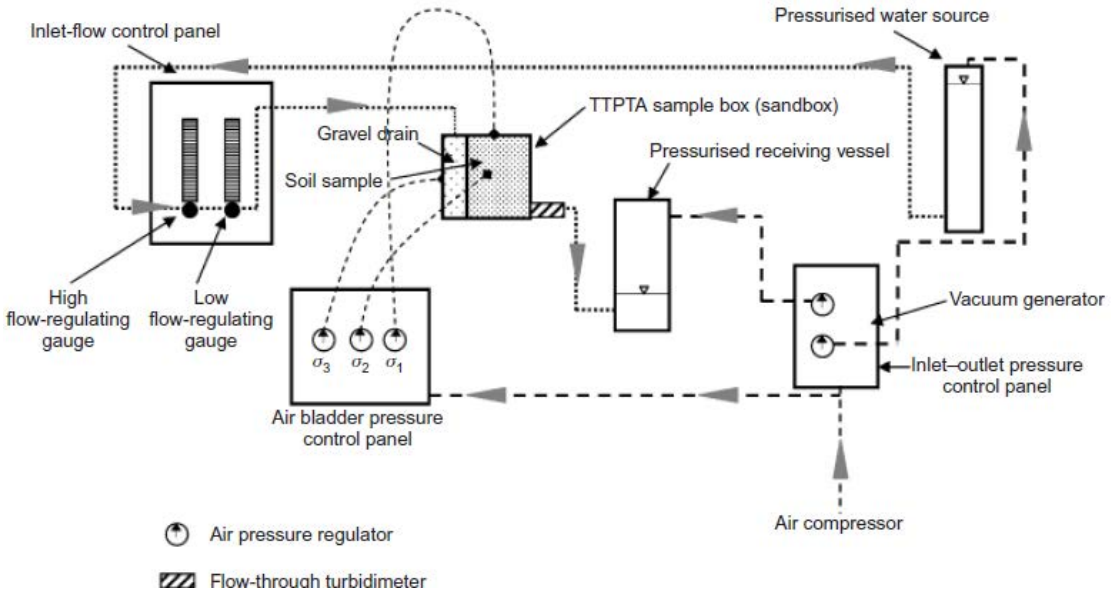

Figure 2.7 Schematic diagram of the piping test apparatus (after Richards and Reddy, 2012)

The apparatus measuring the critical hydraulic gradient improved gradually. In the beginning, the test apparatus was very simple, which only contained a transparent cylinder and some piezometers. Nowadays, the true-triaxial piping apparatus was developed, which contained

the inlet-flow control panel, air bladder pressure control panel, air compressor, sample box, pressurized receiving vessel, and pressurized water resource (Fig 2.7). The effects of the stress state, the seepage direction, the initial porosity, and the seepage flow rate on the critical hydraulic gradient could be investigated.

2.2.3 Stress criterion

The above criteria are obtained based on the macroscopic analysis, which lacks the micromechanical basis. DEM approach can assess the properties of the soils from the respect of the particle scale through establishing the model with numerous idealized particles (Cundall and Strack, 1979). The particles were assumed to be spherical in the DEM approach, and the computation of the relative movement between particles was based on Newton's second law. The velocity, acceleration, and displacement of each particle could be obtained. There is a growing body of literature that recognizes the importance of the study of granular materials through the DEM approach.

The stability of the soils can be assessed based on the coordination number instead of the contact force (Shire and O'Sullivan, 2013). Through the DEM simulations, the stability of the filter increased with the coordination number, which was usually more than four for stable soils. Shire and O'Sullivan (2013) confirmed that a majority of loose fines (fines did not take part in the stress transmission) existed in the unstable soils, which dominated the value of the coordination number. With the process of erosion, the value of the coordination number reduced. The transitions between unstable and stable soils are not clear at the particle level.

Shire *et al.* (2014) continued to carry out 48 DEM simulations on the investigation of factors affecting the stability of the soils. The results showed that the fines content and the relative density had a great influence on the reduction factor α. From the microscopic analysis, the reduction factor α had relations with both the fines content and the grading criterion (D_{15c}/d_{85f}). When the value of D_{15c}/d_{85f} was low, the reduction factor α was approaching

one as the soils were overfilled. While the value of D_{15c}/d_{85f} was high, the ratio of the voids to the fines increased, leading to a decrease of the reduction factor α. The DEM simulations showed that when fines content was smaller than 25%, the soils were underfilled; If the fines content was larger than 35%, the soils were overfilled; If the fines content was between 25% and 35%, the soils were in the transitional state (Shire *et al.*, 2014). These results reflected those of Skempton and Brogan (1994) who found that the fines played a decreasing role in the stress transmission when fines content was below 24% ~ 29% and separated the coarse particles when the fines content was larger than 35% from piping experiments.

Kuwano *et al.* (2016) considered particle gravity in the DEM approach, in which the specimens were prepared by two methods, compression and pluviation. The reduction factor α of the specimens prepared by pluviation was higher than that of the specimens prepared by compression. Kuwano and Shire (2018) simulated the initiation of the suffusion through the coupled Computational Fluid Dynamics (CFD)-DEM approach. The initiation of the suffusion was found to be affected by the combination of particle stress and primary structure. With the gradual erosion of the particles with a low coordination number, the particles with high coordination number began to be washed out.

2.3 Study on the progression of internal erosion

Fines transport and redeposit simultaneously under the seepage flow. The number of eroded fines along with time could be measured through laboratory tests. At the same time, internal erosion is affected by many factors, such as hydraulic gradient, initial fines content, and confining pressure. The DEM approach coupled with many fluid dynamics approaches can be helpful to investigate the erosion process from the perspective of the microscopic scale. Some evolution laws of fines, based on the experimental observations, have been proposed to quantify the internal erosion process.

2.3.1 Laboratory tests of the internal erosion process

Different experimental methods have been proposed to measure the erodibility of the soils,

such as pinhole tests, hole erosion tests, flume tests, and internal erosion tests (Arulanandan *et al.*, 1975; Reddi *et al.*, 2000). A 2mm hole was drilled in the soil core in the pinhole tests, which could be regarded as the preferential flow path. The recorded hole diameter and the flow rate were used to characterize the erodibility of the soils qualitatively. For the hole erosion tests, the diameter of the hole was usually set to 6 mm (Wan and Fell, 2004). Reddi *et al*. (2000) conducted both the hole erosion tests and the internal erosion tests to identify the particles' transportation and reclogging. As the pipe has been formed in the hole erosion tests, the erosion rate of the hole erosion test was larger than that of the internal erosion tests. Particle transportation and reclogging were found to take an important role in the erosion process. Sterpi (2003) conducted the seepage tests on the specimens with 23% initial fines content under the upward seepage flow. The specimen with the larger hydraulic gradient had a larger number of eroded fines.

The permeability showed different trends under different conditions (i.e., soil composition, hydraulic gradient, hydraulic head difference, and flow rate) during the process of seepage tests. Xiao and Shwiyhat (2012) conducted downward seepage tests on the gap-graded soils with a constant hydraulic gradient of 20.8. The permeability showed a decreasing trend. The explanation was that the size of the voids decreased with the clogging of fines, which in turn entrapped the fines again. Ke and Takahashi (2012) conducted upward seepage tests to investigate the hydrological properties of the internally eroded soils with the constant hydraulic head difference. However, the permeability showed an increasing trend during the process of erosion, which resulted from the continuing loss of fines and the subsequent formation of the flow path. More seepage tests under constant flow rate were conducted to investigate the erosion characteristics by Ke and Takahashi (2014a). The sudden increase of the hydraulic gradient was regarded as the sign of the onset of internal erosion. The permeability fluctuated due to the washing out and reclogging of fines. The loss of fines could form the preferential flow paths in the soils, which increased the hydraulic gradient and decreased permeability. However, some relatively large fines could block up these

formed flow paths and increased permeability.

Luo *et al*. (2013) compared the differences between the effect of the long-term hydraulic head and the short-term hydraulic head during the erosion tests (long-term hydraulic head indicates that the hydraulic gradient was kept unchanged during seepage tests for a long time; short-term hydraulic head indicates that the hydraulic head increased gradually until the collapse of the soils). The specimens under the long-term hydraulic head are more likely to be eroded than those under the short-term hydraulic head. At the same time, the soils under higher confining pressure were found to be more difficult to be eroded. The permeability depended on the fate of the fines for the soils under the long-term designated hydraulic head. When the designated hydraulic head was low, the detached fines were easy to be trapped again, leading to an increase in the permeability. However, when the designated hydraulic head was high, the detached fines were mainly washed out, enlarging the voids and decreasing the permeability.

2.3.2 Numerical simulations of the internal erosion progress

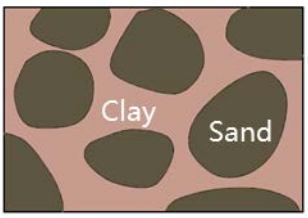

(a) Voids are small

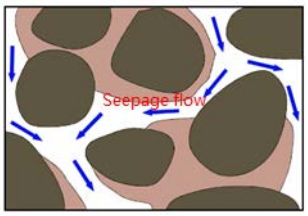

(b) Specimens are easy to be eroded

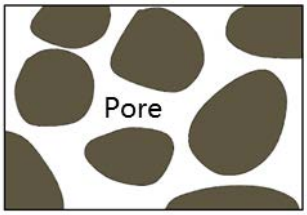

(c) No clay exists

Figure 2.8 Different scenarios of the sand-clay mixtures (after Bonelli and Marot, 2011)

Bonelli and Marot (2011) proposed an erosion law of the sand-clay mixtures under the

seepage flow while ignoring the effects of confining pressure and the volume variation. The erosion was regarded as an interfacial process, which indicated the clay/water interface erosion in particular. The erosion law was established based on some basic assumptions: (a) when the sand was filled with clay, no erosion happened as the voids were small; (b) when some voids existed, the specimens were susceptible to internal erosion; and (c) when no clay existed, the erosion did not occur (Fig. 2.8). The simulation of the internally eroded soils under different hydraulic gradients based on the proposed erosion law agreed well with those from experiments.

Both 2D (Dimension) and 3D Finite Element Method (FEM) approaches were employed to investigate the failure mechanism of the dam induced by internal erosion. The dam failure during the rainy season could be caused by many factors, such as overtopping and seepage flow. The study on the coupled effects of these factors on the failure mechanism of the dam is quite limited. Uzuoka *et al.* (2012) proposed the u-p^a-p^w formulation to study the effect of internal erosion on the failure mechanism of the landslide dam through the 2D FEM approach (u indicates the displacement of the soil skeleton, p^a indicates the pore air pressure, p^w denotes the pore water pressure). The mass exchange between the soil skeleton and pore water was regarded as the process of the eroded fines falling into the pore water. The proposed erosion model, considering the effects of unsaturated soils and mean effective stress, was validated by the experimental tests. The simulation of the Yunokura landslide showed that the erosion occurred in the upstream slope firstly, and then a large flow path formed. The 2D simulation on the piping initiation and progression ignored the hydraulic force from the third dimension and its relative effect on erosion, which could cause the simulation results unreliable. Vandenbore *et al*. (2014) simulated the back-erosion piping (from the downstream to the upstream) in a dam through the 3D FEM approach. The dam was filled with cohesive soils with a designated number of outflow openings. The dam with only one outflow opening was found to be more vulnerable to collapse than that with several outflow openings.

DEM coupled with CFD was firstly employed to give insight into the micromechanical behavior of the internally eroded soils by Tsuji *et al.* (1992). The fluid pressure and fluid velocity could be obtained in the CFD approach. Then, the interaction between particles and fluid was coupled. The variation of porosity was studied based on the coupled CFD-DEM method on both stable and unstable filters under upward seepage flow (Huang *et al.*, 2014). The simulated specimen was prepared with the base soil on the bottom and the filter on the top (Fig. 2.9). For the stable filter, the porosity of the base soil layer near the filter increased at the beginning, and the increasing rate decreased with the progression of the internal erosion. Then, the porosity in this layer began to decrease as the trapped fines filled the voids. Finally, the porosity of the base soil layer near the filter was kept constant. The porosity of the stable filter decreased at the beginning and then kept unchanged along with time. For the unstable filter, the porosity of the base soil increased all the time as fines continued penetrating the filters. The porosity of the unstable filters decreased gradually.

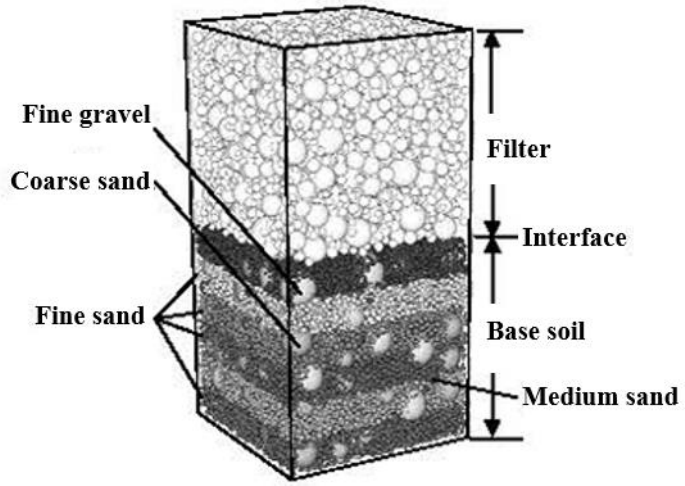

Figure 2.9 Preparation of base soil-filter model (after Huang *et al.*, 2014)

Tao and Tao (2017) used the CFD-DEM approach to study the micro-mechanism of the piping. The piping in essence was the breakage of the equilibrium between particles. The larger increase rate of the pressure difference could result in a smaller critical hydraulic gradient. With the continuation of the piping under the upward seepage flow, both the contact forces and the coordination numbers of soils decreased. As the soils became looser under the

upward seepage flow, the direction of the contact forces transferred from the vertical at the beginning to be more horizontal under large hydraulic forces. Compared with the uniform soils, the nonuniform soils had smaller porosity, which required a larger flow velocity or larger hydraulic gradient for the initiation of the internal erosion.

The upward seepage flow was also simulated on the specimens consisted of 26000 particles with the 26% initial fines content under 50 kPa confining pressure through the CFD-DEM approach (Hu *et al.*, 2019). Fines with low coordination numbers and weak contact force were found to be more prone to be eroded. The gap-graded soils enjoyed a large amount of fines movement and loss of fines under the large hydraulic gradient, while the widely graded soils were seldom eroded. A sudden increase of the hydraulic gradient occurred as the washout of the clusters (gathering of fines), leading to the collapse of the soil skeleton and a decrease in the total volume. The downstream part of the specimens had a larger void ratio after the seepage flow compared with other parts of the specimens, which caused the heterogeneity of the soils along the flow direction (Chang, 2012; Hu *et al.*, 2019).

DEM could be coupled with other fluid methods, such as Pore-scale Finite Volumes (PFV), Lattice Boltzmann Method (LBM), to investigate the evolution of soils subjected to seepage flow. Given that the CFD approach was computationally expensive, Sari *et al.* (2011) simulated the upward seepage flow by injecting the fluid on a point below the soils based on the coupled DEM-PFV approach. The geometry of each void in the PFV approach was calculated with the movement of particles every step. Consequently, the hydraulic forces on particles and the fluxes were computed. The CFD-DEM approach determined the hydraulic force above the particle scale (a group of particles), and the direction of the hydraulic force was that of the averaged fluid velocity. But the DEM-PFV approach determined the hydraulic force at the particle level. The injection forces were in terms of pressure and flux respectively. The threshold injected pressure was around 10 kPa, below which the soils kept stable under seepage flow. When the injected pressure was larger than 10 kPa, the soils were eroded gradually. The imposed flux was set to 2 m^3/s, which could trigger the migration of

fines under seepage flow. The pressure decreased dramatically as the permeability increased after the onset of erosion.

It was found that more fines could be eroded when the direction of the macroscopic seepage flow was consistent with the orientation of the privileged force chain through the DEM-PFV approach (Chareyre *et al.*, 2012). The erosion-induced decrease of particle force chains could lead to an increase in the number of no-contact particles inside the voids (Wautier *et al.*, 2018).

The coupled DEM-LBM approach was employed to investigate the internal erosion progress (Lomine *et al.*, 2013; Sibille *et al.*, 2015). The contact friction law existed among particles in the DEM approach. For cohesive soils, the contact cohesion disappeared upon the broken connections between the particles due to internal erosion. The contact could be reformed again through the re-deposition or clogging. Transportation of the fines was driven by the flow power in the LBM approach. Several lattices were used to represent the fluid domain. The fluid was represented by several groups of particle packages, which stayed on the lattice nodes. Under the flow power, fines in these particle packages moved to nearby lattice nodes. The mass erosion rate was found to have a positive linear relationship with the excess flow power. The simulation results could capture the main features of internally eroded soils under different hydraulic gradients.

The drag force could be computed directly by solving the interaction between the eroded fines and the nodes in the Bonded Particles Method (BPM)-LBM approach while the drag force was calculated through the empirical equation in the CFD-DEM approach. Through the BPM-LBM approach, Wang *et al.* (2017) validated the proposed filter criterion $D_{15c}/d_{85f} \leqslant 4$ and found that the larger hydraulic gradient could cause more fines to move into the filter.

2.3.3 Quantification of the internal erosion process

To quantify the internal erosion process, an empirical exponent function was proposed to

describe the erosion process under different hydraulic gradients along with time, based on the experimental results (Fig. 2.10, Sterpi, 2003). The equation of the eroded fines content was as follows:

$$FC_{er} = FC_0 \left[1 - exp\left(-\left(\frac{t}{t_0}\right)^b \cdot \frac{i^c}{a}\right)\right] \tag{2.6}$$

where FC_{er} is the eroded fines content (percentage by mass), t denotes time, t_0 is the reference time, taken as one hour, i is the hydraulic gradient, a, b, and c are material parameters.

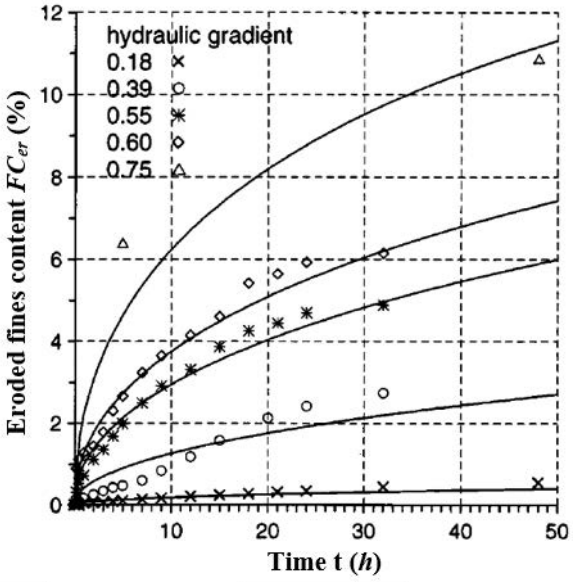

Figure 2.10 Eroded fines content along with the time (after Sterpi, 2003)

By using Eqn (2.6), the remaining fines content can be derived:

$$FC = FC_0 - FC_{er} = FC_0 \cdot exp\left(-\left(\frac{t}{t_0}\right)^b \cdot \frac{i^c}{a}\right) \tag{2.7}$$

Two drawbacks existed in Eqn. (2.7): (a) the erosion could happen at any hydraulic gradient; (b) when the long-term seepage flow was applied to the soils, all the fines were washed out. Thus, the concept of the final density of fines was proposed to avoid the phenomenon that all the fines were washed out after a long seepage time (Cividini and Gioda, 2004). The loss

of fines could be regarded as the change in the density of fines when both coarse particles and fines were considered to be uncompressed. When the flow velocity was large enough, the current density of fines (ρ_f) tended to zero; when the flow velocity was small or zero, almost no fines were washed out. Based on these, a reasonable formulation of the current density of fines under different flow velocities was proposed:

$$\rho_f(v) = \rho_{f0} - \left(\rho_{f0} - \rho_{f\infty}^*\right) \cdot \frac{v}{v^*} \qquad if \quad 0 \le v \le v^* \tag{2.8}$$

$$\rho_f(v) = \rho_{f\infty}^* - \gamma \cdot log\left(\frac{v}{v^*}\right) \qquad if \quad v^* \le v \tag{2.9}$$

where ρ_{f0} is the initial density of fines, $\rho_{f\infty}^*$ is the final density of fines, v^* is the lowest flow velocity applied to the specimen, v is the applied flow velocity, γ is a non-dimensional parameter.

Cividini *et al*. (2009) proposed the evolution law of the final density of fines in the terms of hydraulic gradient and initial density of fines:

$$\rho_{f\infty}^*(\rho_{f0}, i) = \rho_{f0}[(1 - c_0) \cdot \exp(-a_0 \cdot i^{b_0}) + c_0] \tag{2.10}$$

where a_0, b_0, and c_0 are material parameters. Based on the experimental observations, the erosion rate was found to have a linear relation with the square root of the hydraulic gradient, and the erosion rate was also related to the final density of fines. Finally, the equation of the erosion rate was proposed:

$$\frac{\partial \rho_f(\rho_{f0}, i, t)}{\partial t} = d_0 \cdot \sqrt{i} \cdot [\rho_f(\rho_{f0}, i, t) - \rho_{f\infty}^*(\rho_{f0}, i)] \tag{2.11}$$

where d_0 is a material parameter.

2.4 Mechanical behavior of the internally eroded soils

As the on-site internally eroded soils are not easy to obtain, soils with different fines contents are used to mimic the internally eroded soils at the beginning. Shortly afterward, many apparatuses, combining the seepage tests and triaxial tests, were modified to investigate the

mechanical behavior of the internally eroded soils. For further understanding of the effect of internal erosion on the mechanical behavior of soils, the DEM approach was employed from the respects of coordination number, active fines, and so on.

2.4.1 Laboratory tests on the internally eroded soils

The threshold fines content (FC_{th}) is an important indicator of the alteration in the mechanical behavior of soil mixtures, below which the soils are fines-dominated and above which the soils are coarse particles-dominated. Zuo and Baudet (2015) summarized the determination methods of the threshold fines content from the aspects of experiments, analytical and semi-analytical methods. More detailly, factors, such as void ratio, packing density, number of the cycles when the liquefaction occurs, and grain size ratio of coarse particles to fines, can be used to estimate the threshold fines content. When the grain size ratio of coarse particles to fines is large enough, the threshold fines content of the coarse particles-fines mixture is within a small range (Rahman *et al.*, 2009). As the erosion happens in the condition that the fines content is smaller than the threshold fines content, the soils described in this study are mostly coarse particles-dominated.

Soils have different fines contents after internal erosion. Therefore, the study on the mechanical behavior of soils with different fines contents is helpful to understand the mechanism of internal erosion to a certain extent. Previously published studies on the effect of the fines content on the mechanical behavior of the mixtures under the undrained condition are not consistent. A series of undrained triaxial tests were conducted to investigate the effect of the fines content and void ratio on the mechanical behavior of the sand-silt mixtures (Thevanayagam *et al.*, 2002). Soils showed a decreasing trend of deviatoric stress with the increase of fines content under the undrained condition when the intergranular void ratios of the sand-silt mixtures were close to the maximum void ratio of pure coarse particles. When the intergranular void ratios of the sand-silt mixtures were relatively low, the deviatoric stress under the undrained condition increased with fines contents (intergranular

void ratio,$e_s = (e_c + FC)/(1 - FC)$, indicates that all fines were considered as voids; e_c is the void ratio after consolidation; FC denotes the fines content).

Ouyang and Takahashi (2016) conducted the undrained triaxial tests on loose soils with different fines contents. The soils with smaller fines content had higher secant stiffness, peak strength, and deviatoric stress at the critical state than those with larger fines content. Microscopic observations showed that soils with fewer fines had fewer fines jamming, which increased the number of contacts between coarse particles per unit volume.

However, Andrianatrehina *et al*. (2016) found that the deviatoric stress under the undrained condition decreased with the sand in the dense sand-gravel mixtures. The explanation was that force chains were destabilized with the decrease of sand. Mahmoud *et al*. (2016) focused on the influence of fines content and over-consolidation ratio (OCR) on the mechanical behavior of the sand-silt mixtures under the undrained condition. For the mixtures with the same fines content and different OCRs (1, 2, and 4), the deviatoric stress under the undrained condition increased with the OCR. When the OCR was high (e.g., 4), the effect of silt content, ranging from 0% ~ 20%, on the deviatoric stress under the undrained condition was negligible. It could be concluded that the mechanical behavior of the sand-silt mixtures under the undrained condition was governed by the OCR other than the silt content when the silt content was smaller than the threshold fines content.

To investigate the effect of fines on the mixture soils, the maximum shear modulus (G_{max}) of the mixture soils at the small strain level with different fines contents was measured through the resonant column tests (Goudarzy *et al*., 2016). At the same time, the Hardin relation was used to estimate the maximum shear modulus (Hardin and Back, 1966), as shown:

$$G_{max} = A_1 p_a f(e^*) \left(\frac{p}{p_0}\right)^n \tag{2.12}$$

where A_1 and n are material parameters, p_0 is the atmospheric pressure, p is the mean effective stress, $f(e^*)$ is the function of the equivalent void ratio e^* ($e^* = \frac{e_c+(1-b_p)FC}{1-(1-b_p)FC}$, b_p indicates the participation of fines in stress transmission). When the fines content was smaller than the threshold fines content, the equivalent void ratio increased with the fines content, and the maximum shear modulus (G_{max}) at the small strain level decreased with the increase of the fines content. The accuracy of Eqn. (2.12) was highly dependent on the accuracy of the estimation of the equivalent void ratio.

However, soils directly prepared with different fines content cannot comprehensively represent the internally eroded soils, especially the soils with suffosion whose structure changes subjected to the seepage flow. The Cone Penetration Tests (CPTs) were conducted on both the soils with different initial fines contents (ranging from 14.3% ~ 25%) and the soils subjected to seepage flow (Ke and Takahashi, 2012). Original soils with smaller initial fines content had a higher cone resistance. The increase of fines could cause a decrease of contacts between coarse particles per unit volume, resulting in a decrease in the cone resistance. Interestingly, eroded soils with smaller final fines content had a lower cone resistance. Erosion made the soils looser, resulting in a decrease in the cone resistance.

Many drained triaxial tests have been conducted on the eroded soils, which were obtained after the seepage tests. The deviatoric stress of the eroded loose soils at the large strain level was lower than that of the original soils under the drained condition (Ke and Takahashi, 2014a, 2014b, 2015). The change in the deviatoric stress of the internally eroded soils within the small axial strain was studied from the aspect of the normalized secant stiffness (Ke and Takahashi, 2015). The normalized secant stiffness of both original and internally eroded soils was shown in Fig. 2.11. The normalized secant stiffness of the internally eroded soils at the very beginning was larger than that of the original soils, for the seepage flow could strengthen the structure of the soils. The temporary reinforcement collapsed with shearing, causing a sudden drop in the normalized secant stiffness. Finally, the secant stiffness of the

internally eroded soils decreased and became lower than that of the original soils. For eroded dense soils, both peak strength and deviatoric stress at the critical state decreased after erosion under the drained condition (Chen *et al.*, 2016; Li *et al.*, 2017, 2020).

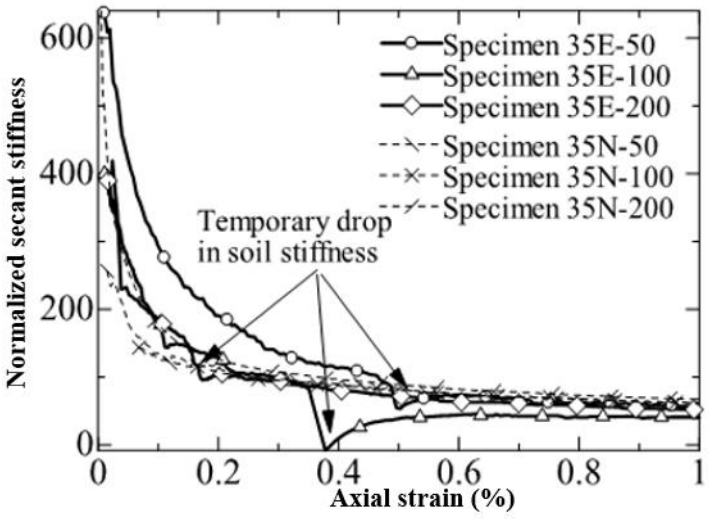

Figure 2.11 Comparisons of the normalized secant stiffness of both original and internally eroded soils (Specimens named with "35" refer to the initial fines content is 35%. "50, 100, 200" indicate the confining pressures, 50 kPa, 100 kPa, 200 kPa, respectively. "E" means internally eroded soils, "N" represents the sample without erosion; after Ke and Takahashi, 2015)

Chang and Zhang (2011) studied the effect of the complex stress state on the hydro-mechanical behavior of the eroded soil. The initial stress states were (50 kPa, 0 kPa), (83 kPa, 100 kPa), (100 kPa, 150 kPa) respectively (the values in the bracket are mean effective stress and deviatoric stress). The structure of the soils became unstable under the larger stress state, resulting in a larger erosion rate and a larger amount of loss of fines. After the seepage test, drained triaxial tests were carried out. Although the soils with a higher initial stress state enjoyed a larger amount of loss of fine, the peak strength of which was higher than that with a lower initial stress state.

A series of undrained cyclic triaxial tests were conducted to understand the cyclic behavior of the soils subjected to internal erosion. Ke and Takahashi (2014b) found that more cyclic loops were needed for the failure of eroded soils compared with original soils. The evaluation of the liquefaction potential on the internally eroded soils depended on the intergranular void

ratio other than the global void ratio (Mehdizadeh *et al.*, 2019). As the total volume decreased with the loss of fines, the intergranular void ratio also decreased, which resulted in a decrease of the liquefaction potential. This study supports evidence from previous observations (Naeini and Baziar, 2004).

Prasomosri and Takahashi (2020) conducted a series of seepage tests on the gap-graded soils with different initial fines contents. Different erosion phenomena were found during the seepage tests: self-filtering happened when fines content was smaller than 20%; no marked volume change was found (suffusion) when initial fines content was 30%; marked volume change occurred (suffosion) when initial fines content ranged from 32.5% to 40%. Undrained triaxial tests on both uneroded and eroded soils with initial fines contents ranging from 0% to 35% were conducted subsequently, which indicated that the undrained mechanical behavior of the eroded soils largely depended on the fines content and related erosion phenomena.

2.4.2 DEM simulation of the mechanical behavior of internally eroded soils

DEM can simulate the mechanical behavior of brittle materials such as rock, concrete, and ceramic, which are difficult to be reproduced by the continuum method. The mechanical behavior such as contraction/dilation, strain-hardening/softening could be realized by the DEM approach (Tavarez and Plesha, 2007).

To understand the micromechanical behavior of soils with different grading curves comprehensively, isotropic compression tests on three types of soils were simulated through the 3D DEM approach (Langroudi *et al.*, 2012). Soils with the grading curve "Cu=3" were internally stable, while soils with the grading curve "G3-a" and "k" were internally unstable (Fig. 2.12). It was found that the average coordination number of stable soils under isotropic compression was larger than that of unstable soils (Fig. 2.13). The perturbations existed in the variation of average coordination number of soils with grading curves "G3-a" and "k". The possible explanation was that the particles with no-contact or one-contact existed inside

the voids, leading to the discontinuation of the coordination number under isotropic compression. Based on the microscopic observations in the force chain of these soils, stable soils had homogenous force networks while unstable soils had heterogenous force networks.

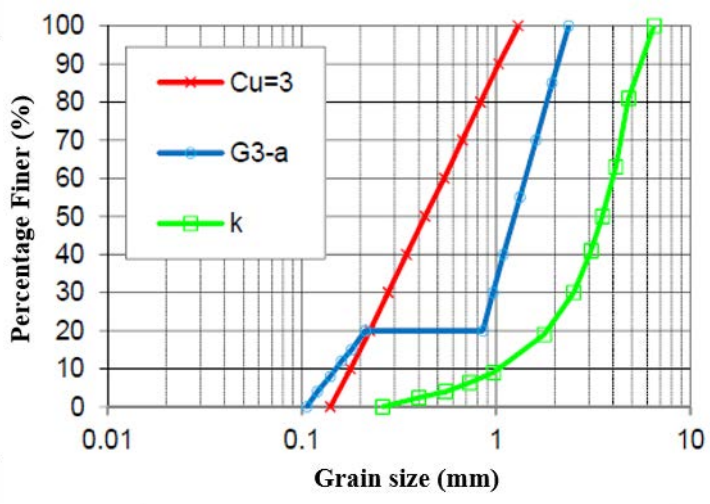

Figure 2.12 Grading curves for three types of soils (after Langroudi *et al.*, 2012)

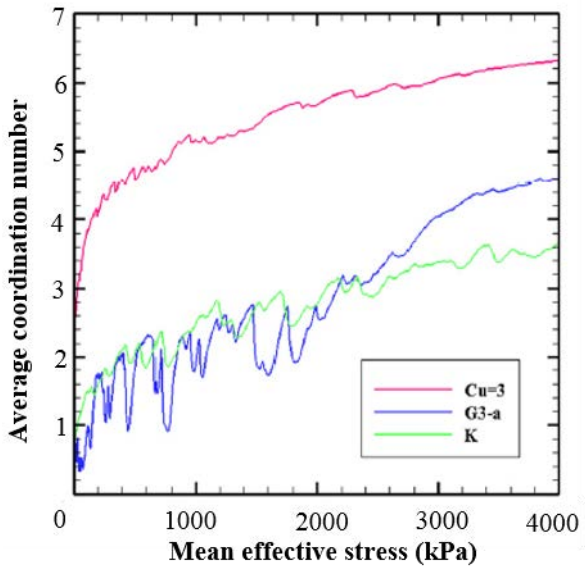

Figure 2.13 Average coordination number under different mean effective stresses (after Langroudi *et al.*, 2012)

The effects of the particle shape and the fines content on the binary mixtures were investigated through the 3D DEM approach (Ng *et al.*, 2016). The particle shape was described by particle radius ratio, sphericity, elongation, and roundness. Compared with the influence of the fines content, the particle shape played a greater role in the peak strength.

However, the particle shape had a negligible impact on the critical void ratio while the fines content played an important role in the critical void ratio. Hosn *et al.* (2016) studied the effect of active fines content on the mechanical behavior of internally eroded soils through the 3D DEM approach. The active fines denoted the fines which took part in the stress transmission. The active fines content was a limit, below which the fines mainly filled the voids and do not transfer the stress. When fines content surpassed the active fines content, the macroscopic mechanical behavior of the soils changed remarkably. Whether or not the values of the threshold fines content and the active fines content were the same depended on the packing density, the mineralogy, and the particle shape.

The effects of the stress ratio on the volumetric characteristics of the soils subjected to internal erosion were studied through the DEM approach, and the dense assemblies of 2D circular particles were used to mimic the soils (Muir Wood *et al.*, 2008). The removal of the non-contact fines could both decrease the volume and increase the void ratio, in which the effect of increasing the void ratio dominated. Fines were directly deleted at different stress ratios. The initial uneroded dense soils showed a dilative trend under the drained triaxial shearing condition. When fines were deleted at a low stress ratio, the internally eroded soils showed contractive behavior. When fines were deleted at a high stress ratio, the internally eroded soils showed dilative behavior.

To study the effect of different erosion processes on the mechanical behavior of internally eroded soils, two erosion scenarios (i.e., deleting the fines randomly and deleting the fines with fewer contacts) were simulated through the 3D DEM approach (Zhang *et al.*, 2019). The internally eroded soils from deleting the fines with fewer contacts showed higher initial stiffness but lower deviatoric stress at the critical state compared with those from random deletion of the fines. Hu *et al*. (2019) obtained the internally eroded soils under the seepage flow through the CFD approach, after which the triaxial shearing on the internally eroded soils was simulated through the DEM approach. The internally eroded soils showed a reduction in the peak strength and similar deviatoric stress at the critical state compared with

the original soils. The void ratio at the critical state of the internally eroded soils was higher than that of the original soils.

2.5 Constitutive models considering internal erosion

Currently, some constitutive models have been modified to simulate the mechanical behavior of the soils subjected to internal erosion. The review of the modification of the constitutive model considering internal erosion will be presented from the aspects of the model parameter study, the mobilized friction angle variation, the critical state line variation, and the porosity variation.

2.5.1 Review on model parameter study considering the effect of internal erosion

Through the information from the triaxial tests simulated by the DEM approach, the influence of the erosion on the model parameters could be analyzed. Wang and Li (2015) classified the effects of erosion into four aspects: the loose effect, force network damage, force network relaxation, and variation of the critical state. The designated number of fines were directly removed at the specified stress state to simulate the erosion process. Depending on the DEM simulations of the internally eroded soils under different mass erosion percentages, the relations between the state-based elastoplastic model parameters (i.e., void ratio, critical state line related parameters, the stress reduction) and mass erosion percentage were established quantitatively. The simulation made by the modified state-based elastoplastic model agreed well with those from DEM simulations.

The Duncan-Chang E-B model was used to simulate the triaxial tests of both uneroded soils and internally eroded soils with different cumulative fines losses (Zhang and Chen, 2017). As it was difficult to obtain the on-site soils, the soils prepared in the laboratory had the same grading curves as the on-site soils. The internally eroded soils were prepared with fewer fines while keeping the porosity the same as the on-site internally eroded soils. Through the back analysis and the regression analysis, the relations between the model parameters (volumetric strain parameters and shear deformation parameters) and the cumulative fines

loss were derived quantitatively. The Duncan-Chang E-B model considering different cumulative fines losses could be used to describe the erosion-induced variation of mechanical behavior.

2.5.2 Constitutive models focusing on the erosion-induced variation of mobilized friction angle

Hicher (2013) investigated the effects of erosion on mechanical behavior at the particle level. The impact of removing fines on mechanical behavior was presented in two aspects: the decrease in the contacts between particles and the decrease of the mobilized friction angle. The post-erosion void ratio was linked with the mobilized friction angle, which was then incorporated into the microstructural model. And the critical state line was considered unchanged. The change in the number of contacts per unit volume caused by internal erosion was also considered in the microstructural model. From the numerical simulation, it was found that the erosion-induced deformation was very large at the high stress ratio. The diffuse failure, which occurred at the low stress level and without any plastic strain localization, was found during the triaxial shearing on the internally eroded soils (Daouadji *et al.*, 2011). This microstructural model was validated by the DEM simulations.

2.5.3 Constitutive models focusing on the erosion-induced variation of the critical state line

Many researchers focused on the erosion-induced variation of the critical state line when studying the constitutive model considering the effect of internal erosion. To quantify the effect of internal erosion on the grading curves, the grading ratio (R_D) of the maximum grain size to the minimum grain size was proposed (Muir Wood and Maeda, 2007). And the grading state index ($I_G = \frac{lnR_D}{2B_s}$, B_s is a constitutive parameter, Fig. 2.14) was proposed, which could be employed to estimate the evolution of both specific volume and critical state line (Muir Wood *et al.*, 2010). The variation of both specific volume and critical state line could be reflected by the state parameter (Ψ), which was a hardening parameter in the Severn-Trent

sand model. The Severn-Trent sand model considering the loss of fines could capture the main features of the internally eroded soils.

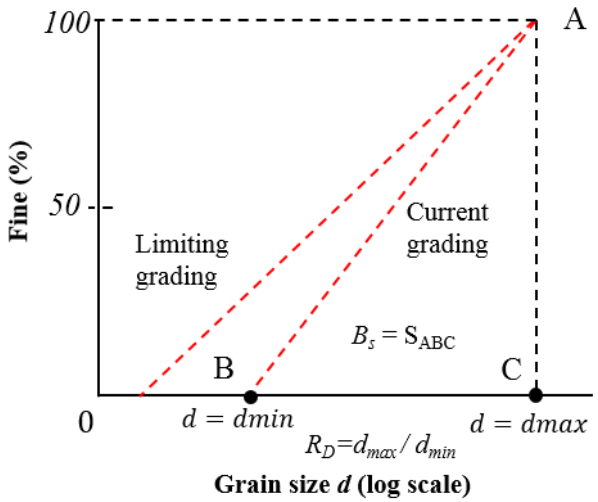

Figure 2.14 The definition of the grading ratio (R_D) and the constitutive parameter B_s (after Muir Wood *et al.*, 2010)

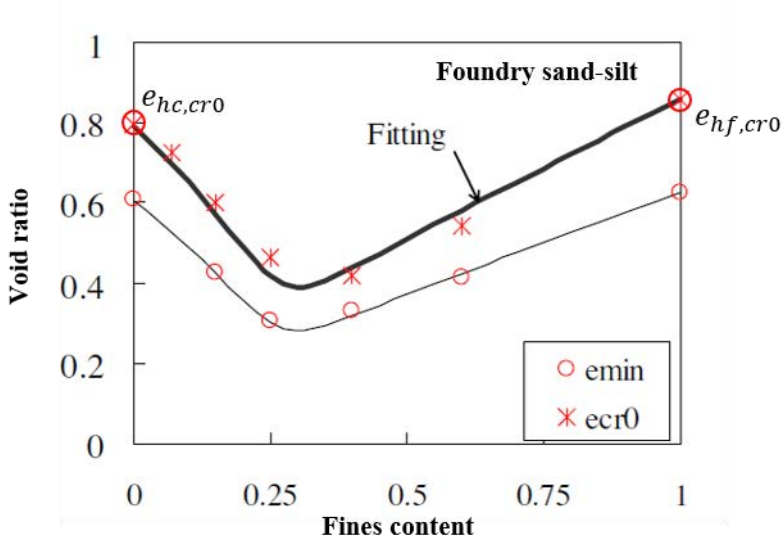

Figure 2.15 The variation of void ratio under different fines contents (after Yin *et al.*, 2014)

It was found that the minimum void ratio of the foundry sand-silt mixture decreased with the fines content firstly, and then increased with the fines content (Fig. 2.15). The reference critical void ratio (e_{cr0}) along with different fines contents was found to have a similar trend. The predictive equation of the reference critical void ratio under different fines contents was firstly proposed by Yin *et al*. (2014), as shown in the equation:

$$e_{cr0} = \left[e_{hc,cr0}(1-FC) + a_e FC\right]\frac{1-\tanh[\xi(FC-FC_{th})]}{2} + e_{hf,cr0}\left(FC + \frac{1-FC}{(R_d)^{m_e}}\right)\frac{1+\tanh[\xi(FC-FC_{th})]}{2} \quad (2.13)$$

where $e_{hc,cr0}$ is the initial critical void ratio for the pure coarse particles, $e_{hf,cr0}$ is the initial critical void ratio for the pure fines, a_e and ξ are material parameters, m_e is a coefficient ($0 < m_e < 1$).

The slope of the normal compression line (λ) was assumed to be unchanged after erosion. The critical state line with different fines contents could be obtained based on Eqn. (2.13). The variation of the critical state line was then incorporated into the elastoplastic model, which could predict the mechanical behavior of the soils under different fines contents. Soils had different fines contents after the seepage tests, then it was natural to think that Eqn. (2.13) could also be employed to predict the critical state line of soils subjected to seepage flow. Yang *et al*. (2018) treated the hydro-mechanical effects on the soils as a two-step process. Firstly, the porosity and the permeability increased due to the seepage flow. Secondly, the continuing loss of fines increased the void ratio and the critical state line. The mass change model and the modified elastoplastic constitutive model were coupled to investigate the phenomenon of internal erosion and the subsequent variation of mechanical behavior. To simulate the real scale problems, both 2D and 3D dike-on-foundation models were established (Yang *et al*., 2018, 2020). The effects of the leakage cavity size and the hydraulic head difference between the upstream and downstream on the development of the sinkhole were studied.

2.5.4 Constitutive models focusing on the erosion-induced variation of porosity

The erosion process and mechanical failure could affect each other. The migration of the fines could cause an increase in the porosity and the rearrangement of the soils, resulting in a strength decrease for most cases. Meanwhile, the external stress could cause stress concentration, leading to soil damage in a certain location, which in return caused the transportation of fines among the voids formed by coarse particles. Stavropoulou *et al*. (1998)

divided the total stress into two partial stresses for the fluid phase and the solid phase. The equation was constructed as:

$$\sigma_{ij} = {\sigma_{ij}}^{(1)} + {\sigma_{ij}}^{(2)} \tag{2.14}$$

$${\sigma_{ij}}^{(1)} = (1-\phi)\overline{\sigma_{ij}} \quad , \quad {\sigma_{ij}}^{(2)} = -\phi p^{w}\delta_{ij} \tag{2.15}$$

where σ_{ij} is the total stress, ${\sigma_{ij}}^{(1)}$ is the partial stress of the solid part, ${\sigma_{ij}}^{(2)}$ is the partial stress of the fluid part, ϕ is the porosity, $\overline{\sigma_{ij}}$ is the stress related to the strain, δ_{ij} is the Kronecker symbol. The cohesion decreased with the increase of porosity. Through the numerical simulations based on proposed equations, the erosion-induced deformation and failure near the wellbore were analyzed.

The erosion-induced porosity (ϕ_{er}) was proposed as an internal variable, which was regarded as the irreversible strain (Rousseau Q. *et al.*, 2018, 2020). In this case, the hardening law of the pre-consolidation pressure (p_c) was established in terms of ϕ_{er}. The predictive equation of porosity-dependent friction angle at critical state was also proposed, varying from the maximum friction angle to the minimum friction angle with the increase of ϕ_{er}. The extended Sinfonietta-Classica constitutive model considering the variation of ϕ_{er} could reproduce the strength reduction and the volumetric strain variation of the internally eroded soils observed from the experimental results (Nova, 1989).

2.6 Summary

Study on the internal erosion mainly focuses on four aspects, i.e., the initiation of internal erosion, the internal erosion process, the variation of mechanical behavior for the eroded soils, and the constitutive model considering internal erosion. Normally, the initiation of the erosion is thought to be difficult under the higher confining pressure. However, a special situation exists that the higher confining pressure could cause the collapse of the arch and a smaller hydraulic gradient is required for the initiation of the erosion. To quantify the internal erosion process, the equation expressing the fines considering initial fines content and

hydraulic gradient has been proposed. However, other factors (e.g., confining pressure, flow velocity) may also affect the internal erosion process, which needs to be considered in the predictive equation of fines. The modifications of the constitutive model for the eroded soils are mainly from the aspects of the critical state line, friction angle of shearing at the critical state line. Internal erosion is also thought to change the size of the yield surface, which should be considered in the modification of the constitutive model. The simulated results from these modified constitutive models are seldom compared with the experimental results. Besides, computation considering both the seepage tests and the subsequent triaxial shearing is quite limited.

[This page intentionally left blank]

CHAPTER 3

QUANTIFICATION OF SEEPAGE-INDUCED INTERNAL EROSION

3.1 Introduction

Many researchers have conducted seepage tests on unstable soils to investigate the changes in the soil properties. At the same time, some also study the effects of factors (i.e., initial fines content, hydraulic gradient, grain size, and flow direction) on the transportation of fines. Besides these experimental studies, the predictive equation of the fines content after erosion considering the initial fines content and the hydraulic gradient has been proposed. However, the limited study focuses on the effect of the confining pressure on the particle transportation. At the same time, few researchers quantify the effect of the cumulative fines loss on the erosion-induced volume change.

To understand the evolution process of the soils in detail, typical seepage tests under different conditions are firstly recalled in this chapter. The erosion-induced variations of basic properties such as the particle size distribution, the fines content, and the void ratio are analyzed under different conditions. Moreover, the heterogeneity of the eroded soils along the flow direction is also described. Secondly, the predictive equation of the fines content considering the effects of the initial fines content, the flow velocity, and the confining pressure is proposed. Besides, the predictive equation of erosion-induced volumetric strain is proposed based on the experimental results. Finally, post-erosion void ratios, estimated based on the erosion-induced volumetric strain and the cumulative fines loss, are compared with those from experimental results.

3.2 Experimental investigations

3.2.1 Seepage tests of loose sand under different confining pressures

Ke and Takahashi (2014a) conducted seepage tests and drained triaxial tests on loose gap-graded soils successively. Generally, the definition of dense or loose sand depends on the relative density. However, the maximum and minimum void ratios cannot obtain for most cases selected in this study. The sand, whose deviatoric stress reaches the peak strength and then decreases (showing the softening trend) under the drained condition, is defined as the dense sand. The sand, whose deviatoric stress increases gradually and reaches the critical state (showing the hardening trend) under the drained condition, is defined as the loose sand (Craig, 2004). The silica Nos. 3 and 8 sands, functioning as coarse particles and fines respectively, were washed to remove the impurities. The properties of silica sand used in the experiment are summarized in Table 3.1. The cylinder-shaped specimens were prepared by the mixture of silica No.3 and No.8 sands with the moist tamping method (Ladd, 1978). The grain size of silica No.8 sand was smaller than 1 mm and the grain size of silica No.3 was found to be larger than 1 mm. Specimens had initial fines contents of 15%, 25%, and 35% in the mass ratio of fines to initial total soils. As the threshold fines content of the mixtures, obtained from the relation of the maximum/minimum void ratio and different fines contents (Fig. 3.1), was around 35%, the specimens were categorized as coarse particles dominated soils (Yang *et al.*, 2005; Ke, 2015; Wang *et al.*, 2018).

Table 3.1 Property of silica sand for Ke and Takahashi (2014a)

Property	Silica No.3	Silica No.8
Specific gravity	2.63	2.63
Median grain size (d_{50}, mm)	1.72	0.16
Effective grain size (d_{10}, mm)	1.37	0.087
Maximum void ratio	1.009	1.333
Minimum void ratio	0.697	0.703

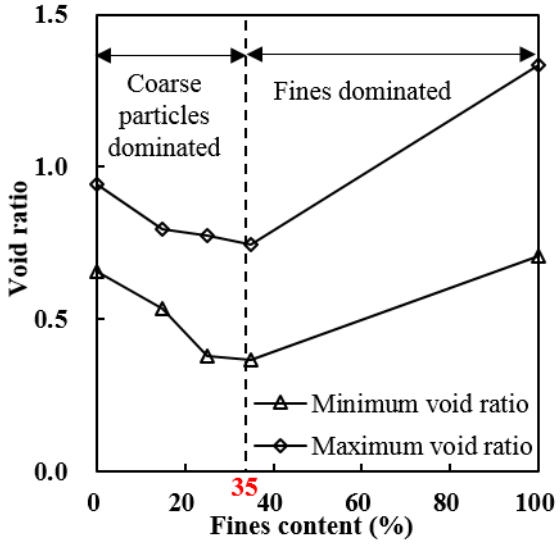

Figure 3.1 Maximum and minimum void ratios along with fines contents (Data from Ke, 2015)

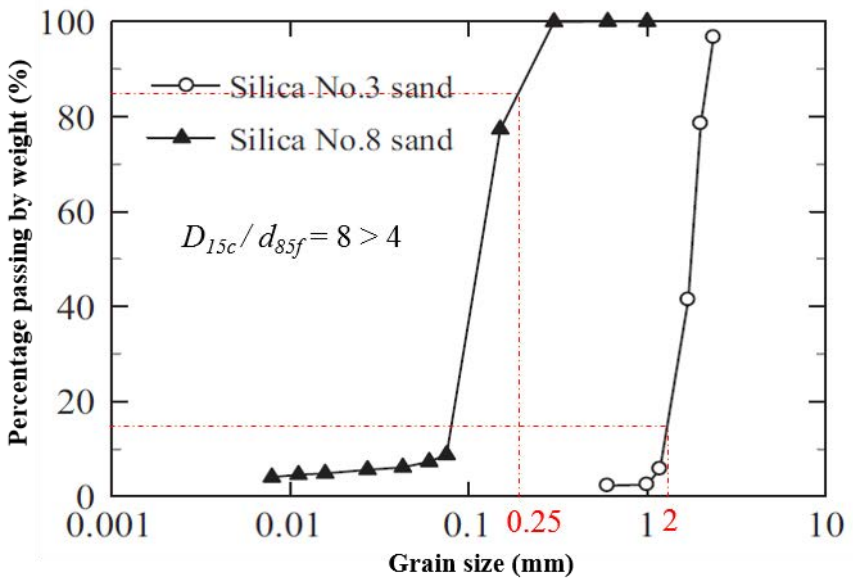

Figure 3.2 Grading curves of both silica No.3 and No.8 sands (after Ke and Takahashi, 2014a)

The mixture specimens were classified as internally unstable soils based on criteria proposed by previous researchers (when $D_{15c}/d_{85f} > 4$ or H/F < 1, the specimen is considered to be internally unstable, Fig. 3.2, Kezdi, 1979; Kenney and Lau, 1985). After the specimens were put in the triaxial cell, they were saturated and consolidated. Then different confining pressures were applied to the specimens, 50 kPa, 100 kPa, and 200 kPa, respectively (Ke and Takahashi, 2014a, 2015). As the bottom mesh has 1mm openings, fines could flow

through this mesh by the hydraulic force.

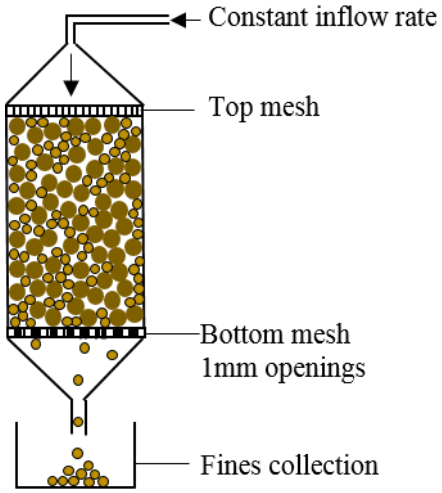

Figure 3.3 Schematic diagram of downward seepage test

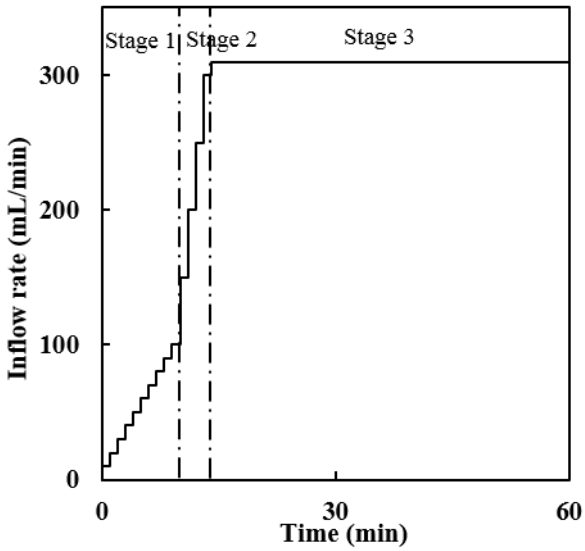

Figure 3.4 Inflow rate for seepage test (after Ke and Takahashi, 2014a)

Figure 3.3 briefly shows the apparatus assembly of seepage tests. The downward flow was applied to the specimen with an increasing inflow rate from zero to 310 mL/min (5.17×10^{-6} m^3/s). The whole inflow process was divided into three stages as shown in Fig. 3.4 to avoid the collapse of structures formed by coarse particles (Fannin, 2015). In Stage 1, the flow rate increment was 10 (mL/min)/min for 10 minutes until the flow rate reached 100 mL/min. In Stage 2, the flow rate increment was 50 (mL/min)/min for 4 minutes until the flow rate reached 300 mL/min. Finally, in Stage 3, the flow rate was increased to the target value (310

mL/min), and the flow rate was kept constant for at least 3 hours. During the seepage tests, downward discharge effluent along with fines flowed into the eroded soil collection unit through a pipe. The cumulative fines that remained in the light tray were continuously measured by a highly sensitive waterproofed load cell. Axial and lateral strains could also be measured. When no visible fines and effluent could be observed from the collection unit, the seepage tests were terminated.

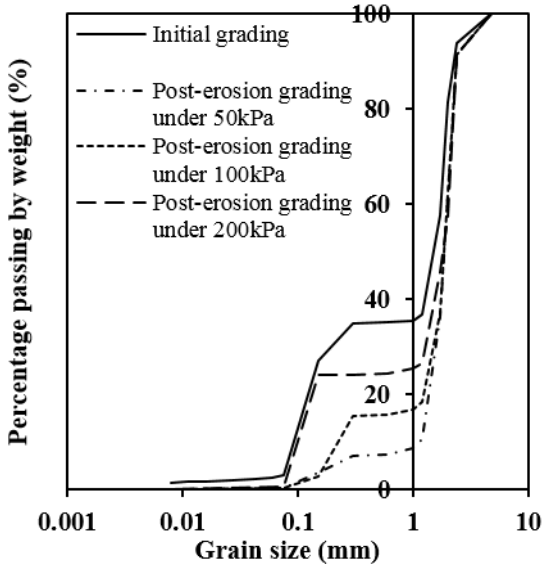

Figure 3.5 Particle size distribution curves before and after erosion under different confining pressures (Experimental data from Ke, 2015)

Figure 3.5 illustrates post-erosion grading curves under different confining pressures (i.e., 50 kPa, 100 kPa, 200 kPa). Comparing with the initial grading curve, the post- erosion grading curves shift downward clearly in the fines fraction. The amount of this shifting of grading curves depends on the applied confining pressure. The uniformity coefficient and curvature coefficient for the uneroded and eroded specimens are calculated and summarized in Table 3.2. Based on the criteria (when both $C_u \geqslant 6$, $1 < C_c < 3$ are met, the sand is regarded as well graded sand; otherwise, it is regarded as poorly graded sand), both uneroded sand and eroded sand are classified as poorly graded sand. Both the curvature coefficient and uniformity coefficient varied dramatically due to erosion.

Table 3.2 Change in material properties and other parameters after erosion for the soils with different confining pressures for Ke and Takahashi (2014a)

Specimens	d_{10}	d_{30}	d_{60}	C_u	C_c	ΔFC	FC_∞	e_c	e_{er}	ε_v^{er}
35N-50	0.10	0.21	1.73	17.3	0.25	0%	35%	0.55	0.55	0
35E-50	1.15	1.60	1.88	1.63	1.18	29.25%	8.1%	0.55	1.01	3.91%
35E-100	0.21	1.55	1.88	8.95	6.09	23.04%	15.5%	0.56	0.92	3.65%
35E-200	0.10	1.28	2.02	20.2	8.11	13.81%	24.6%	0.54	0.77	2.82%

Note: C_u represents the uniformity coefficient; C_c represents the curvature coefficient; ΔFC represents the cumulative fines loss (mass ratio of eroded fines to initial total soils); FC_∞ denotes the final fines content, which indicates the initial fines content for the uneroded soils and the post-erosion fines content for the eroded soils; e_c means the void ratio after consolidation; e_{er} means the post-erosion void ratio; ε_v^{er} indicates the erosion-induced volumetric strain.

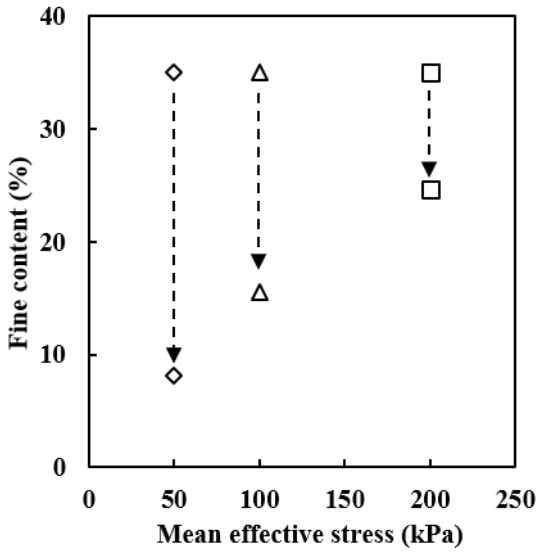

Figure 3.6 Erosion-induced change in fines content for different initial mean effective stresses (Experimental data from Ke and Takahashi, 2014a)

Figure 3.6 presents erosion-induced changes in fines content for the different initial confining pressures. For 50 kPa initial confining pressure, the specimen experienced the largest fines content loss, and the fines content decreased from 35% to 8.1%. With the higher confining pressure, the loss of fines was less compared to the case under 50 kPa initial confining pressure. Bendahmane *et al.* (2008) observed that the increase in the confining pressure would result in a decrease in the maximum erosion rate. The higher initial mean

effective stress may have caused tighter interlocking between particles, which made it more difficult for small particles to migrate under seepage flow. The same tendency can be seen in the tests reported here. Before the seepage test, the void ratio was almost the same for all the cases (cf. Fig. 3.7). The erosion made the void ratio larger, especially in the case under 50 kPa initial confining pressure, and the void ratio increased from 0.55 to 1.01. After the seepage tests, the measured volumetric strain ranged from 2.5% to 4%.

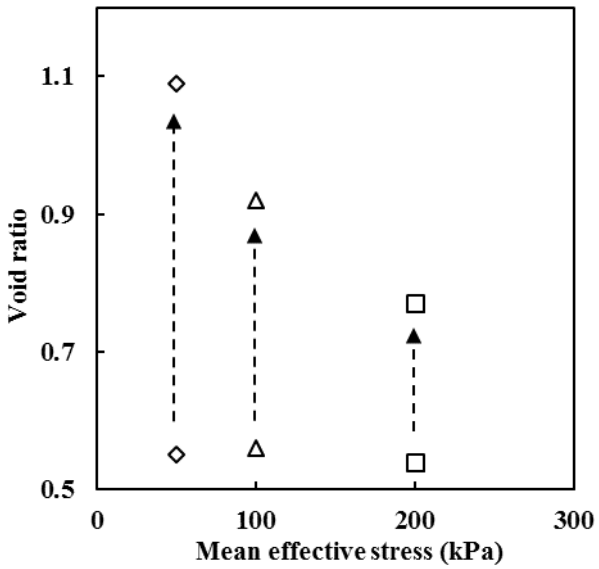

Figure 3.7 Erosion-induced change of void ratio for different initial mean effective stresses (Experimental data from Ke and Takahashi, 2014a)

3.2.2 Seepage tests of loose sand with different initial fines contents

The specimens with 15%, 25%, and 35% initial fines contents were also subjected to seepage flow under the 50 kPa confining pressure (Ke and Takahashi, 2014a). Figure 3.8 shows the post-erosion grading curves of the soils with different initial fines contents. Comparing with the initial grading curve, post-erosion grading curves also shift downward clearly in the fines fraction. The specimen with 35% initial fines content has the largest shift, while those with 15% and 25% initial fines contents have a similar amount of shift. The curvature coefficient and uniformity coefficient and other material properties for specimens with erosion are calculated and summarized in Table 3.3. The uniformity coefficient decreased while the curvature coefficient increased after internal erosion.

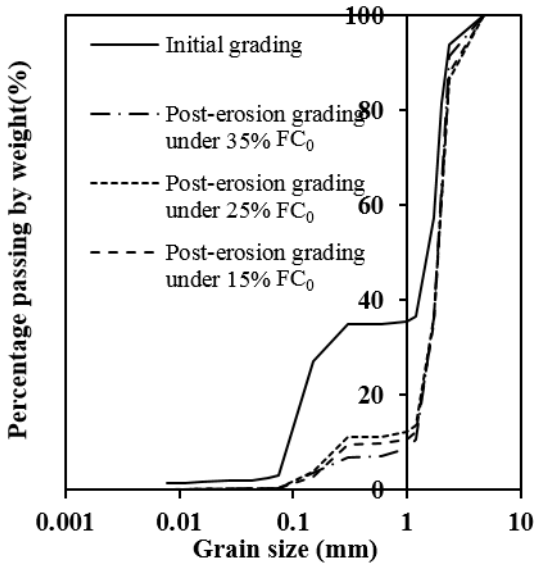

Figure 3.8 Particle size distribution curves before and after erosion under different initial fines contents (FC_0 denotes the initial fines content; Experimental data from Ke and Takahashi, 2014a)

Table 3.3 Details of material properties of the silica mixtures with different initial fines contents before and after erosion for Ke and Takahashi (2014a)

Specimens	d_{10}	d_{30}	d_{60}	C_u	C_c	ΔFC	FC_∞	e_c	e_{er}	ε_v^{er}
35N-50	0.10	0.21	1.73	17.3	0.25	0%	35%	0.55	0.55	0
35E-50	1.15	1.60	1.88	1.63	1.18	29.2%	8.1%	0.55	1.01	3.91%
25E-50	0.28	1.56	2.01	7.29	4.37	15.1%	11.6%	0.57	0.81	0.8%
15E-50	0.69	1.58	2.01	2.93	1.81	4.9%	10.6%	0.68	0.78	0.01%

Figure 3.9 presents the change of fines content for specimens with different initial fines contents under the same confining pressure (50 kPa). The specimen with larger initial fines content has a relatively larger change of the fines content. Ke and Takahashi (2012) also found that the soils with larger initial fines content had a larger fines content loss. The possible explanation may be that a large number of fines do not participate in the stress transmission in the soils with larger initial fines content and are easier to be washed out under seepage flow.

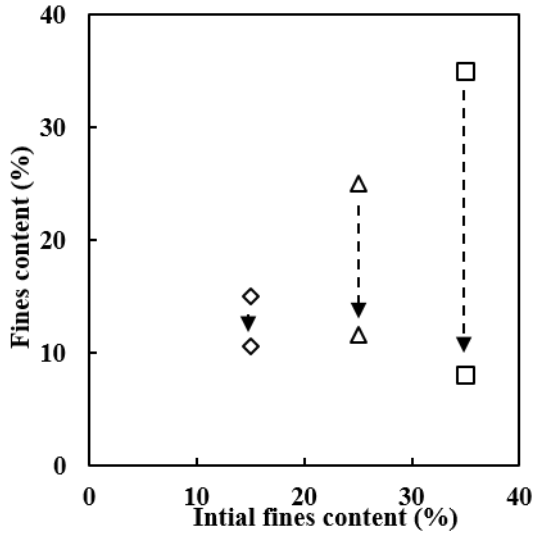

Figure 3.9 Erosion-induced change of fines content for different initial fines contents (Experimental data from Ke and Takahashi, 2014a)

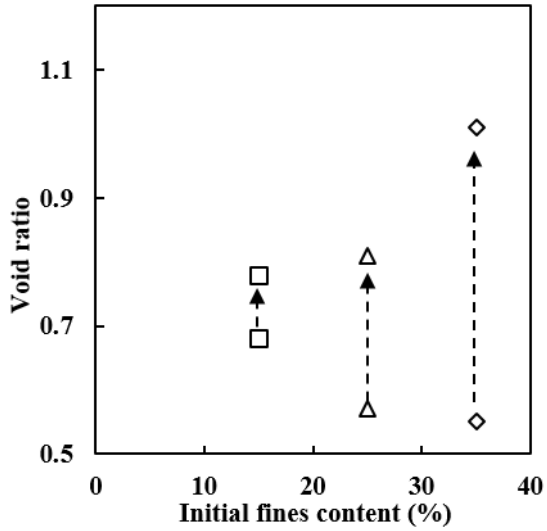

Figure 3.10 Erosion-induced change of void ratio for different initial fines contents (Experimental data from Ke and Takahashi, 2014a)

Figure 3.10 describes the variation of the void ratio for soils under different initial fines contents. The initial void ratios of the soils with different initial fines contents were different; the specimen with the smaller initial fines content had a larger initial void ratio but the relative density was the same. The soils were coarse particle-dominated, in which fines filled the voids formed by coarse particles. The void ratio increased after the seepage tests. The specimen with 35% initial fines content experienced the most loss of fines, resulting in the largest increase of the void ratio after erosion. The soils with 15% initial fines content had

the lowest cumulative fines loss (i.e., 4.9%), whose volume was almost unchanged after erosion.

3.2.3 Seepage tests of dense soils with different cumulative fines losses

Chen *et al.* (2016) investigated the variations of the material properties of the dense soils subjected to seepage flow. The test apparatus contained four systems, i.e., the triaxial system, the pressurized water supply system, the soil collection system, and the water collection system (Chang and Zhang, 2011). The table salt functioning as a part of fines was added into the soils during the sample preparation. The 50 kPa confining pressure was applied to the specimen. In the beginning, the carbon dioxide was put into the specimen to increase the saturation degree. Then, the pressurized water supply system supplied the seepage water with a relatively low hydraulic gradient for around 36 hours. When all the salt was dissolved through the seepage water, the seepage test was terminated. Two groups of dense soils were studied: Group A, the soils with 20% initial fines content had cumulative fines losses 0%, 5%, and 15% after the salt dissolution; Group B, the soils with 35% initial fines content had cumulative fines losses 0%, 10% and 30% after the salt dissolution. The material compositions and physical properties of the dense soils are summarized in Table 3.4. As the C_c of the Group B soil is smaller than one, the Group B soil is classified as poorly graded soils.

Table 3.4 Material compositions and physical properties of soils with different initial fines contents subjected to internal erosion for Chen *et al.* (2016)

Samples	Coarse	Fines	FC_0	C_u	C_c	Types
20N-50	Completely decomposed granite	Leighton Buzzard sand	20%	-	-	Group A
35N-50	Completely decomposed granite	Leighton Buzzard sand	35%	16.7	0.09	Group B

Note: "-" indicates that the information is not given.

The change of material properties of two groups of dense soils subjected to seepage water was studied by Chen *et al.* (2016). The material properties of soils before and after erosion are summarized in Table 3.5. The larger the cumulative fines loss, the larger the erosion-induced volumetric strain. The specimen B3 had a 30% cumulative fines loss, whose erosion-induced volumetric strain was quite large. As the salt accounts for 30% of the total mass in specimen B3 during preparation, much salt takes part in the force transmission. After the salt dissolution, the original soil structure collapses. The rearrangement of soils can cause a decrease in volume.

Table 3.5 Details of material properties of the dense soils before and after erosion for Chen *et al.* (2016)

Specimens	FC_0	ΔFC	FC_∞	e_c	e_{er}	ε_v^{er}
A1	20%	0%	20%	0.461	0.461	0%
A2	20%	5%	15.8%	0.461	0.514	1.51%
A3	20%	15%	5.9%	0.461	0.644	4.32%
B1	35%	0%	35%	0.377	0.377	0%
B2	35%	10%	27.8%	0.377	0.476	3.58%
B3	35%	30%	7.1%	0.377	0.593	19.06%

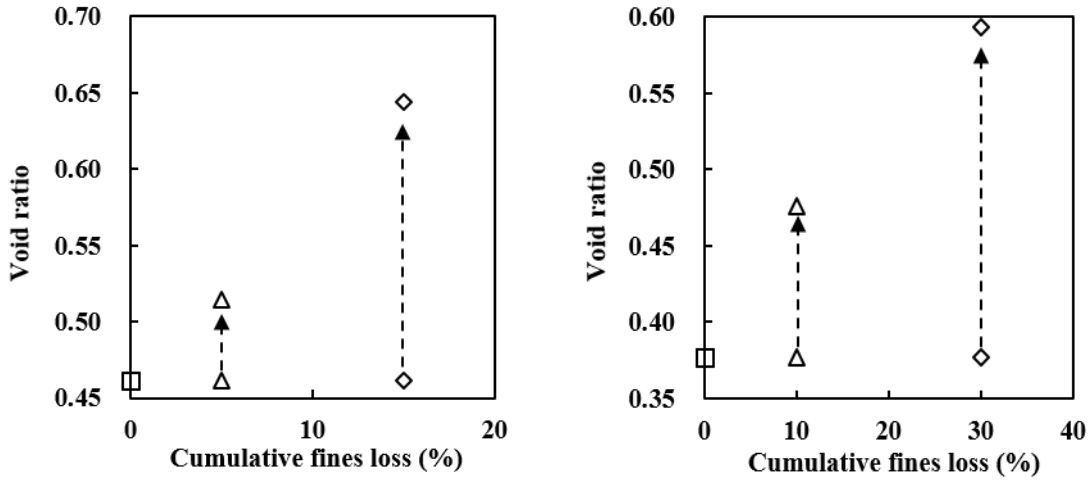

(a) Group A soils (b) Group B soils

Figure 3.11 Erosion-induced change of void ratio for different cumulative fines losses (Experimental data from Chen *et al.*, 2016)

Since the amount of the cumulative fines loss was designated (the amount of salt in the specimen), we only studied the variations of voids ratio after erosion. The initial void ratios of the specimens without erosion were the same. Figure 3.11 indicates that the void ratios for both Groups A and B soils increase with the cumulative fines loss. The specimen with the larger cumulative fines loss had a larger increase in the void ratio.

3.2.4 Seepage-induced grading heterogeneity of the soils

Seepage flow in an upward or downward direction can both cause the heterogeneity of the specimen. Heterogeneity in this study mainly refers to the variations of the grading curve, the fines contents, the void ratio of different layers in the specimen along the seepage direction. Figure 3.12 describes the differences of the grading curves in the different parts of specimens with 35% initial fines content under 50 kPa confining pressure after erosion (Ke and Takahashi, 2014a). The downward seepage water was applied to the specimen, and the specimen was divided into the upper layer and bottom layer. The loss of fines in the upper layer was more than that in the bottom layer, which was in line with that of previous studies (Kenney and Lau, 1985).

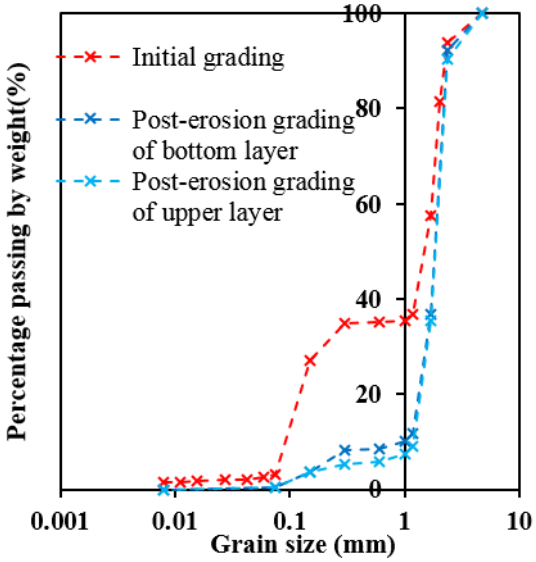

Figure 3.12 Particle size distribution curves of different parts for the specimen after erosion (Experimental data from Ke and Takahashi, 2014a)

Li *et al.* (2020) studied the effects of particle size distribution heterogeneity of soils under

seepage flow. The specimens were prepared by the gap-graded soils with a large value of C_u, whose physical properties were summarized in Table 3.6. Seepage water could pass through the specimens in both upward and downward directions with a constant hydraulic head. The silica 60 G and 5 mm basalt functioned as the fines while the 10mm basalt functioned as the coarse particles. The initial fines content was around 32%, and the coarse particles mainly formed the bearing skeleton. The specimens underwent different amounts of downward seepage water (i.e., 8×10^{-3} m^3, 24×10^{-3} m^3, and 48×10^{-3} m^3) under 50 kPa confining pressure. After the seepage tests, the fines contents of different parts of the specimen along the flow direction were different, which resulted in heterogeneity.

Table 3.6 Materials and properties of soils with 32% initial fines content for Li *et al.* (2020)

Sample	Coarse	Fines	d_{60} (mm)	d_{30} (mm)	d_{10} (mm)	FC_0	C_u	C_c	Particle description
32N-50	10mm Basalt	Silica 60G, 5mm Basalt	6.9	0.97	0.02	32%	284.6	5.6	Sub-angular

Note: d_X indicates grain size when X % of mass passing is finer in the grading curve.

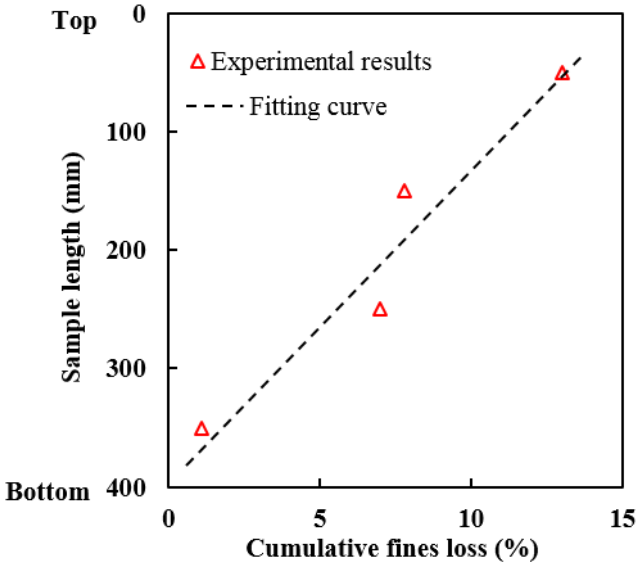

Figure 3.13 Erosion-induced change of fines content for different sample lengths (Experimental data from Li *et al.*, 2020)

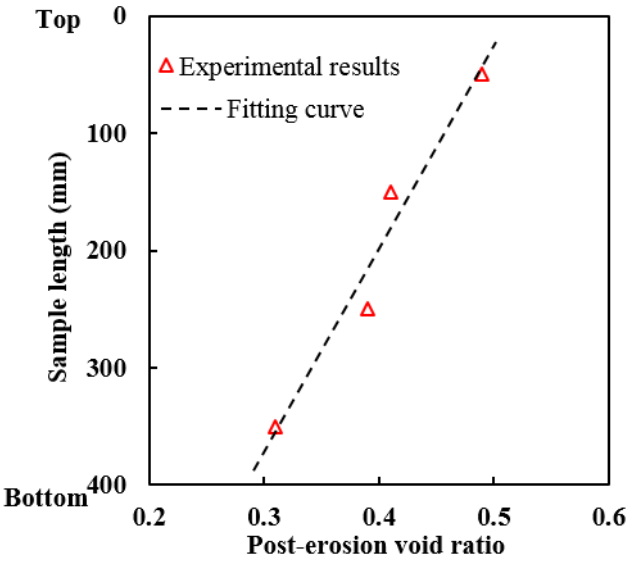

Figure 3.14 Erosion-induced change of post-erosion void ratio for different sample lengths (Experimental data from Li *et al.*, 2020)

The specimen under 24×10^{-3} m^3 downward seepage water was considered to study the heterogeneity of the eroded soils in more detail. The eroded specimen was divided into four parts along the flow direction. The midpoint of each part was assumed to represent the whole layer. Figure 3.13 shows that the top layer has a larger cumulative fines loss compared with the bottom layer. The cumulative fines losses of the middle two layers were almost the same. The transportation and re-deposition of fines happened simultaneously during erosion in the middle two layers. The top layer underwent the most fines transportation and the fewest fines re-deposition, while the bottom layer had the opposite phenomenon. The change of post-erosion void ratio along the specimen length is illustrated in Fig 3.14, which shows that the void ratio of the top layer has the largest increase as a result of the largest loss of fines in this layer. The post-erosion void ratio decreased linearly with the distance from the top of the specimen. Hu *et al.* (2019) simulated the specimens under the upward seepage flow through the CFD-DEM simulation. They divided the specimen into three parts (top part, middle part, and bottom part). The top part also had the largest loss of fines and the highest increase of void ratio, while the bottom part enjoyed the least loss of fines and the lowest increase of void ratio. Under both downward and upward directions of seepage flow, the top layer has the largest loss of fines. Thus, another factor (particle gravity) is thought to affect the

variations of loss of fines and void ratio in different layers. As the particle size distribution curve of the soils has an important effect on the mechanical behavior of the eroded soils (Muir Wood *et al.*, 2010), the heterogeneity of particle size distributions for different layers also affects the mechanical behavior of the eroded soils.

3.3 Quantification of the internal erosion process

3.3.1 Predictive equation of the fines content during the erosion process

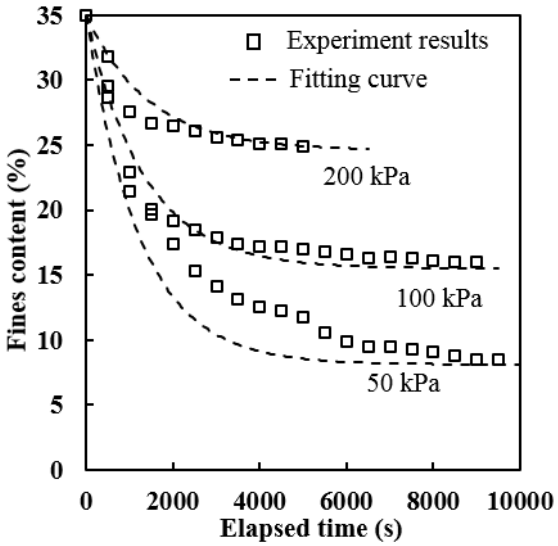

Figure 3.15 Fines contents along with time under different confining pressures Experimental data from Ke and Takahashi, 2014a)

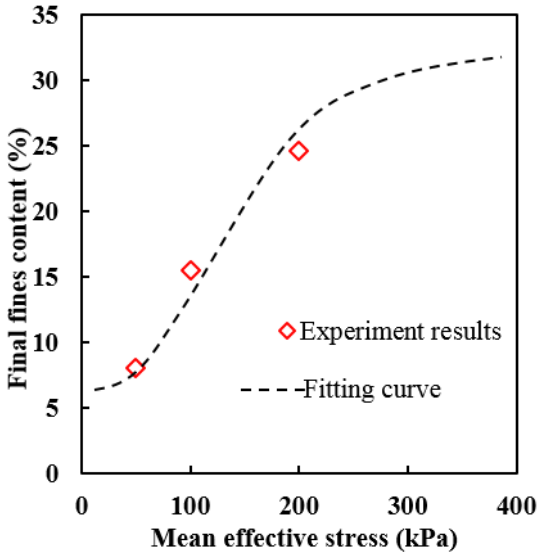

Figure 3.16 Change of final fines contents under different confining pressures (Experimental data from Ke and Takahashi, 2014a)

When the seepage flow was applied to the unstable soils, the variation of fines contents under different confining pressures against elapsed time could be obtained. It took some time for the initiation of erosion by seepage flow. However, in the following evaluation, the elapsed time before erosion was ignored for simplification. As depicted in Fig. 3.15, the fines contents decrease with the continuing inflow and tend to converge to certain values (Ke and Takahashi, 2014a). It is also noticeable from this figure that a specimen under higher confining pressure has less loss of fines. Figure. 3.16 shows that final fines content is a monotonic increase function of the mean effective stress (soils with 35% initial fines content under different confining pressures 50 kPa, 100 kPa, and 200 kPa). The fines will be difficult to be eroded when the confining pressure is high. Fines are expected to be eroded mostly when the confining pressure is close to zero, under which there is no external constraining force preventing fines from transporting.

Figure 3.17a shows the change of fines content with different initial fines contents (15%, 25%, 35%) under 50 kPa confining pressure (Ke and Takahashi, 2014a). The fines content decreases with the elapsed time and finally tended to converge to a certain value. The erosion rate depends on the initial fines content. The specimen with larger initial fines content has a larger erosion rate.

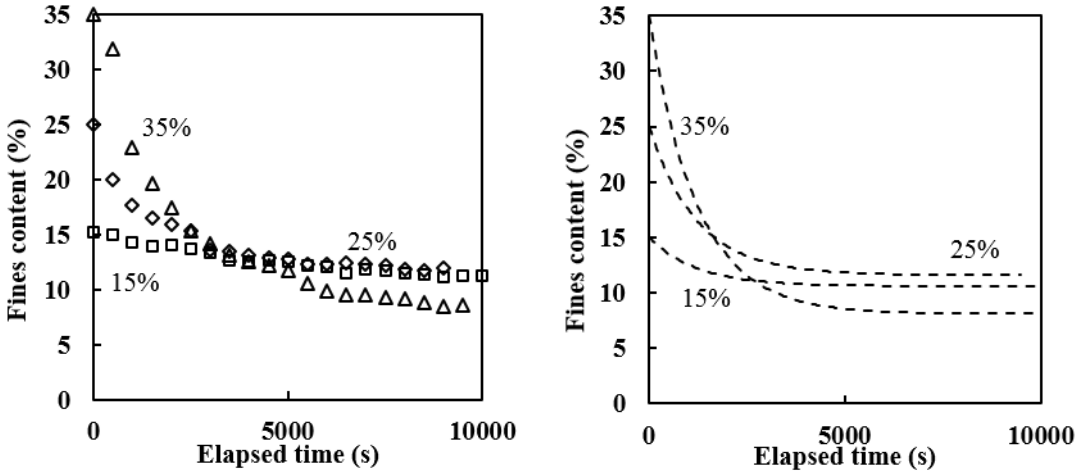

(a) Experimental results (b) Prediction curves

Figure 3.17 Fines content against elapsed time with different initial fines contents (15%, 25%, 35%) under 50 kPa confining pressure (Data from Ke and Takahashi, 2014a)

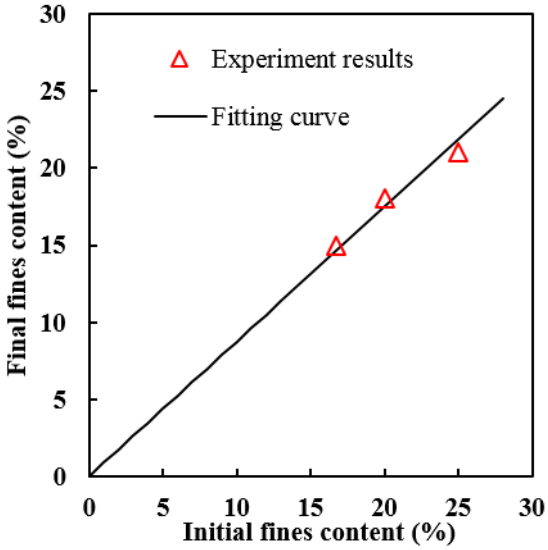

(a) Specimens subjected to upward seepage flow with different initial fines contents (16.7%, 20%, and 25%, Experimental data from Ke and Takahashi, 2012)

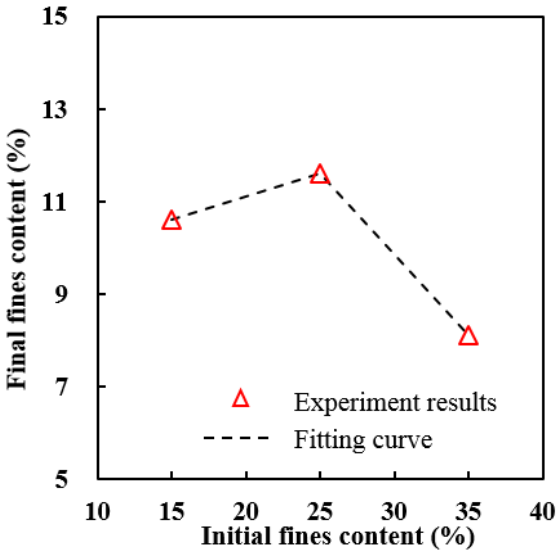

(b) Specimens subjected to downward seepage flow with different initial fines contents (15%, 25%, and 35%, Experimental data from Ke and Takahashi, 2014a)

Figure 3.18 Change of final fines contents with different initial fines contents

Tomlinson and Vaid (2000) also found that confining pressure made a difference in the final fines content; meanwhile, both flow velocity and initial fines content could cause the change of finial fines content. It is believed that the specimen with the larger initial fines content has the larger final fines content after erosion (Sterpi, 2003). A series of the soils subjected to the upward seepage flow under very low confining pressure with 16.7%, 20%, and 25% initial fines contents were conducted by Ke and Takahashi (2012). Figure 3.18a shows that

the final fines content has a positive linear relationship with the initial fines content for the eroded soils. However, no clear relation between the final fines content and the initial fines content can be found in another series of the soils that underwent the downward seepage flow with 15%, 25%, and 35% initial fines contents under 50kPa confining pressure (Fig. 3.18b, Ke and Takahashi, 2014a).

Cividini *et al.* (2009) regarded the decrease of non-dimensional density of fines as the loss of fines. The long-term non-dimensional density of fines was a function of the initial non-dimensional density of fines and hydraulic gradient. The change of fines can be expressed as the variation of the fines content, the equation of the final fines content considering the effect of initial fines content and the hydraulic gradient is proposed:

$$FC_{\infty}(FC_0, i) = FC_0 \cdot [(1 - d_1)exp(-a_1 \cdot i^{b_1}) + d_1] \tag{3.1}$$

where a_1, b_1, and d_1 are fitting parameters. From the fitting of the experimental data, a_1, b_1, and d_1 are taken as 1.1, 2.2, and 0.05 for the soil with 23% initial fines content under different hydraulic gradients (Fig. 3.19). With the increase of hydraulic gradient, the final fines content decreases rapidly firstly, and then decreases slowly, finally tends to be constant (close to zero).

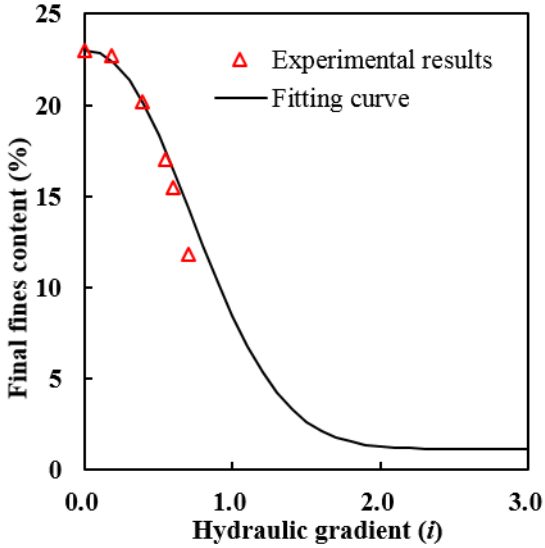

Figure 3.19 Change of final fines content with different hydraulic gradients (Experimental data from Sterpi, 2003)

However, the effect of confining pressure has not been considered. In this subsection, the effect of the hydraulic gradient is replaced by the effect of flow velocity. Also, the effect of confining pressure on the variation of fines content is studied. In the formulation, the flow velocity is normalized by reference velocity, and confining pressure is normalized by reference confining pressure, where reference velocity v_{ref} equals to 0.0001 m/s and reference confining pressure p_{ref} equals to 1 kPa. Final fines content $FC_\infty(FC_0, v_{nor}, p_{nor})$ is constructed as a function of initial fines content FC_0, normalized flow velocity v_{nor}, and normalized confining pressure p_{nor}.

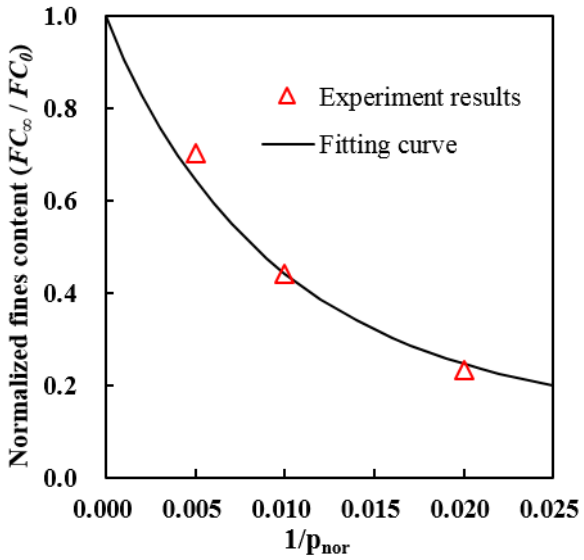

Figure 3.20 Normalized finial fines content along the reciprocal of normalized confining pressure (Experimental data from Ke and Takahashi, 2014a)

Experimental data in Fig. 3.20 show the change of the normalized final fines content FC_∞/FC_0 along with the parameter $1/p_{nor}$ for specimens with 35% initial fines content and different confining pressures (50 kPa, 100 kPa, and 200 kPa). As we can see, the normalized final fines content decreases with the increase of $1/p_{nor}$, and the normalized final fines content equals one when $1/p_{nor}$ converges towards zero (which means the confining pressure is very high). At the same time, the final fines content increases with the initial fines content (cf. Fig. 3.18a). The equation of the final fines content is proposed:

$$FC_\infty(FC_0, v_{nor}, p_{nor}) = FC_0 \cdot \left[(1-d_1)exp\left(-a_1 \cdot (v_{nor})^{b_1} \cdot (\frac{1}{p_{nor}})^{c_1}\right) + d_1\right] \quad (3.2)$$

where a_1, b_1, c_1, and d_1 are fitting parameters. From the fitting of the experimental data (Fig. 3.20), a_1, b_1, c_1, and d_1 are taken as 6.5, 0.95, 0.95, and 0.12 for the soils with 35% initial fines contents under different confining pressures (50 kPa, 100 kPa, and 200 kPa).

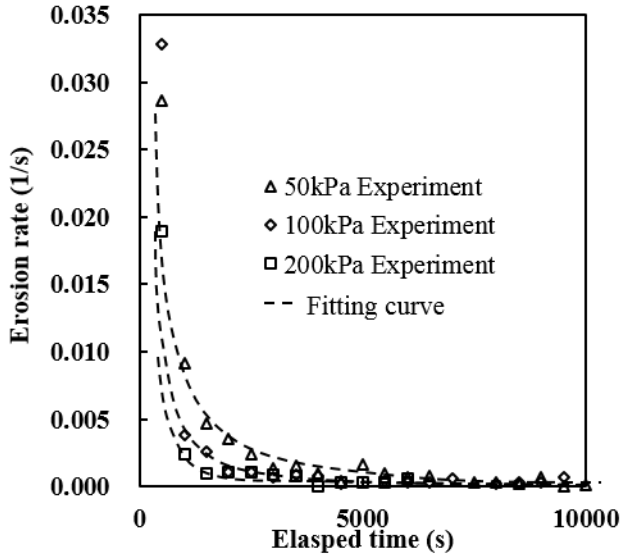

Figure 3.21 Trends of erosion rate with elapsed time under different confining pressures (Experimental data from Ke and Takahashi, 2014a)

Figure 3.21 shows the trend of erosion rate along elapsed time for the specimens under different confining pressures. The erosion rate denotes the fines content change per unit time. The erosion rate follows the conditions: (a) for all cases with different confining pressures, it decreases monotonically with time and finally tends to zero; and (b) it decreases with the increase of confining pressure. Previous research indicated that the erosion rate also depended on the root of the hydraulic gradient (Cividini *et al.*, 2009). The change of hydraulic permeability was small after the onset of internal erosion, which was assumed to be unchanged during erosion for simplification. And then the hydraulic gradient could be replaced by flow velocity (Bowman and Hunter, 2017). Consequently, the following equation of current fines content $FC(FC_0, v_{nor}, p_{nor}, t)$ is proposed:

$$\frac{\partial FC(FC_0, v_{nor}, p_{nor}, t)}{\partial t} = -e_1 \cdot (v_{nor})^{0.5} \cdot \left(\frac{1}{p_{nor}}\right)^{e_2} \cdot (FC - FC_\infty) \tag{3.3}$$

Based on this, the function of FC can be obtained by integration:

$$FC = (FC_0 - FC_\infty) \cdot \exp\left[-e_1 \cdot (v_{nor})^{0.5} \cdot \left(\frac{1}{p_{nor}}\right)^{e_2} \cdot t\right] + FC_\infty \quad (3.4)$$

where e_1=0.00035 and e_2=0.12, the predictive equation of Eqn. (3.4) can capture the features of the experimental results under different confining pressures (cf. Fig. 3.15). At the same time, if we know the final fines content of the specimens with 15%, 25%, and 35% initial fines contents under 50 kPa confining pressure, Eqn. (3.4) can also estimate the variation of the fines content for the soils with different initial fines contents during internal erosion well (cf. Fig. 3.17b). Eqns (3.2) and (3.4), considering the effect of flow velocity and confining pressure, are suitable for the prediction of the fines content of the eroded soils obtained through the loss of fines under the seepage flow, but not suitable for the prediction of the fines content of the eroded soils obtained through the salt dissolution.

3.2.2 Estimation of the erosion-induced volumetric strain

The erosion-induced change in volume of the soils under seepage flow was found in some experiments (Xiao and Shwiyhat 2012; Ke and Takahashi, 2014a, 2015; Chen *et al.*, 2016). However, no volume change also happened when soils were subjected to the seepage flow (Fannin and Slangen, 2014; Li *et al.*, 2020). The possible explanation may be that the soils are constituted by two parts: the stable skeleton (mainly formed by coarse particles) and the migratable particles that do not contribute to the stress transmission (mainly fines). When the cumulative fines loss is small, or the skeleton is competent enough, the volume may be unchanged even the internal erosion occurs due to the seepage flow (suffusion). Contrarily, when the loss of the fines is large, or the skeleton collapses by the large seepage force, the volume may change dramatically (suffosion).

It is important to find the relation between erosion-induced volumetric strain and the cumulative fines loss for the modeling of the internally eroded soil behavior. As the maximum cumulative fines loss exists for any binary mixture under seepage flow and both coarse particles and fines are nearly incompressible, the maximum erosion-induced

volumetric strain $\varepsilon_{v\max}^{er}$ may also exist for the soils subjected to the seepage flow.

In this subsection, the variation of the erosion-induced volumetric strain from two cases is investigated. For the loose soils, the experiments conducted by Ke and Takahashi (2014a) were analyzed. Chen *et al.* (2016) investigated the variations of the material properties of the dense soils subjected to seepage flow. Generally, the erosion-induced volumetric strain of dense soils is expected to be smaller than that of the loose soils. However, the erosion-induced volumetric strain of dense soils is much larger than that of the loose soils in this study (Fig. 3.21b). The explanation is that the salt is used to mimic the erosion of the dense soils and the salt dissolution can also cause a decrease in the soil volume. Here, it is assumed that depending on the cumulative fines loss ΔFC, the erosion-induced volumetric strain varies from 0 to the maximum volumetric strain $\varepsilon_{v\max}^{er}$. The equation of the erosion-induced volumetric strain is proposed as:

$$\varepsilon_v^{er} = \frac{1}{2}\varepsilon_{v\max}^{er}\left(1+\tanh\left(\frac{1}{l}(\Delta FC - A_2)\right)\right) \tag{3.5}$$

where A_2 is the threshold, l is a parameter deciding the smoothness of the fitting curve, the curve is much smoother when the value of l is larger (Fig. 3.22a). From the fitting of the experimental data (Fig. 3.22b), $\varepsilon_{v\max}^{er}$, A_2, l are taken as 20%, 19%, and 0.095 for dense soils (Group B, Chen *et al.*, 2016); 4.2%, 16%, and 0.055 for loose soils (Ke and Takahashi, 2014a). The range of the fitting parameter l is suggested to be $0 < l < 0.1$. When $l > 0.1$, it is difficult to predict the phenomenon that volume does not change when the cumulative fines loss is small through Eqn. (3.5). The internal erosion occurs when the soils are unstable, which suggests that Eqn. (3.5) is suitable for the most gap-graded soils and the eroded soils obtained through salt dissolution.

The erosion-induced volumetric strain is also affected by the confining pressure, but this effect is not considered in Eqn. (3.5). From the fitting curve, we can know that the erosion-induced volumetric strain is almost zero when the cumulative fines loss is less than 5% for loose soils. When the cumulative fines loss is more than 25%, the volumetric strain of loose

soils shows almost the greatest value but becomes insensitive to the amount of the loss of fines. The change of volumetric strain for dense soils has a similar trend.

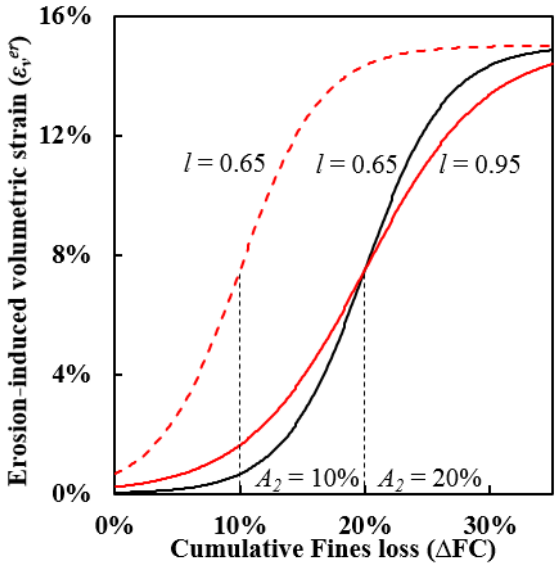

(a) Change of the hyperbolic tangent function with A_2 and l

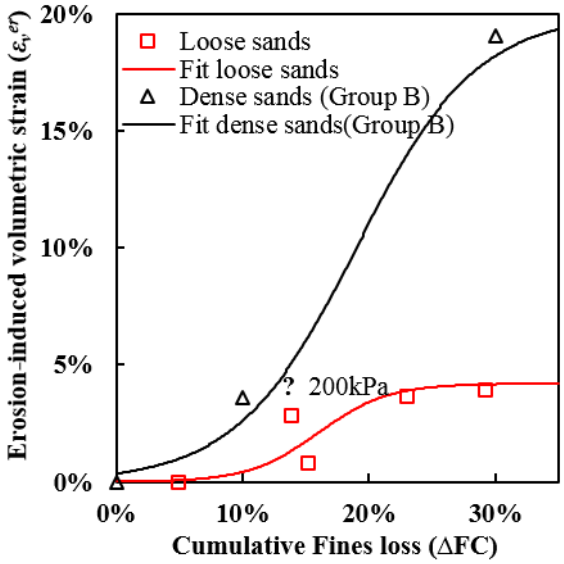

(b)Fitting of erosion-induced volumetric strains of both the loose and dense soils

Figure 3.22 Erosion-induced volumetric strain against cumulative fines loss (Experimental data of loose sand from Ke and Takahashi, 2014a; Experimental data of dense sand from Chen *et al.*, 2016)

Figure 3.23 shows the seepage tests required for the determination of the erosion parameters. The number and type of seepage tests depend on the many conditions (e.g., confining pressure, initial fines content, and flow velocity). When only confining pressures are different, a series of seepage tests under different confining pressures with the same initial

fines contents and constant flow velocity need to be conducted. However, when initial fines contents and flow velocities change, more seepage tests considering the variations of initial fines contents and flow velocity need to be conducted.

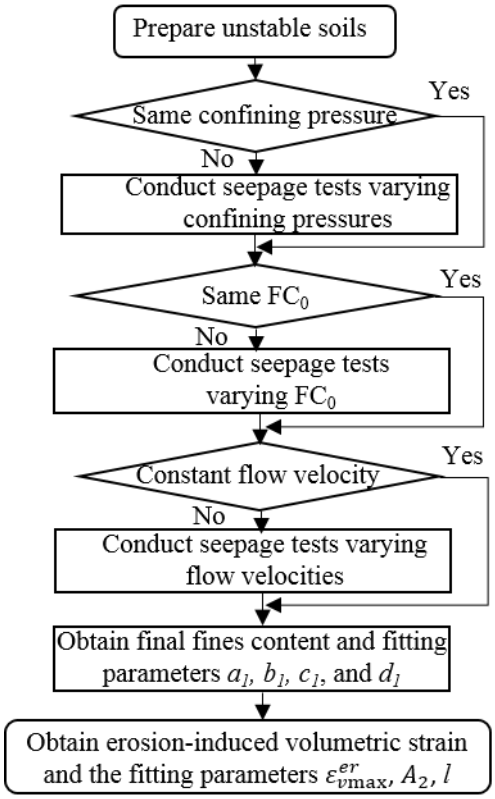

Figure 3.23 Flowchart for determining required seepage tests and erosion parameters

3.2.3 Estimation of the post-erosion void ratio

The void ratio of the specimen increases after the seepage test. Sterpi (2003) divided the total specimen into voids and solid and proposed three hypotheses about the variation of void ratio and volumetric strain after the seepage test: (1) the total volume of the specimen kept constant, which noted that the volumetric strain was zero. Eroded fines could cause the increase of voids and the decrease of the solid; (2) all eroded fines were washed out while the voids did not change, which caused the variation of volumetric strain; (3) the void ratio of the specimen were unchanged with the loss of both the voids and the solid (Fig. 3.24). The specific gravities of both fines and coarse particles are assumed to be the same, and then the percentage by volume of eroded particles can be expressed as the percentage by mass of

eroded particles (ΔV_s=ΔFC).

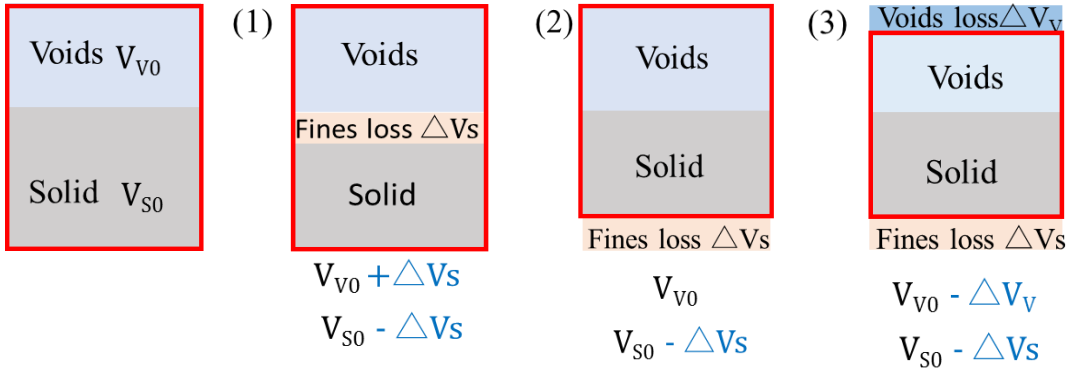

Figure 3.24 Three hypotheses of the change in void ratio and volumetric strain (V_{V0} represents the initial volume of the voids; V_{s0} denotes the initial volume of the solid; ΔV_s means the volume change induced by the loss of fines; ΔV_V means the volume change induced by the loss of voids)

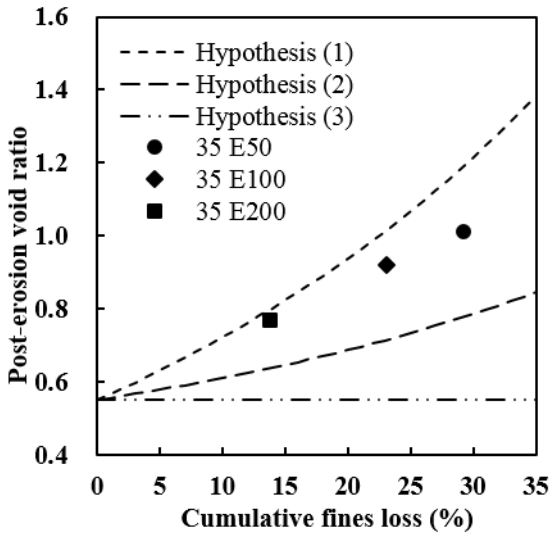

Figure 3.25 Change in the void ratio of internally eroded soils with different confining pressures along with the cumulative fines loss (Experimental data from Ke and Takahashi, 2014a)

The void ratios before and after erosion and the cumulative fines loss for both loose and dense soils are summarized in Tables 3.2, 3.3, and 3.5. As mentioned above, the specimens with higher confining pressure have fewer eroded fines, which results in relatively smaller fines content variation. The trends of the void ratio change of the internally eroded soils under different confining pressures along different cumulative fines loss are plotted based on three hypotheses (Fig. 3.25). As the initial void ratios of specimens after consolidation with 35% initial fines contents under different confining pressures (50 kPa, 100 kPa, and

200 kPa) are quite close, the initial void ratio after consolidation in this figure is determined by average value for simplification, yields e_c=0.55 (Fig. 3.25). The prediction curves of post-erosion void ratio under different initial fines contents and different cumulative fines losses are plotted in Figs. 3.26 and 3.27, respectively.

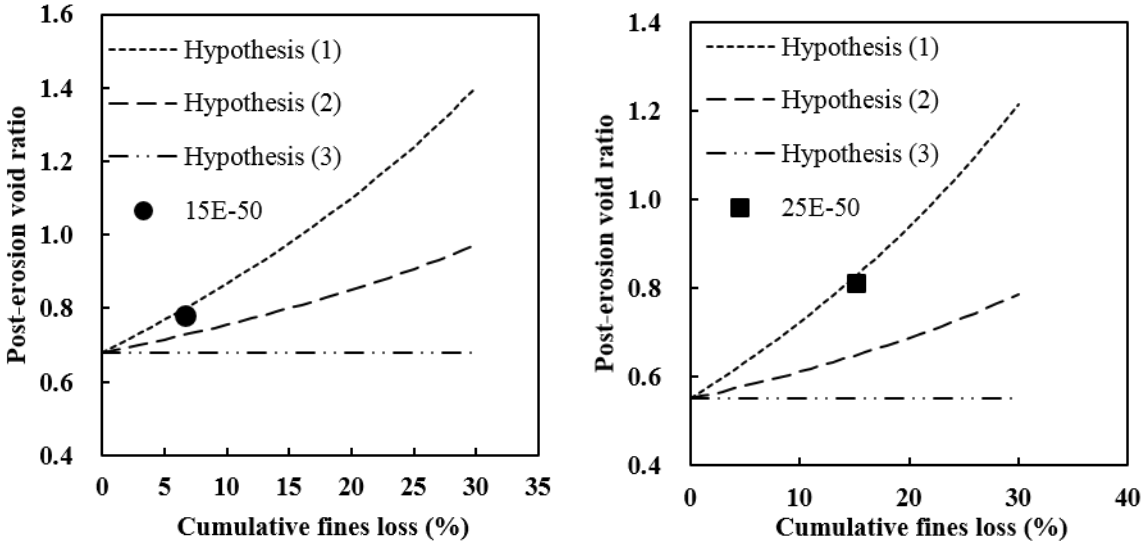

(a) Soils with 15% initial fines content (b) Soils with 25% initial fines content

Figure 3.26 Change in the post-erosion void ratio with different initial fines contents along with the cumulative fines loss (Experimental data from Ke and Takahashi, 2014a)

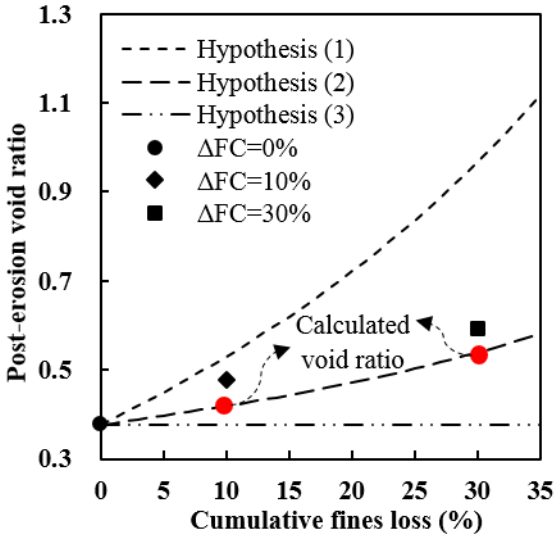

Figure 3.27 Change in the void ratio of the eroded dense soils (Group B, Experimental data from Chen *et al.*, 2016)

The experimental results drop between prediction curves obtained through hypotheses (1) and (2), while hypothesis (3) shows that no change of void ratio happens with the increase

of the cumulative fines loss. Compared with the prediction curve by hypothesis (2), experimental results are closer to that by hypothesis (1) for most cases. The equation used in hypothesis (1) is shown below:

$$e_{H1} = \frac{e_c + \Delta FC}{1 - \Delta FC} \tag{3.6}$$

where e_c is the void ratio after the consolidation, e_{H1} is the post-erosion void ratio calculated based on hypothesis (1). For the case (Group B, Chen *et al.*, 2016), the experimental results are closer to prediction results calculated by hypothesis (2), which are underestimated (Fig. 3.27).

The prediction curves for hypothesis (1) are closer to the experimental results but overestimate for most cases, which results from the ignorance of the effect of the volumetric strain. If we know the erosion-induced volumetric strain, we can estimate the post-erosion void ratio (Ke and Takahashi, 2014a). Then the equation considering the effect of the volumetric strain is as follow:

$$e_{er} = (1 - \varepsilon_v^{er}) \left(\frac{e_c + \Delta FC}{1 - \Delta FC} \right) - \varepsilon_v^{er} \tag{3.7}$$

where ΔFC is also regarded as a percentage by volume when the specific gravities of both the coarse particles and fines are the same. The post-erosion void ratios from both experimental and prediction results calculated by Eqn. (3.7) are plotted in Fig. 3.28, from which we can know that Eqn. (3.7) can be used to estimate the post-erosion void ratios by considering the cumulative fines loss and erosion-induced volumetric strain, i.e., Eqn. (3.7) is suitable for the prediction of post-erosion void ratio for the gap-graded soils and the eroded soils obtained after the salt dissolution. For the dense soils with 30% cumulative fines loss, the calculated post-erosion void ratio is larger than that from the experiment (question mark in Fig. 3.28a). This discrepancy could be attributed to the post-erosion void ratio of soils with 30% cumulative fines loss was closer to the prediction curve calculated by hypothesis (2) (Fig. 3.27). The seepage scenario of the hypothesis (2) is that the loss of fines (dissolution

of the salt) does not increase the voids dramatically, but decreases the solid.

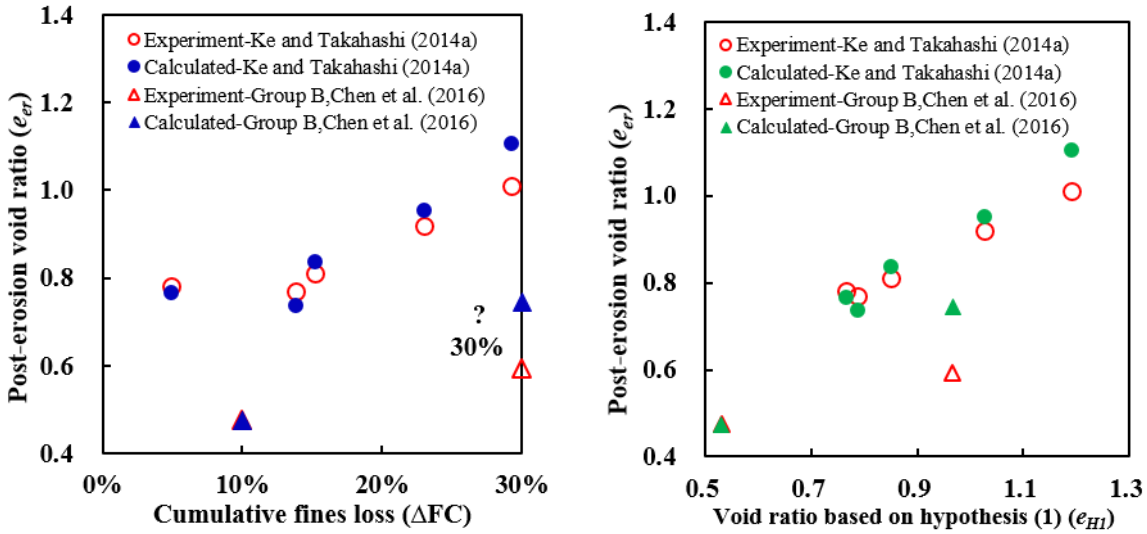

(a)Variation with cumulative fines loss (b)Variation with void ratio e_{H1}

Figure 3.28 Post-erosion void ratios comparison between experimental and calculated results

3.3 Summary

Several series of laboratory erosion tests on gap-graded soils under different conditions have been discussed in this chapter. The post-erosion grading curves shift downward in the fines fraction for all erosion tests. Compared with the effect of initial fines content, the amount of this shifting for grading curves depends more on the applied confining pressure. The soils with higher confining pressure and smaller initial fines content have less loss of fines, resulting in a smaller increase in post-erosion void ratio compared with those of lower confining pressure and larger initial fines content.

The heterogeneity exists along the flow direction through the specimen. From the top to the bottom of the internally eroded soils with the downward flow, both the cumulative fines loss and the post-erosion void ratio are found to decrease linearly with the distance from the top of the specimen. The top layer of the eroded soils also has the largest amounts of loss of fines in the upward flow through CFD-DEM simulation. Therefore, gravity is thought to affect the movement of fines under the seepage flow.

The predictive equation of the fines content incorporated with the mean effective stress, the

initial fines content, and the flow velocity have been proposed. The fines content of the soils under constant flow velocity decreases gradually, finally tending to converge to a certain value. The proposed predictive equation can capture the main features of the variations of the fines content during erosion under different confining pressures and different initial fines contents. There should be a positive correlation between the final fines content and the initial fines content (Cividini et al., 2009). However, some specimens with different initial fines contents do not show this relation, which needs further study.

The volumetric strain is almost zero when the cumulative fines loss is very small. At the same time, the volumetric strain of the internally eroded soils shows approximately the highest value when the cumulative fines loss is large enough. It becomes insensitive to the amount of the loss of fines when the cumulative fines loss is large. Based on these phenomena, a hyperbolic tangent function is employed to predict the variation of the erosion-induced volumetric strain along with the cumulative fines loss. At last, the equation incorporated with cumulative fines loss and volumetric strain has been employed to predict the post-erosion void ratio, which is important to study the mechanical behavior of the internally eroded soils.

[This page intentionally left blank]

CHAPTER 4

PARAMETER STUDY ON CONSTITUTIVE MODEL FOR SANDY SOILS CONSIDERING THE INFLUENCE OF INTERNAL EROSION

4.1Introduction

There remains a need for further investigations on the variations of model parameters caused by internal erosion concerning the experimental evidence (Chang *et al.* 2014; Ke and Takahashi, 2014a, 2014b, 2015; Ouyang and Takahashi, 2015; Li *et al.*, 2017, 2020; Mehdizadeh *et al.*, 2017). In this chapter, firstly, the variation of mechanical behavior of the soils after different erosion phenomena (suffosion and suffusion) under both drained and undrained triaxial tests are introduced. The effects of fines content and intergranular void ratio on the soil structure are discussed. After confirming the good reproducibility of the subloading Cam-clay model for uneroded specimens under the drained condition, the mechanical response of the soils with suffosion under the drained condition is simulated using the same model. Finally, the evolutions of key parameters with suffosion-related parameters are examined and analyzed.

4.2 Experimental investigations in literature

To investigate the change in the mechanical behavior of the internally eroded soils, many researchers have conducted both the drained and undrained triaxial tests. The effects of the erosion phenomena (suffusion and suffosion) and intergranular void ratio on the variation of both the drained and undrained mechanical behavior will be discussed in detail.

4.2.1 Mechanical behavior of the soils after suffosion

Ke and Takahashi (2015) performed seepage and drained triaxial tests to understand the mechanical behavior of the loose soils with suffosion. Figure 4.1a shows the changes of

deviatoric stress with axial strain. For the same initial confining pressure, the deviatoric stress of the eroded specimen is smaller than that of the uneroded specimen at the relatively large axial strain level. However, the deviatoric stress of the eroded specimen is larger than that of the uneroded specimen when the axial strain is small (less than 1%, Fig. 4.1b). As for the volumetric strain change, no large difference can be seen among the cases, and the volumetric strain for the eroded specimens is slightly smaller than that of the uneroded one (Fig. 4.1c).

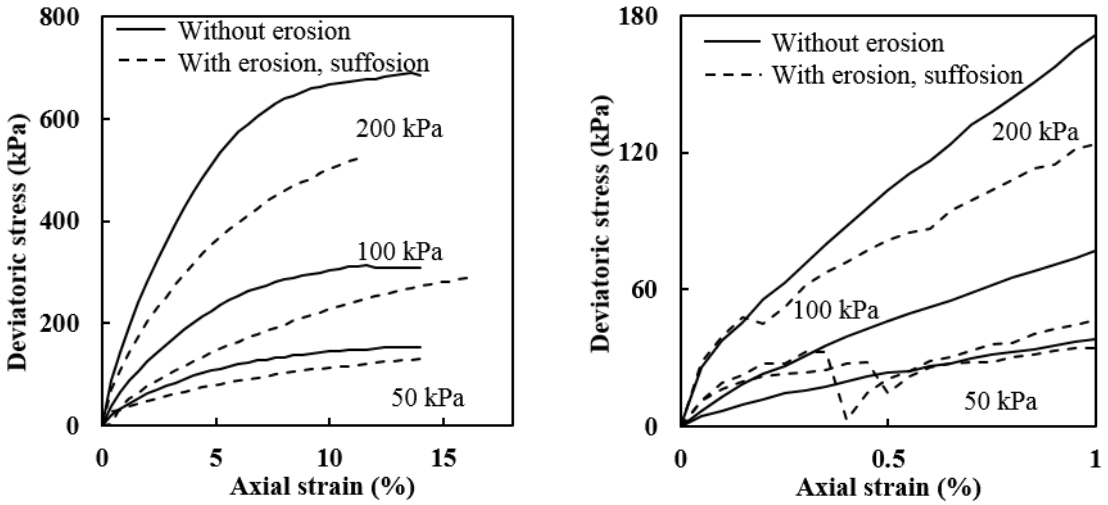

(a)Deviatoric stress-axial strain response (b)At the small axial strain level

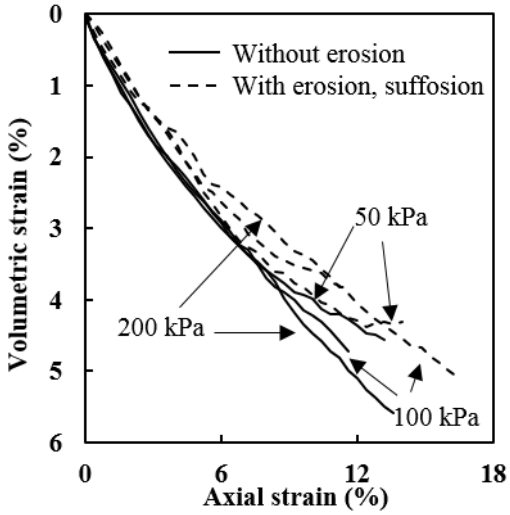

(c)Volumetric strain-axial strain response

Figure 4.1 Mechanical behavior of both uneroded and eroded specimens under drained triaxial shearing tests (Experimental data from Ke and Takahashi, 2015)

The volumetric strain is defined as the volume change divided by the initial total volume ($\varepsilon_v = \Delta V/V_0 = \Delta V/(1+e_{bs})$). The volumetric strain is affected by two factors, volume

change (ΔV) and the initial void ratio before shearing (e_{bs}). The ΔV of the internally eroded soils during triaxial shearing is larger than that of the uneroded soils during triaxial shearing. At the same times, the e_{bs} also increases after suffosion-type erosion. When the effect of the void ratio increment is larger than that of the volume change, the volumetric strain of the internally eroded soils becomes less than that of the uneroded soils.

Li *et al.* (2017) performed similar tests. After the seepage tests, the drained triaxial shearing tests were performed to study the effect of suffosion on the dense specimens. With the loss of fines, the peak strength decreased (Fig. 4.2a), which was consistent with experimental results by many researchers (Ke and Takahashi, 2014a, 2015; Chen *et al.*, 2016 among others). It is worth noting that deviatoric stress at the critical state showed a minor change. The dense soils became less dilative or became contractive with the loss of fines. This suffosion process changes the soils from a dense state to a loose state; hence, it is expected to make the dense soils more contractive (Fig. 4.2b).

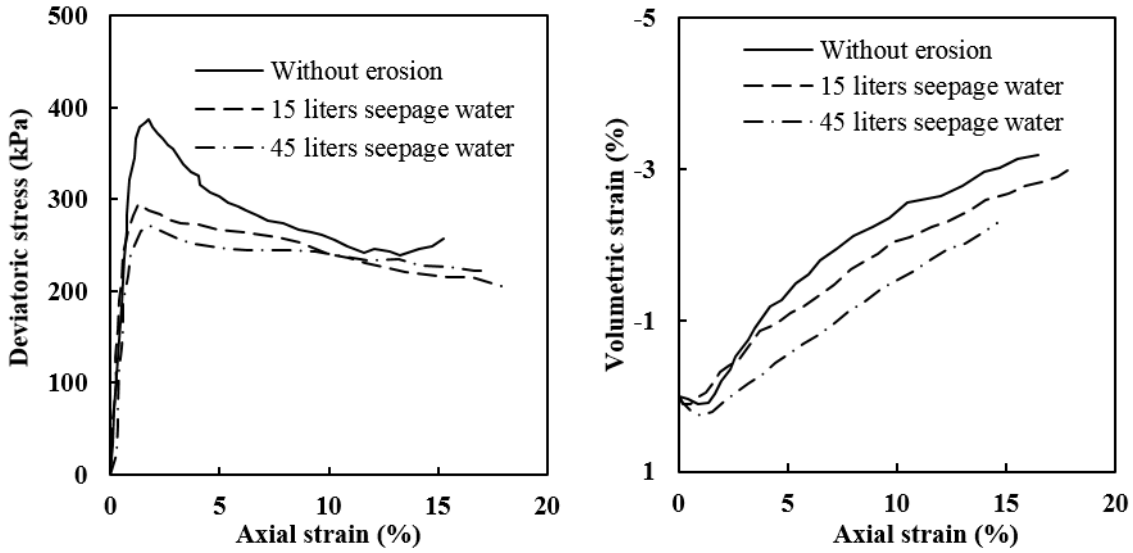

(a)Deviatoric stress-axial strain response (b)Volumetric strain-axial strain response

Figure 4.2 Drained mechanical behavior of both uneroded and eroded specimens (Experimental data from Li *et al.*, 2017)

Xiao and Shwiyhat (2012) studied the effects of the suffosion on the undrained mechanical behavior of the mixture of sand and kaolinite clay. The original soils were prepared by the mixture of poorly graded river sand and the non-expansive kaolinite clay (accounting for 10%

of the total mass). Three kinds of gap-graded soils were obtained through removing the soils of the grain sizes from 1.18 mm to 0.3 mm (#16×#50), from 0.6 mm to 0.3 mm (#30×#50), and from 0.6 mm to 0.15 mm (#30×#100) respectively. The seepage tests were performed on the gap-graded soils, after which the undrained triaxial shearing tests were conducted. The details of both uneroded and eroded specimens are summarized in Table 4.1. Figure 4.3 shows the comparison of the deviatoric stresses of the uneroded and internally eroded soils. Both the peak strength and deviatoric stress at the critical state of the internally eroded soils were larger than those of the uneroded soils for all three cases.

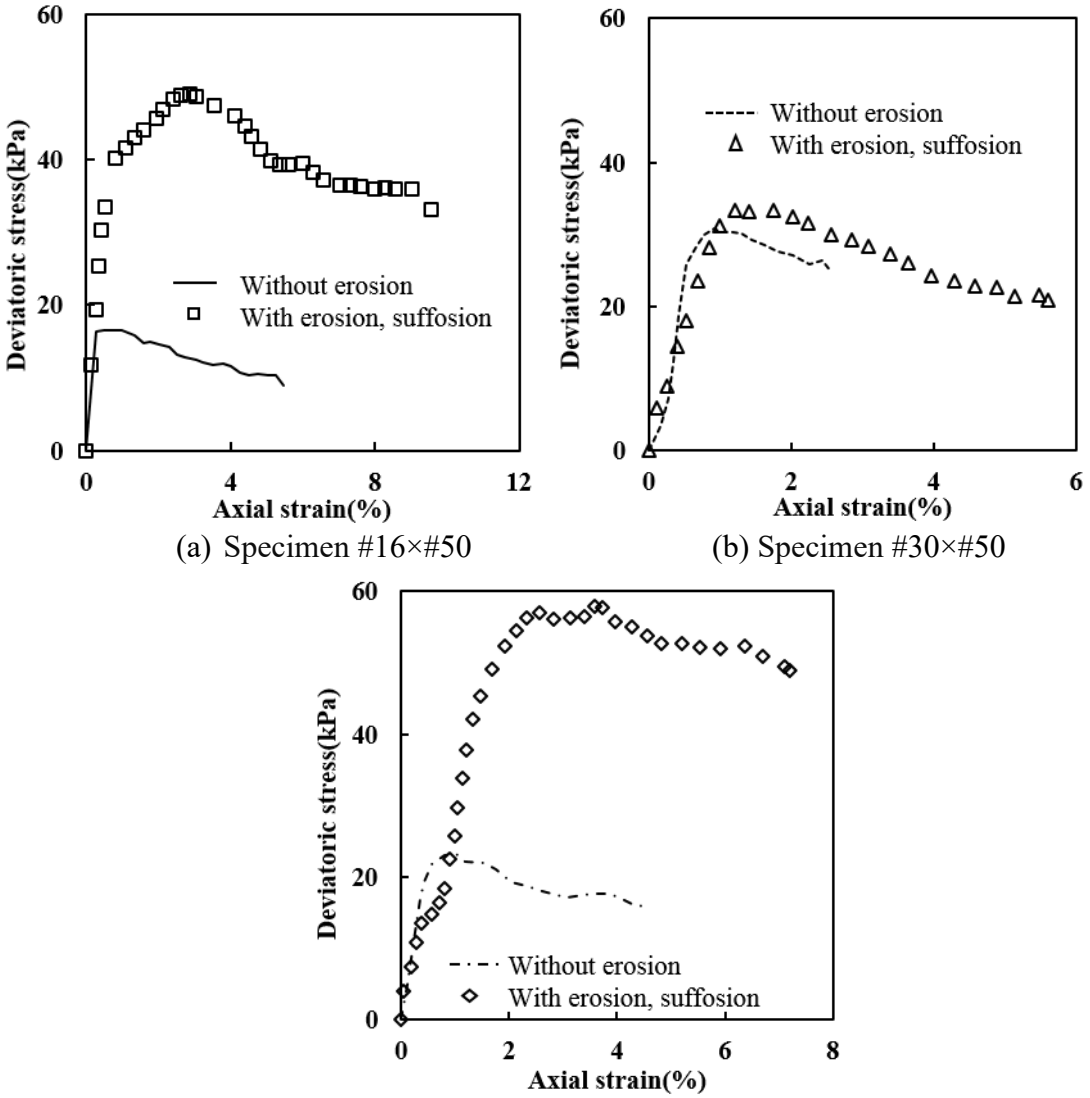

(a) Specimen #16×#50

(b) Specimen #30×#50

(c)Specimen #30×#100

Figure 4.3 Mechanical behavior of specimens without and with suffosion under undrained triaxial shearing (Experimental data from Xiao and Shwiyhat, 2012)

Table 4.1 Details for sand and kaolinite clay mixtures with and without suffosion for Xiao and Shwiyhat (2012)

Specimens	Dry density	Relative density	e_c	ε_v^{er}	e_{er}
#16×#50N	1.88 g/cm^3	86.0%	0.43	-	-
#16×#50E	1.86 g/cm^3	85.1%	0.43	0.62%	0.44
#30×#50N	1.95 g/cm^3	93.0%	0.37	-	-
#30×#50E	1.79 g/cm^3	85.2%	0.37	0.32%	0.50
#30×#100N	1.95 g/cm^3	93.0%	0.37	-	-
#30×#100E	1.79 g/cm^3	85.1%	0.37	0.75%	0.50

Table 4.2 Basic properties of uneroded soils and seepage tests results for Ouyang and Takahashi (2016)

Specimens	FC_0	FC_∞	e_{ini}	e_c	ε_v^{er}	e_{er}	e_s
15N-50	15%	15%	0.68	0.67	-	0.67	0.96
15E-50	15%	8.75%	0.68	0.67	0.2%	0.80	0.98
25N-50	25%	25%	0.61	0.54	-	0.54	1.05
25E-50	25%	13.10%	0.61	0.54	1.9%	0.81	1.06
35N-50	35%	35%	0.61	0.59	-	0.59	1.45
35E-50	35%	13.00%	0.61	0.59	10.2%	0.99	1.29

Note: e_{ini} indicates the initial void ratio before consolidation.

Ouyang and Takahashi (2016) investigated the change in the structure of the internally eroded soils subjected to suffosion through recorded microscopic images. The specimens were prepared by the mixture of silica No. 3 and No. 8 sands with 15%, 25%, and 35% initial fines contents. The increase in the flow rate is the same as that conducted by Ke and Takahashi (2014a). The changes in fines contents and void ratios after suffosion are summarized in Table 4.2. To study the effects of suffosion on the mechanical behavior of the soils, undrained triaxial tests on both uneroded and eroded soils were conducted. Figure 4.4 shows the deviatoric stress-axial strain curves of the uneroded and eroded soils under the

undrained condition. Both the peak strength and deviatoric stress at the critical state of the internally eroded soils are larger than those of the uneroded soils.

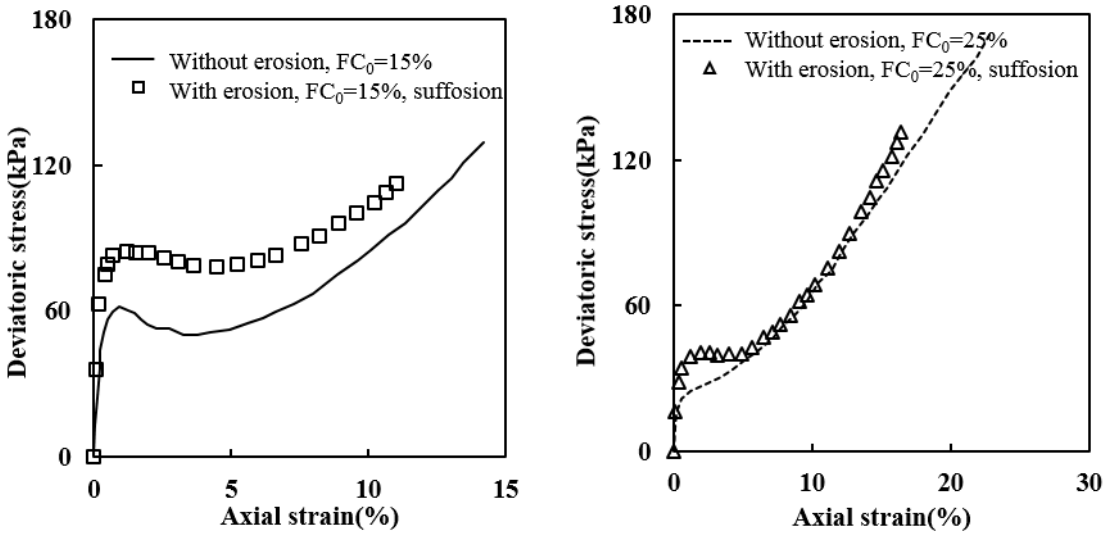

(a) Specimen with 15% initial fine content (b) Specimen with 25% initial fine content

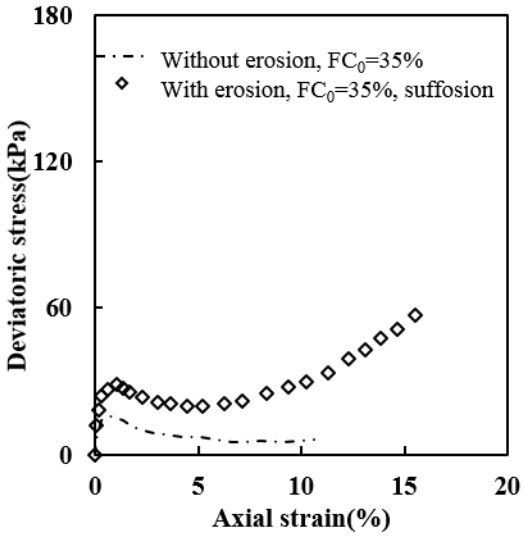

(c) Specimen with 35% initial fine content

Figure 4.4 Undrained stress-strain curves of the uneroded and eroded soils (Experimental data from Ouyang and Takahashi, 2016)

Prasomsri and Takahashi (2020) conducted seepage tests on the soils with different initial fines contents. Here, the seepage tests with 25% and 32.5% initial fines contents are recalled. The variations of the fines content and the void ratio are summarized in Table 4.3. The suffosion happened in soils with 32.5% initial fines content because significant change existed in the volume after the seepage tests. After the seepage tests, undrained triaxial tests

were conducted on the internally eroded soils. It was found that the mechanical behavior of the eroded soils had a relation with the fines content and the erosion phenomena. When suffosion happened, deviatoric stress at a large axial strain level was larger than that of the uneroded soils (Fig. 4.5). The rearrangement happened during suffosion, which caused an increase of deviatoric stress at the large strain level.

Table 4.3 Basic properties of both uneroded and eroded soils for Prasomsri and Takahashi (2020)

Specimens	FC_0	FC_∞	e_c	ε_v^{er}	e_{er}	e_s
25N-50	25%	25%	0.58	-	-	1.10
25E-50	25%	24.2%	0.59	0.01%	0.65	1.18
32.5N-50	32.5%	32.5%	0.54	-	-	1.28
32.5E-50	32.5%	31.4%	0.54	1.15%	0.60	1.34

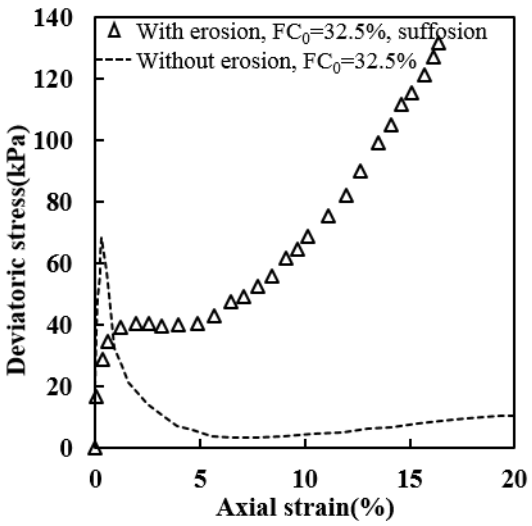

Figure 4.5 Undrained stress-strain curves of soils with and without suffosion (Experimental data from Prasomsri and Takahashi, 2020)

In a word, both the total volume and the number of fines decrease after suffosion in their tests (Fig. 4.6). The decrease in the total volume indicates the collapse of the original structure and the rearrangement of the new structure, which plays an important role in the mechanical behavior of the soils after suffosion.

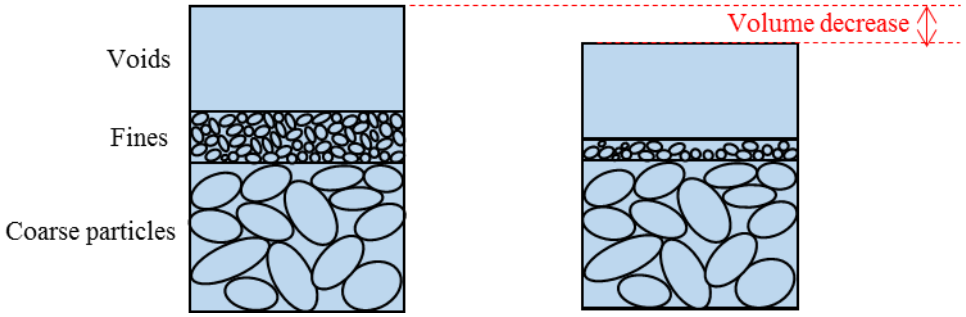

Figure 4.6 Description of the suffosion-type erosion

Under the drained triaxial shearing condition, the effect of this rearrangement was not obvious at the large strain level. Deviatoric stress of eroded soils was smaller than that of uneroded soils at the large strain level (Ke and Takahashi, 2015; Chen *et al.*, 2016; Li *et al.*, 2017). However, this rearrangement could cause an increase of stiffness for eroded loose soils within a small strain level, which was weak and easy to collapse with straining.

Under the undrained triaxial shearing condition, the deviatoric stresses of the soils with suffosion were larger than those of uneroded soils (Xiao and Shwiyhat, 2012; Ouyang and Takahashi, 2016; Prasomsri and Takahashi, 2020). Xiao and Shwiyhat (2012) thought that the increase in both peak strength and deviatoric stress at the critical state of the soils after suffosion was attributed to the loss of saturation after seepage tests. To validate their thoughts, they re-saturated the specimens after the seepage tests. However, the peak strength and deviatoric stress at the critical state of the eroded and subsequent re-saturated soils were still larger than those of the uneroded soils. It was believed that the re-saturation process could rearrange the soil structure. Ouyang and Takahashi (2016) focused on the change of the soil structure caused by seepage flow through the microscopic observation. It was found that some fines could coat the coarse particles while other fines filled the voids formed by coarse particles. From the microscopic observation, most fines were jammed around the coarse particles after the suffosion, which strengthened the structure of the soils.

4.2.2 Mechanical behavior of the soils after suffusion

To understand the effects of the fines content, the global void ratio, and the intergranular

void ratio on the mechanical behavior of the sandy silts, Thevanayagam *et al.* (2002) conducted several series of undrained triaxial tests. Two groups of soils are discussed in this subsection. The global void ratios were about 0.60 for Group C soils while the intergranular void ratios were almost the same, around 0.67 for Group D soils, summarized in Table 4.4. The soils were prepared by the mixture of host sand (F55, Foundry Sand) and the crushed silica fines (silts, silica No.40) with different initial fines contents, 0%, 7%, and 15% respectively. These fines contents were smaller than the threshold fines content (around 25% in this case). For suffusion, the intergranular void ratios are the same after the seepage tests. Therefore, Group D soils could be employed to investigate the mechanical behavior of the soils after the suffusion. The undrained triaxial tests were conducted on both Group C and D soils.

Table 4.4 Basic material properties of two groups of soils (Groups C and D) for Thevanayagam *et al.* (2002)

Group	FC_0	d_{10} (mm)	d_{30} (mm)	d_{60} (mm)	Cu	Cc	e_c	e_s
C	0%	0.16	0.22	0.27	1.7	1.1	0.598	0.598
C	7%	-	-	-	-	-	0.596	0.716
C	15%	0.018	0.19	0.25	13.6	8.2	0.584	0.864
C	15%	0.018	0.19	0.25	13.6	8.2	0.595	0.876
D	0%	0.16	0.22	0.27	1.7	1.1	0.665	0.665
D	7%	-	-	-	-	-	0.558	0.675
D	15%	0.018	0.19	0.25	13.6	8.2	0.423	0.674

Figure 4.7a shows that when the global void ratios and the initial confining pressures are the same for all cases of the Group C soils, the increase of the fines contents can increase the fragility. However, the increase of fines contents can decrease the fragility when the intergranular void ratios are similar for the Group D soils (Fig. 4.7b). The functions of fines in the soils could vary with the change of the intergranular void ratios (Thevanayagam *et al.*, 2002). When the intergranular void ratio is larger or close to the maximum void ratio of pure

host sand (Group C soils), the fines may support the coarse grain skeleton and reduce the coarse-coarse contacts, which could increase the fragility. When the intergranular void ratio is relatively low (Group D), the fines around the coarse particles strengthen the structure, providing a cushioning effect.

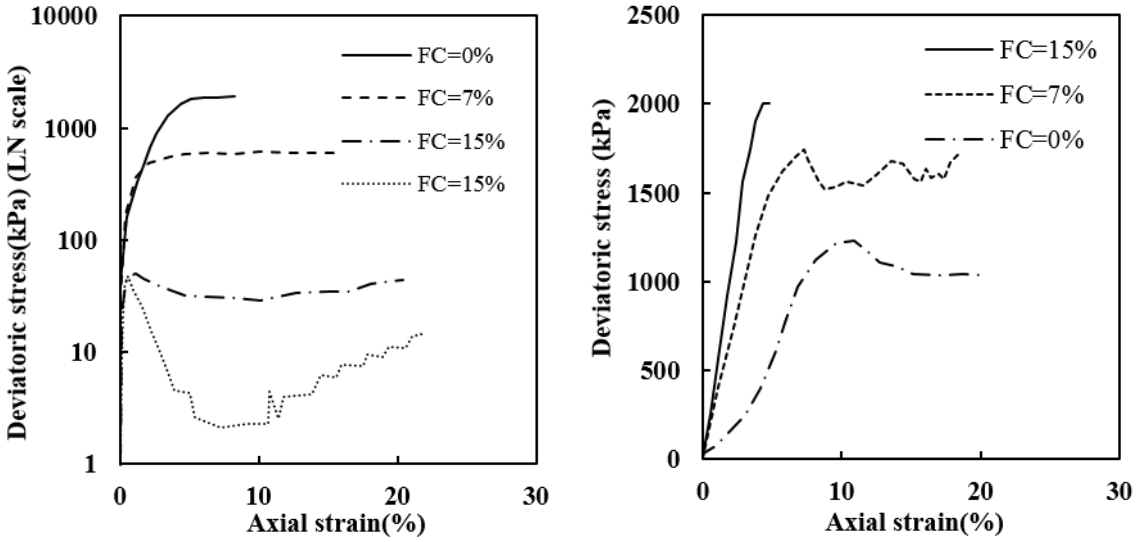

(a) Group C soils (b) Group D soils

Figure 4.7 Undrained mechanical behavior of the soils under different initial fines contents (Experimental data from Thevanayagam *et al.*, 2002)

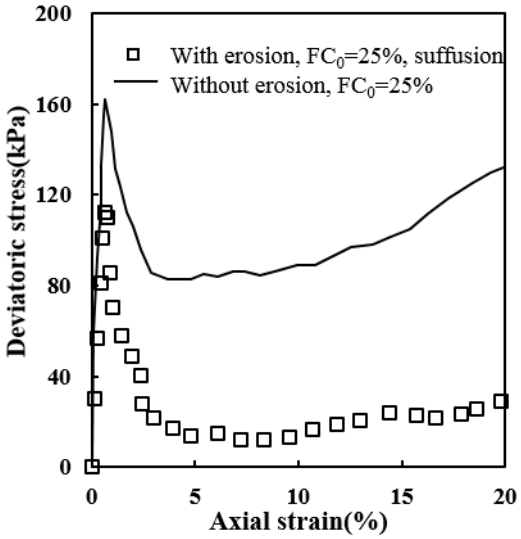

Figure 4.8 Undrained stress-strain relations for both uneroded and eroded specimens with 25% initial fine content (Experimental data from Prasomsri and Takahashi, 2020)

Figure 4.8 shows the variation of the deviatoric stress for soils with 25% initial fines content after suffusion (Prasomsri and Takahashi, 2020). The basic properties of the soils with 25%

initial fines content are summarized in Table 4.3. When suffusion happened, deviatoric stresses of internally eroded soils at both peak state and large axial strain level decreased compared with those of uneroded soils.

On the whole, when the intergranular void ratio of soils was lower than the maximum void ratio of the pure coarse particles, the loss of fines after suffusion increased the fragility (collapse potential) under the undrained condition. Figure 4.9 shows that the intergranular void ratio of the soils kept unchanged after suffusion. The fines could strengthen the soil structure, and the loss of fines could cause a decrease in the soil strength. (Group D, Thevanayagam *et al.*, 2002; Li *et al.*, 2020; Prasomsri and Takahashi, 2020).

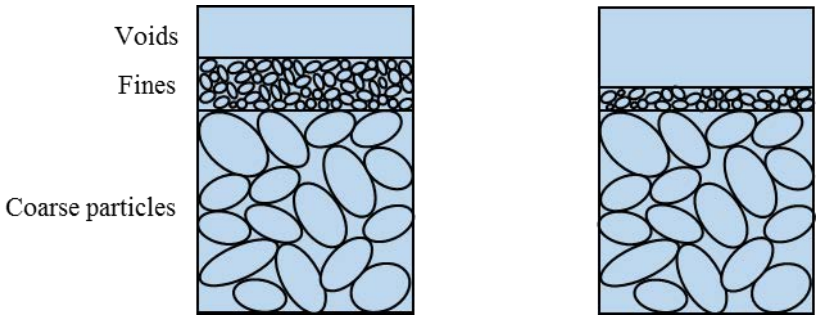

Figure 4.9 Description of the suffusion while the intergranular void ratio is relatively low

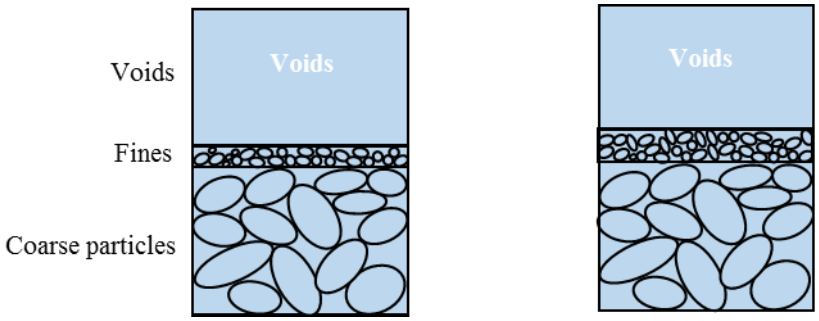

Figure 4.10 Description of the suffusion while the intergranular void ratio is close to the maximum void ratio of the pure coarse particles

However, a special situation existed for soils with different initial fines contents under the undrained condition. When the intergranular void ratio of soils was close to the maximum void ratio of the pure coarse particles, the fines have a lubrication effect on the soil structure (Fig. 4.10). The increase of the fines may increase the fragility (collapse potential), leading to a decrease of deviatoric stress under the undrained condition (Group C, Thevanayagam *et*

al., 2002).

4.3 Constitutive model used

4.3.1 Model description

Hashiguchi (1989) proposed the concept of the subloading surface, which could describe the plastic deformation of the material even inside the normal yield surface and realize the smooth of stress-strain behavior under loading. The current stress state point is always on the subloading surface, and the normal yield surface can expand or contract with the movement of the subloading surface. The subloading surface is geometrically similar to Cam-clay (normal) yield surface, as shown in Fig. 4.11.

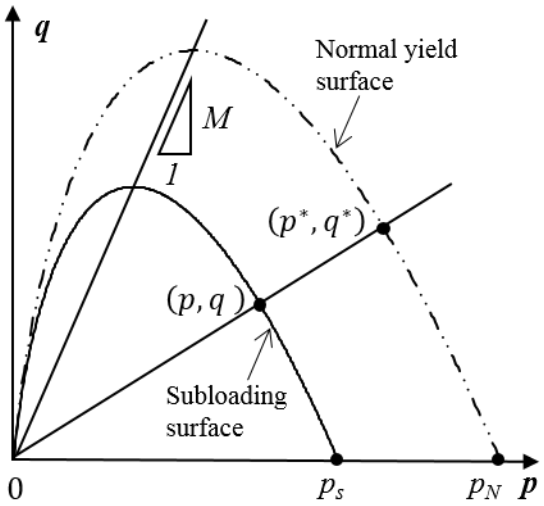

Figure 4.11 Subloading surface and normal yield surface

In the *p*-*q* space, the yield function of the normal yield surface, similar to the yield surface of the original Cam-clay model ($f = Mln\frac{p}{p_0} + \frac{q}{p} = 0$), can be expressed as:

$$f = MDln\frac{p^*}{p_N} + D\frac{q^*}{p^*} = \frac{\lambda - \kappa}{1 + e_0} ln\frac{p^*}{p_N} + D\frac{q^*}{p^*} = C_p ln\frac{p^*}{p_N} + D\frac{q^*}{p^*} = 0 \qquad (4.1)$$

where $C_p = \frac{\lambda-\kappa}{1+e_0}$ (Zhu *et al.*, 2013), D is a material constant ($D = \frac{C_p}{M}$, Shibata, 1963), λ is the slope of the normal compression line in *e*-ln *p* space, κ is the slope of swelling line

in *e*-ln *p* space. *p* is mean effective stress ($p = \frac{\sigma_1 + 2\sigma_3}{3}$, σ_1 is the axial stress, σ_3 is the radial stress, all mean stresses p in this dissertation represent mean effective stresses), and q is deviatoric stress ($q = \sigma_1 - \sigma_3$). *M* (critical stress ratio) is the slope of the critical state line in *p*-*q* space; e_0 is the initial void ratio; p_s and p_N are intersection points of the subloading and normal yield surfaces and mean effective stress axis; p^* and q^* are mean effective stress and deviatoric stress on the normal yield surface, respectively.

The current stress state (p, q) is on the subloading surface. By considering the concept of subloading surface, Eqn. (4.1) can be rewritten as:

$$f = C_p \left[ln\frac{p}{p_0} - \left(ln\frac{p_N}{p_0} - ln\frac{p_N}{p_s} \right) \right] + D\frac{q}{p} = 0 \tag{4.2}$$

where p_0 is the reference pressure, taken as 98 kPa. The plastic volumetric strain caused by isotropic compression from p_0 to p_N, is expressed as:

$$\varepsilon_v^p = C_p ln\frac{p_N}{p_0} \tag{4.3}$$

where $R = \frac{p_S}{p_N}$ is stress ratio that corresponds to the size ratio of subloading surface to normal yield surface, and is also the reciprocal of over-consolidation ratio. By using Eqn. (4.3), the subloading surface can be written as:

$$f = C_p ln\frac{p}{p_0} - \varepsilon_v^p - C_p lnR + D\frac{q}{p} = 0 \tag{4.4}$$

Since the current stress state point has to be on the subloading surface all the time, the following consistency conditions have to be satisfied:

$$df = \frac{\partial f}{\partial p}dp + \frac{\partial f}{\partial q}dq + \frac{\partial f}{\partial R}dR - \frac{1}{C_p}\varepsilon_v^p = 0 \tag{4.5}$$

When the associated flow rule is adopted to the subloading surface, the plastic strain increments can be calculated as:

$$d\varepsilon_v^p = \Lambda \frac{\partial f}{\partial p} \quad , \quad d\varepsilon_q^p = \Lambda \frac{\partial f}{\partial q} \tag{4.6}$$

where Λ is the plastic multiplier (non-negative), $d\varepsilon_v^p$ is the plastic volumetric strain increment, $d\varepsilon_q^p$ is the plastic shear strain increment. The evolution rule of R is as follows (Hashiguchi, 1989):

$$dR = U d\varepsilon_q^p \tag{4.7}$$

where $U = -m_R lnR \cdot \frac{1}{D}$, and m_R is a material constant.

By substituting Eqns. (4.6), (4.7) into (4.5), Λ can be obtained:

$$\Lambda = \frac{\frac{\partial f}{\partial p} dp + \frac{\partial f}{\partial q} dq}{\frac{1}{R}\frac{\partial f}{\partial q} + \frac{1}{C_p}\frac{\partial f}{\partial p}} \tag{4.8}$$

From this plastic multiplier, the following constitutive equation can be obtained:

$$\begin{pmatrix} dp \\ dq \end{pmatrix} = \boldsymbol{D}_{ep} \begin{pmatrix} d\varepsilon_v \\ d\varepsilon_q \end{pmatrix} \tag{4.9}$$

where ε_v is the volumetric strain ($\varepsilon_v = \varepsilon_1 + 2\varepsilon_3$, ε_1 is the axial strain; ε_3 is the radial strain); ε_q is the shear strain ($\varepsilon_q = \frac{2}{3}(\varepsilon_1 - \varepsilon_3)$). The elastoplastic stiffness matrix in Eqn. (4.9) can be written as:

$$\boldsymbol{D}_{ep} = \boldsymbol{D}_e - \frac{\boldsymbol{D}_e \partial \boldsymbol{f} \partial \boldsymbol{f}^T \boldsymbol{D}_e}{\partial \boldsymbol{f}^T \boldsymbol{D}_e \partial \boldsymbol{f} + H} \tag{4.10}$$

where $\boldsymbol{D}_e = \begin{bmatrix} K & 0 \\ 0 & 3G \end{bmatrix}$, $\partial \boldsymbol{f}^T = \begin{Bmatrix} \frac{\partial f}{\partial p} & \frac{\partial f}{\partial q} \end{Bmatrix}$, G is the shear modulus and K is the bulk modulus. G and K can be expressed by the following equations (Richart *et al.*, 1970):

$$G = G_0 \frac{(2.97 - e)^2}{1 + e} \sqrt{pp_0} \quad , \quad K = G \frac{2(1 + \nu)}{3(1 - 2\nu)} \tag{4.11}$$

where G_0 is a material constant (Li and Dafalias, 2000), e is the void ratio, ν is Poisson's

ratio. ε_v^p and R are hardening parameters, and the hardening function can be written as:

$$H = \frac{1}{R}\frac{\partial f}{\partial q} + \frac{1}{C_p}\frac{\partial f}{\partial p} \tag{4.12}$$

4.3.2 Model performance for uneroded soil

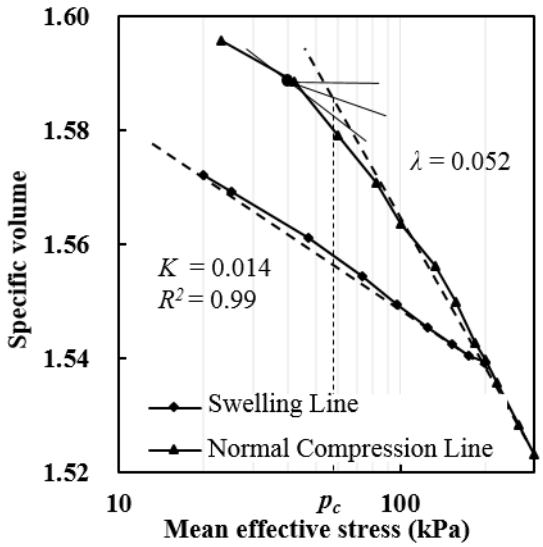

Figure 4.12 Isotropic volume change of uneroded specimen (Experimental data from Ke, 2015)

Under the drained triaxial shearing condition, the deviatoric stress of the eroded soils at the large axial strain decreased after both suffosion and suffusion (Ke and Takahashi, 2015; Li *et al.*, 2020). The effect of the erosion type differences (suffosion and suffusion) cannot be ignored in the study of the constitutive model for the soil under the drained condition. The effect of suffosion on the model parameters is considered in this chapter. Drained triaxial tests on soils with and without suffosion conducted by Ke and Takahashi (2015) are considered to examine the capability of the constitutive model. Key parameters in the model above are λ, κ, M, e_0, and the initial value of R. Isotropic compression test has been conducted on uneroded specimens with 35% initial fines content. The specific volume variation along with mean effective stress is plotted in Fig. 4.12. As the normal compression line (NCL) is not straight along with the mean effective stress, it is divided into two distinct regions. The first one is the elastic rebound curve under the low stress while the other is the elastoplastic linear compression curve under the higher stress (Gregory *et al.*, 2006). Since

the greater part of the normal compression curve is approximately straight for the soil used, the slope of the normal compression line is expressed as λ ($\lambda = \frac{e_1 - e_2}{\ln (p_2/p_1)}$). The value of λ can be estimated by the fitting of the higher-stress part of the compression curve. Since the swelling line (SL) is straight, the slope of the swelling line (κ) can be directly fitted. As the estimated pre-consolidation pressure (p_c) is 70 kPa, the initial stress ratio (R_0) for the case with 50 kPa confining pressure is estimated as 0.71 (see Fig. 4.12) and is set 1.0 for the other cases. Poisson's ratio is assumed 0.2 for all the tests.

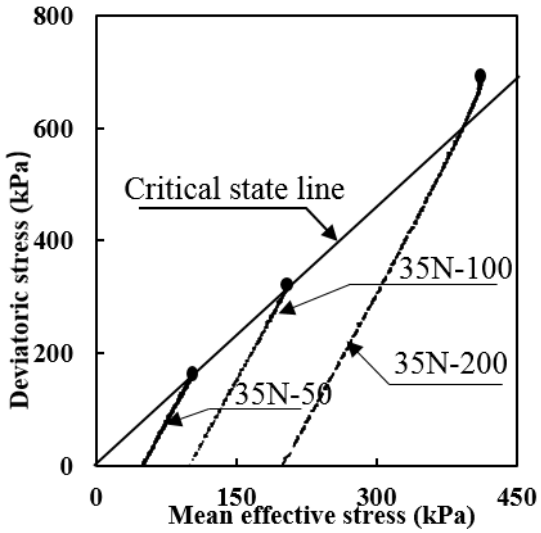

Figure 4.13 Effective stress paths in drained triaxial tests on uneroded specimens (Experimental data from Ke and Takahashi, 2015)

When deviatoric stress of the specimen shows the constant value with increasing the axial strain and keeping the volume constant, the soils can be regarded as in the critical state, and *M* (stress ratio at the critical state) can be determined from the effective stress paths (Fig. 4.13). The stress-strain curves (cf. Fig. 4.1) show that the deviatoric stress increases gradually and reaches a peak value with the axial strain. However, as the experiments were terminated at the axial strain from 12% to 18%, the eroded samples have not reached the critical state. To estimate the deviatoric stress at the critical state of the eroded samples, the fitting with a hyperbolic function was proposed (Ferreia & Bica, 2006):

$$q = \frac{\varepsilon_1}{a_2 + b_2 \varepsilon_1} \tag{4.13}$$

where a_2 and b_2 are material constants, which can be determined by the fitting. $1/b_2$ is regarded as the deviatoric stress at the critical state.

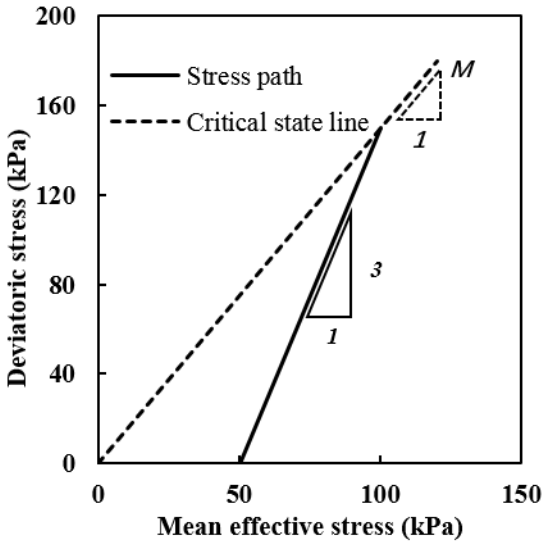

Figure 4.14 Critical state line and stress path in *p*-*q* space

For the drained triaxial shearing tests, the slope of the stress path is three in the *p*-*q* space (Fig. 4.14). The slope of the critical state line (M) can be estimated by the parameter b_2 above. For triaxial shearing tests, the angle of shearing resistance at the critical state (φ) can be obtained from the equation as below:

$$M = \frac{6sin\varphi}{3 - sin\varphi} \tag{4.14}$$

Based on the back analysis, we estimate the parameter for the evolution of R as m_R, equals 0.2. The material constant G_0 is estimated as 100 MPa, which is assumed to be the same under different confining pressure as Eqn. (4.11) has considered the effect of confining pressure. Parameters used in the simulations are summarized in Table 4.5. Simulation results are plotted in Fig. 4.15 (Sim. represents simulation results and Exp. represents experiment results). From Fig. 4.15, it can be said that the subloading Cam-clay model can reasonably capture the features of uneroded specimens under the drained condition.

Table 4.5 Parameters for original soils for Ke and Takahashi (2015)

Specimens	λ	κ	M	R_0	e_c
35N-50	0.052	0.014	1.65	0.71	0.55
35N-100	0.052	0.014	1.65	1.0	0.56
35N-200	0.052	0.014	1.65	1.0	0.54

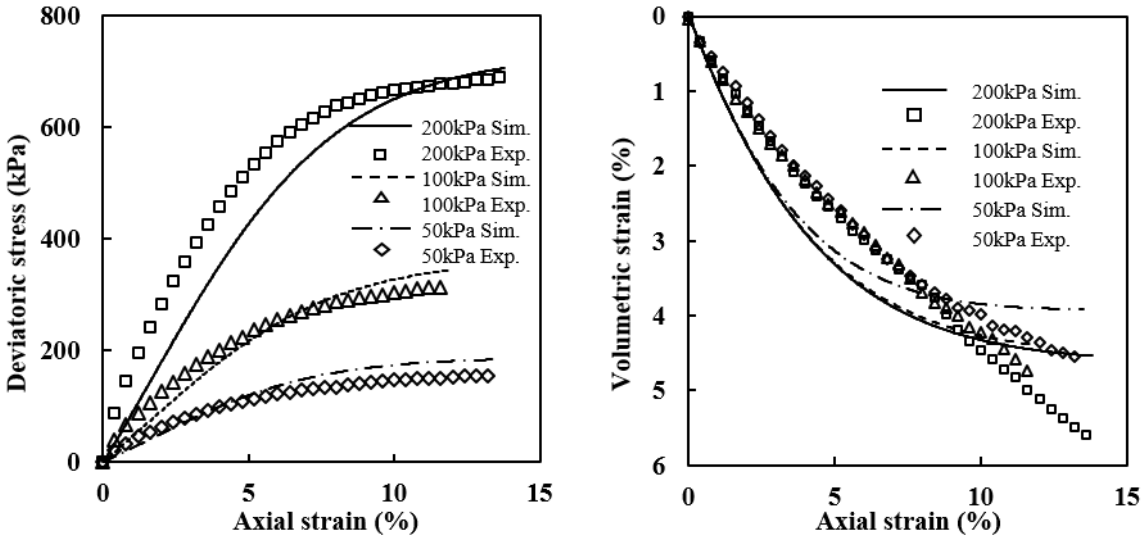

(a)Deviatoric stress-axial strain response (b)Volumetric strain-axial strain response

Figure 4.15 Comparisons between drained triaxial shearing test and prediction by the subloading Cam-clay model for uneroded specimens (Experimental data from Ke and Takahashi, 2015)

4.4Model parameter study considering the effect of suffosion

The fines content of the soils whose voids formed by coarse particles are full of fines is called the transitional fines content (FC_{th}) (Yang *et al.*, 2005; Andrianatrehina *et al.*, 2016). In this chapter, FC_{th} is determined from the minimum value of e_{max} and e_{min}. The FC_{th} is determined to be 35%, at which both maximum and minimum void ratios show a trough (cf. Fig. 3.1).

4.4.1 Influence of fines content on the angle of shearing resistance at the critical state

Table 4.6 summarizes the previous studies on the variations of fines contents on the soil shear strength. There are both positive correlation and negative correlation between fines

content and shear strength, which means the shear strength or angle of the shear resistance is also affected by other factors, such as void ratio, mineral composition, particle shape, particle size distribution, the method of specimen preparation and so on. For Samples 6 and 7, shearing tests on the internally eroded soils were also conducted. They were prepared by binary poorly graded sand, after a certain period of seepage flow, both angles of shearing resistance at peak and critical state became smaller with the loss of non-plastic fines.

Table 4.6 Influence of fines content on shear strength

Samples	Drained/ Undrained	Ranges of fines content	Types of fines	Positive/Negative Correlation	Reference
1	Undrained	3%-18%	Plastic	Negative	Ishihara (1993)
2	Undrained	10%-40%	Plastic	Negative	Pitman *et al.* (1994)
2'	Undrianed	0%-40%	Non-plastic	Positive	Pitman *et al.* (1994)
3	Undrained	12%-27%	Non-plastic	Negative	Thevanayagam *et al.* (1997)
4	Undrained	6%-27.5%	Plastic	Negative	Yin (1999)
5	Undrained	0%-30%	Non-plastic	Negative	Chien *et al.* (2002)
6	Undrained	0%-20%	Non-plastic	Positive	Ni *et al.* (2004)
6'	Undrained	0%-20%	Plastic	Negative	Ni *et al.* (2004)
7	Undrained	0%-15%	Non-plastic	Positive	Murthy *et al.* (2007)
8	Undrained	0%-50%	Non-plastic	Negative	Belkhatir *et al.* (2010)
9	Drained	25%-35%	Non-plastic	Positive	Chang *et al.* (2014)
10	Drained	5%-35%	Non-plastic	Positive	Chen *et al.* (2016)

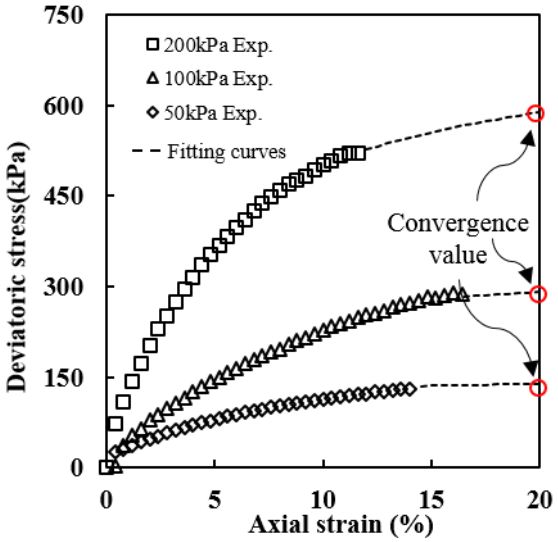

Figure 4.16 Determination of the deviatoric stress at the critical state of eroded specimens (Experimental data from Ke and Takahashi, 2015)

The initial fines contents (FC_0) are 35% for all specimens in the case of Ke and Takahashi (2015). The deviatoric stress at the critical state (convergence value) of eroded specimens under 50 kPa, 100 kPa, and 200 kPa initial mean effective stresses are obtained through Eqn. (4.13) as shown in Fig.4.16, based on which the angle of shearing resistance at the critical state (φ) can be calculated through Eqn. (4.14). Final fines contents (FC_∞) and the angles of shearing resistance at the critical state (φ) of both uneroded and eroded specimens under 50 kPa, 100 kPa, and 200 kPa initial mean effective stresses are summarized in Table 4.7. The relation between the angle of shearing resistance at the critical state and final fines content is fitted as a linear function with the equation shown below (Fig. 4.17):

$$\varphi = a_3 \cdot FC_\infty + b_3 \tag{4.15}$$

where a_3=14.5, and b_3=34.8. The angle of shearing resistance at the critical state decreases with the decrease of final fines content, which is the same as the previous results (Samples 9 and 10) described above.

Table 4.7 Influence of final fines content on the angle of shearing resistance at the critical state for Ke and Takahashi (2015)

Specimens	FC_∞	φ(°)
35N*	35.0%	40.3
35E200	24.6%	37.6
35E100	15.5%	37.1
35E50	8.1%	36.2

Note: 35N* denotes uneroded specimens with 35% initial fines content under 50 kPa, 100 kPa, and 200 kPa confining pressures.

Here, only the final fines content is considered as an explaining variable. However, as the seepage-induced suffosion not only makes the fines content smaller but also makes the void ratio larger, this decrease of the angle of shearing resistance at the critical state with the decrease of the final fines content may have also been affected by the increase of the void ratio. Since the separation of these effects cannot be made in the experiment, the contribution

of the void ratio increase cannot be explicitly expressed in this study. Presumably, the impact of the loss of fines is not large on change in the angle of shearing resistance at the critical state. The relationship between the angle of the shearing resistance and the final fines content for the uneroded soils is also added in Fig. 4.17. The uneroded soils were directly prepared with 15%, 25%, and 35% initial fines contents, on which triaxial tests were conducted under 50 kPa confining pressure. The angle of shearing resistance of the eroded soils is found to be smaller than those of the uneroded soils with the same fines content, which is attributed to two reasons. Firstly, fines with more angularities are assumed to be easily eroded. Uneroded soils have more angular fines than eroded soils with the same fines content. Secondly, the heterogeneity of particle size distribution along with the seepage direction of the eroded soils exists after erosion. Li *et al*. (2020) also found that both peak strength and deviatoric stress at the critical state of the soils with heterogeneous particle size distribution were smaller than those with homogeneous particle size distribution. Figure 4.17 also indicates that the heterogeneity of particle size distribution changes the trend of the angle of shearing resistance, which needs more experimental study in the future.

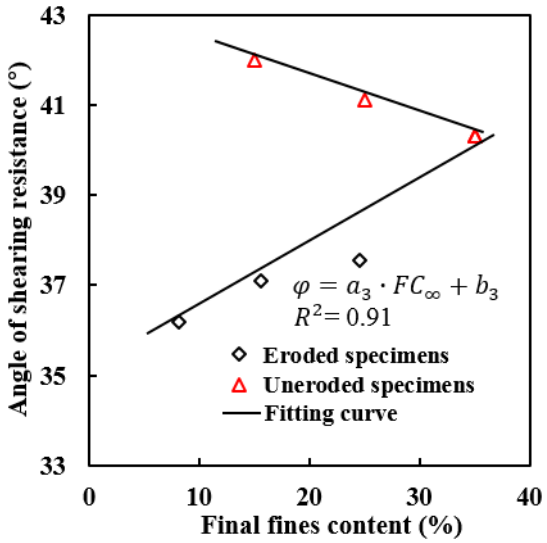

Figure 4.17 Angle of shearing resistance at the critical state versus final fines content (Experimental data of uneroded soils from Ke and Takahashi 2014a, Experimental data of eroded soils from Ke and Takahashi, 2015)

4.4.2 Influence of suffosion on the slope of the NCL (λ)

Isotropic compression tests have been conducted on both eroded and uneroded specimens, and curves of specific volume changes with mean effective stress are plotted in Fig. 4.18. Eroded specimen refers to the sample remaining 13% fines content after suffosion under 50 kPa confining pressure with 35% initial fines content. The eroded specimen was firstly loaded to 100 kPa and then was unloaded down to 20 kPa. Isotropic loading was then conducted until the load reached 200 kPa, after which the eroded specimen was unloaded to 20 kPa again. At last, the isotropic compression was given to the specimen up to 300 kPa. The uneroded specimen had 35% initial fines content. The isotropic compression started from 20 kPa. Firstly, the specimen was loaded to 100 kPa. Secondly, the specimen was unloaded to 20 kPa, after which the specimen was loaded to 200 kPa. Then, the specimen was unloaded to 20 kPa again. Finally, the isotropic compression was given to the specimen up to 300 kPa (Fig. 4.18). By suffosion, the normal compression line is shifted upward, and its slope increases. However, we can observe that the swelling line of the eroded specimen is almost parallel to that of the uneroded specimen, which means that suffosion has a minor effect on the slope of the swelling line (Fig. 4.18).

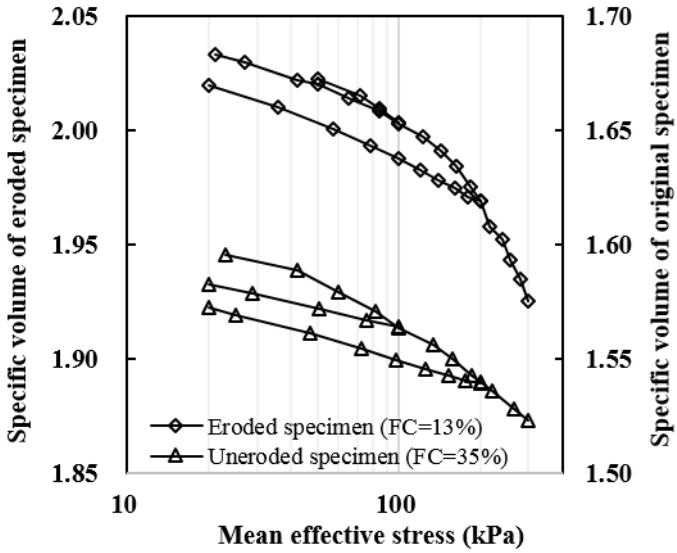

Figure 4.18 Normal compression lines and swelling lines for eroded and uneroded specimens (Experimental data from Ke, 2015)

Comparing to the variations of the slope of the swelling line (κ) with suffosion, a marked change in the slope of the normal compression line (λ) can be seen. Therefore, within the scope of this study, it is reasonable to ignore the suffosion-induced change of κ. Based on the observation in the isotropic compression tests, we estimate the values of λ and R_0 with different losses of fines from back analysis for simulation on the eroded specimens. In this study, the increase of stiffness at the small strain level for eroded specimens in the deviatoric stress-axial strain curve obtained in the experiment is ignored for simplicity. The G_0 is assumed unchanged during the simulation for both uneroded and eroded specimens based on the observation above.

4.4.3 Simulation of eroded specimens and evaluation of the slope of NCL (λ)

Figure 4.19 shows the simulation results for the eroded specimens. Here, λ and R_0 are considered to be fitting parameters, which are obtained by trial and error to fit the stress-strain response of the experimental results for eroded soils. The numerical simulation can capture the basic features of eroded specimens under the drained triaxial shearing condition. The predicted deviatoric stress is smaller than the experimental one at the smaller strain level, which could be due to the rearrangement of soil particles after the seepage test. This rearrangement would have reinforced the soil structure in the experiment. However, at the larger strain level, the predicted deviatoric stress is larger than the experimental result. It is supposed that the structure formed has been destroyed under the larger deviatoric stress. In other words, interlocking formed by clogged fines may have been broken in this stage in the experiment, but this appears less in the simulation. The predicted volumetric strains under 50 kPa, 100 kPa confining pressures are almost the same as the experimental ones at the larger strain level. The final axial strain under 200 kPa confining pressure stops around 11%, at which the predicted volumetric strain is larger than the experimental result. However, the predicted and experimental volumetric strains under 200 kPa may well be similar in the larger axial strain. When it comes to the volumetric strains under all mean effective stresses in the axial strain from 0 ~ 10%, all volumetric strains are overestimated. This is presumably

because Poisson's ratio is kept unchanged during the simulation. Parameters obtained from this back analysis are summarized in Table 4.8.

Table 4.8 Parameters for eroded specimens for Ke and Takahashi (2015)

Specimens	λ	M	R_0	e_{er}	FC_∞
35E-50	0.072	1.47	0.67	1.01	8.1%
35E-100	0.069	1.51	0.83	0.92	15.5%
35E-200	0.064	1.53	0.94	0.77	24.6%

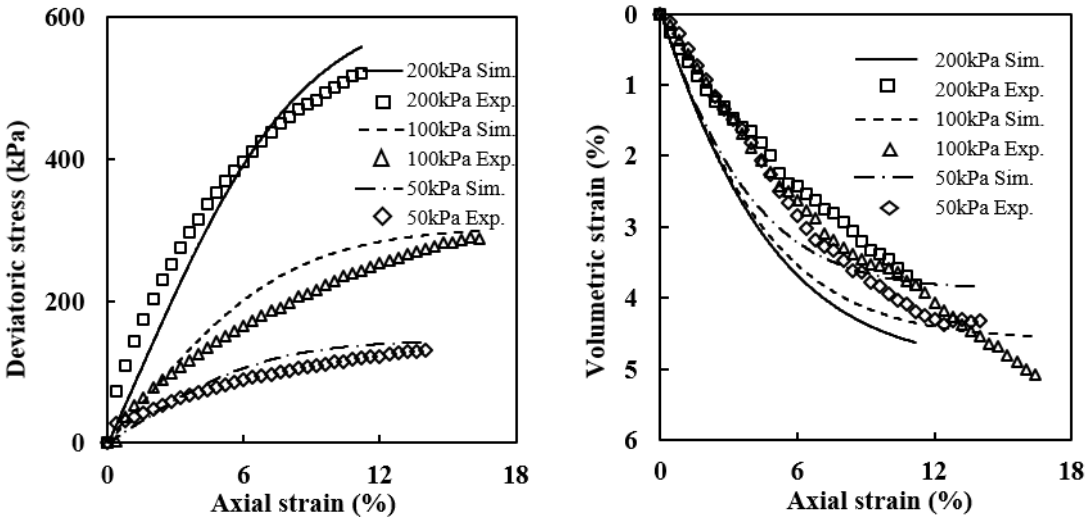

(a)Deviatoric stress-axial strain response (b)Volumetric strain-axial strain response

Figure 4.19 Predictions of mechanical behavior of eroded specimens under drained triaxial shearing (Experimental data from Ke and Takahashi, 2015)

The slope of the normal compression line (λ) can be estimated with a linear empirical equation with a single soil parameter such as liquid limit for clay. For high plastic soils, as both water content and void ratio have a linear relation with liquid limit, they can also be used for estimation of the slope of the normal compression line (Al-Khafaji and Andersland, 1992). The compression of sand is mostly affected by its structure and particle re-orientation (Sowers, 1979). For both low plastic soils and high plastic sand and silts, Sowers (1979) found the linear relation between the void ratio and the compression index. A similar expression will be used later to examine the relation between the slope of the normal compression line and the void ratio before shearing.

During the process of suffosion, the loss of fines may result in a larger void ratio, accompanied by the rearrangement of particles. Soils with a larger void ratio may produce larger volume change under isotropic compression. Both fines content and void ratio may have effects on the compression index. Here it is assumed that the void ratio has a greater impact on the compression index compared with fines content, and the void ratio is chosen as an explaining variable in the formulation of the compression index. The values of void ratio before shearing and slope of normal compression line for both uneroded and eroded specimens are summarized in Tables 4.5 and 4.8, and the relation between the slope of normal compression line and initial void ratio before shearing is fitted as shown in Fig. 4.20 with the equation below:

$$\lambda = a_4 \cdot e_{bs} + b_4 \tag{4.16}$$

where a_4=0.045, b_4=0.028, e_{bs} denotes the initial void ratio before shearing, which includes the initial void ratio of the uneroded soils after consolidation and the post-erosion void ratio of the internally eroded soils. The slope of the normal compression line increases with an increasing void ratio before shearing due to suffosion.

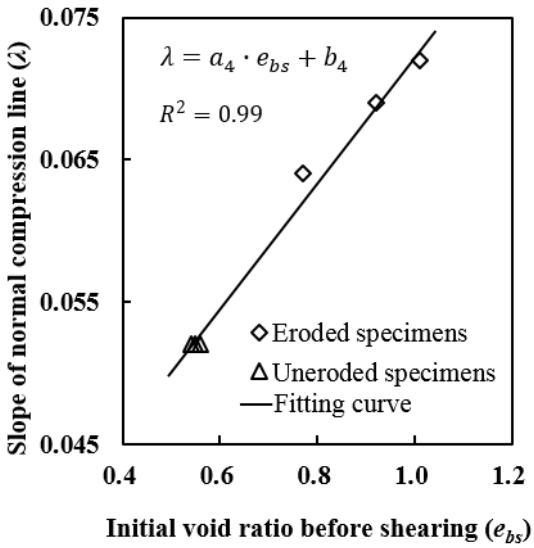

Figure 4.20 Change in the slope of normal compression line with initial void ratio before shearing (Experimental data from Ke and Takahashi, 2015)

4.4.4 Influence of initial void ratio before shearing on the initial stress ratio

The initial stress ratio (R_0) for the eroded soil is estimated by back analysis. The over-consolidation properties of the soils can be examined by the reciprocal of the initial stress ratio. As the initial stress ratio denotes the size ratio of the initial subloading surface to the initial normal yield surface, the smaller value of the initial stress ratio corresponds to the larger over-consolidation ratio or highly structured nature of the soil.

Both fines content and void ratio change with seepage flow. The fines continue decreasing and tend to be unchanged under a constant flow rate. The void ratio of the soils increases gradually, during which the new arrangement is formed. Hájek *et al.* (2009) selected void ratio as the state variable to simulate the mechanical behavior of soils with different over-consolidation ratios. It is reasonable to select the initial void ratio to be an explaining variable for the initial stress ratio in this study. Both coarse particles and fines take part in the force chain when the fines content is around 35%. However, with the increase of the void ratio, more coarse particles take part in the force chain. In this case, more pressure may act on the supporting structures (Hanna and Romhein, 2008), which causes an increase in the over-consolidation ratio. The interlocking prior to shearing seems stronger after suffosion, along with an increase in the void ratio, which also makes the over-consolidation ratio larger (Mahmoudi *et al.*, 2018).

Figure 4.21 plots the estimated initial stress ratio against the initial void ratio before shearing for different confining pressures. With the increase of the initial void ratio before shearing, the initial stress ratio decreases, which means the suffosion makes the over-consolidation ratio larger or makes the soil highly structured condition. However, the impact of the suffosion-induced structure reinforcement is small when we focus on the variation of the initial stress ratio. At the same time, this temporary reinforcement is easy to fade with the continuing triaxial shearing.

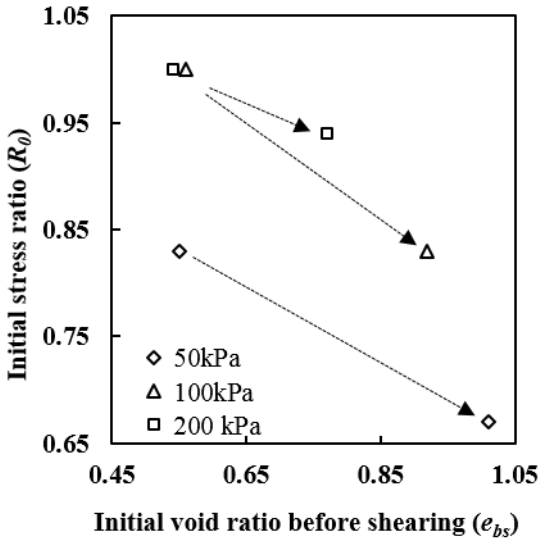

Figure 4.21 Estimated initial stress ratio against the initial void ratio before shearing for Ke and Takahashi (2015)

4.5 Summary

Seepage tests followed by both drained and undrained triaxial shearing are studied to investigate the variations of mechanical behavior of the soils subjected to internal erosion. The erosion phenomena and intergranular void ratio play an important role in the alteration of mechanical behavior. For suffosion, the drained deviatoric stress of eroded soils is smaller than that of uneroded soils, while the undrained deviatoric stress of eroded soils is larger than that of uneroded soils. The volumetric strain of eroded loose soils shows a minor change and decreases, while the eroded dense soils become contractive under the drained condition in many of the literature. For suffusion, when the intergranular void ratio is relatively low, the deviatoric stress of eroded soils is smaller than that of uneroded soils under the undrained condition. When the intergranular void ratio is close to the maximum void ratio of the pure coarse particles, the increase of fines causes a decrease in the deviatoric stress under the undrained condition.

The subloading Cam-clay model predicts the stress-strain behavior of the original soils under the drained condition well. Parameter study of the soils with suffosion under the drained condition is conducted based on the subloading Cam-clay model. It is identified that the

slope of the normal compression line (λ) and initial stress ratio (R_0) are the key parameters to characterize the suffosion effects on the mechanical behavior of the gap-graded sandy soils. Through back analysis, evolutions of the slope of the normal compression line and initial stress ratio are quantified. Since the larger void ratio soil exhibits the larger volume change, the initial void ratio before shearing is selected as an explaining variable for the slope of the normal compression line, and it is found that the slope of the normal compression line has a positive correlation with the initial void ratio before shearing. The initial void ratio before shearing can also be the explaining variable for the initial stress ratio, and it is found that the initial stress ratio decreases with the increase of the initial void ratio before shearing. This means that the suffosion makes the over-consolidation ratio larger or makes the soil highly structured condition.

Based on the experimental observations, the internally eroded loose soils show a sudden change in the deviatoric stress at the smaller axial strain level (less than 1%). In the present study, this feature is ignored for simplicity. However, this may be associated with the reinforcing effect of the clogged fines (Ke and Takahashi, 2015), and further studies regarding this effect would be worthwhile.

CHAPTER 5

MODIFICATION OF THE SUBLOADING CAM-CLAY MODEL

5.1Introduction

The constitutive models with reasonable accuracy, which can express the strength and deformation characteristics of the internally eroded soils, are required to solve the geotechnical problems. In this chapter, the modified subloading Cam-clay model incorporated with the normal yield surface for the internally eroded soils is proposed. In the following sections, the development of the normal yield surface for eroded soils is presented in detail. The determination method of the erosion-related model parameters is also explained.

5.2 Modified model description

The modified model is based on the subloading Cam-clay model. Liu and Carter (2002) proposed a new structured Cam-clay model based on the modified Cam-clay model, which introduced the effect of structure. Through the change in the initial yield surface, volumetric strain, and shear strain, the proposed model could predict the mechanical behavior of the structured soils. Considering the influence of temperature on the mechanical behavior of granular materials, the subloading Cam-clay model was modified by introducing the concept the equivalent stress (Zhang *et al.*, 2012). The subloading surface was also modified to model the mechanical behavior of cement-treated soils (Gai and Sánchez, 2019). The increased amount of cement is a process that strengthens the soils.

The erosion has different effects, i.e., the deviatoric stress at the large strain level decreases after the erosion for both loose and dense soils under the drained triaxial shearing condition. The volumetric strain of eroded loose soils decreases while the eroded dense soils become

less dilative or become contractive after erosion. The normal yield surface of the eroded soils varies after the internal erosion. The following modified subloading Cam-clay model is inspired by the modified model for the cement-treated soils by Gai and Sánchez (2019).

5.2.1 Modified normal yield surface of eroded soils

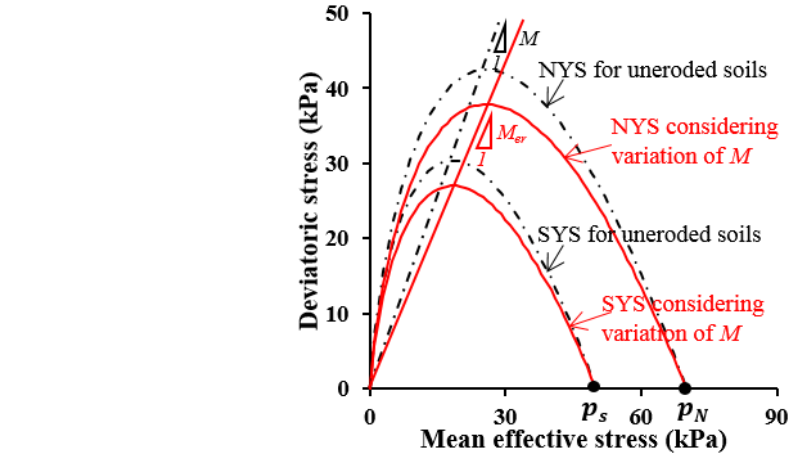

(a)Variation of the shape of the yield surface

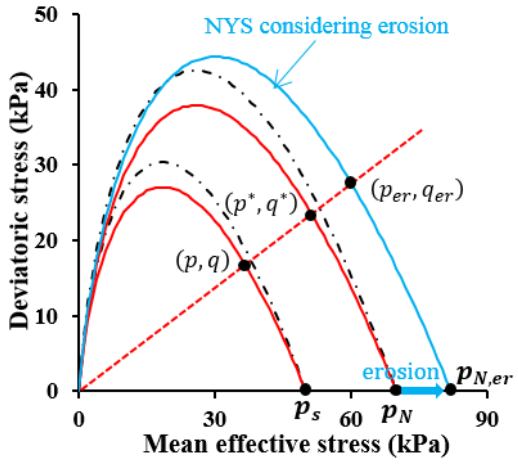

(b)Variation of yield surface for loose soils

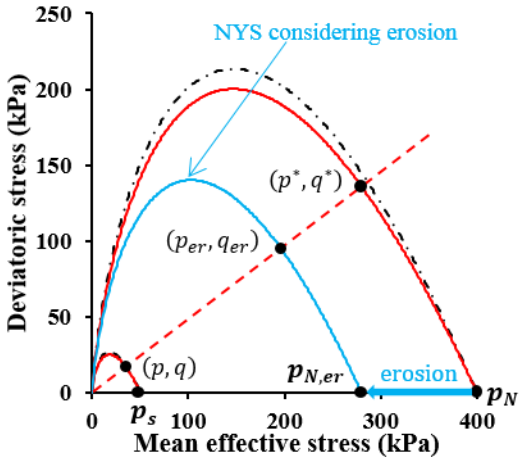

(c)Variation of yield surface for dense soils

Figure 5.1 Concept of normal yield surface for the eroded soils (a and b: data from 35N-50 and 35E-50, Ke and Takahashi 2015; c: data from 35E-50 of Group B with 10% cumulative fines loss, Chen *et al*., 2016; NYS: normal yield surface; SYS: subloading yield surface)

Based on the analysis in Subsection 4.4.1, the critical stress ratio (M) decreases after erosion, which can cause the change of shape for the yield surface (Fig. 5.1a). From the variation of the initial stress ratio (R_0) after erosion in Subsection 4.4.4, we can know that the normal yield surface of the loose soils expands after erosion, which indicates that the structure of

the loose soils is reinforced after the seepage tests, but this kind of reinforcement was weak and easy to collapse. However, the erosion could cause the shrinkage of the normal yield surface for the dense soils as the deviatoric stress decreases and the volumetric strain becomes contractive after erosion. The concept of the normal yield surface of eroded soils is shown in Figs 5.1b and 5.1c.

Based on the geometrical relations between different yield surfaces, we can obtain:

$$\frac{p}{p_S} = \frac{p_{er}}{p_{N,er}} = \frac{p^*}{p_N} \tag{5.1}$$

$$\frac{q}{p} = \frac{q_{er}}{p_{er}} = \frac{q^*}{p^*} \tag{5.2}$$

where (p, q) represents the current stress state; (p_{er}, q_{er}) is the stress state point on the normal yield surface for the eroded soil; (p^*, q^*) is the stress state point on the normal yield surface for the uneroded soil. p_s, $p_{N,er}$, p_N are the intersections of subloading surface, normal yield surface for the internally eroded soils, and normal yield surface for the uneroded soils with the mean effective stress axis respectively.

The normal yield surface for the eroded soils can be expressed as:

$$f = C_p \ln \frac{p_{er}}{p_{N,er}} + D \frac{q_{er}}{p_{er}} = 0 \tag{5.3}$$

Similarity ratio (stress ratio) R, $0 < R \leq 1$, is the size ratio of the subloading yield surface to the normal yield surface of uneroded soils:

$$R = \frac{p}{p^*} = \frac{q}{q^*} = \frac{p_S}{p_N} \tag{5.4}$$

Similarity ratio of the eroded soils R_{er}, is the size ratio of the normal yield surface for the eroded soils to the normal yield surface for the uneroded soils:

$$R_{er} = \frac{p_{er}}{p^*} = \frac{q_{er}}{q^*} = \frac{p_{N,er}}{p_N} \tag{5.5}$$

For eroded loose soils, $R_{er} \geq 1$. When R_{er} decreases, the effect of erosion-induced

reinforcement decreases. When the effect of the erosion does not exist, R_{er} equals to one. For eroded dense soils, $R \leq R_{er} \leq 1$. When R_{er} gets closer to R, the effect of over-consolidation disappears. When the effect of the erosion does not exist, R_{er} also equals to one.

The normal yield surface for the eroded soils can be written as below:

$$f = C_p \ln\left(\frac{p_{er}}{p_0} \cdot \frac{p_0}{p_{N,er}}\right) + D\frac{q_{er}}{p_{er}} = 0 \tag{5.6}$$

where p_0 is the reference stress.

If we assume that, for the normally and isotropically consolidated eroded soils, the plastic volumetric strain can be obtained as:

$$\varepsilon_v^p = C_p \ln\frac{p_{N,er}}{p_0} \tag{5.7}$$

Equation (5.6) can be written as:

$$f = C_p \ln\frac{p_{er}}{p_0} - \varepsilon_v^p + D\frac{q_{er}}{p_{er}} = 0 \tag{5.8}$$

This equation can be rearranged in the form of the current stress state (p, q) as below:

$$f = C_p \ln\left(\frac{p}{p_0} \cdot \frac{p_{er}}{p^*} \cdot \frac{p^*}{p}\right) - \varepsilon_v^p + D\frac{q}{p} = 0 \tag{5.9}$$

Substituting Eqns. (5.4) and (5.5) into Eqn. (5.9), we can obtain the following subloading surface of the eroded soils:

$$f = C_p \ln\frac{p}{p_0} + C_p \ln R_{er,l} - C_p \ln R - \varepsilon_v^p + D\frac{q}{p} = 0 \tag{5.10}$$

5.2.2 Plastic potential, flow rule, and consistency condition

The associated flow rule is applied to the subloading surface. The plastic volumetric strain increment and plastic shear strain increment can be obtained from the following equations:

$$d\varepsilon_v^p = \Lambda \frac{\partial f}{\partial p} \tag{5.11}$$

$$d\varepsilon_q^p = \Lambda \frac{\partial f}{\partial q} \tag{5.12}$$

in which Λ is the plastic multiplier. The hardening law of R is expressed as:

$$dR = -\frac{m_R}{D} \ln R \cdot d\varepsilon_q^p \tag{5.13}$$

where m_R is a material constant, determined by the degrading rate of the over-consolidation.

The construction of the evolution law of R_{er} considers that the increment of R_{er} is related to the plastic shear strain increment. Then the evolution law of R_{er} is expressed as:

$$dR_{er} = h_0 \cdot \left(\frac{1}{R_{er}} - 1\right) \cdot d\varepsilon_q^p \tag{5.14}$$

where h_0 is a material constant, which is determined by the degrading rate of the effect caused by erosion.

Since the current stress state remains on the subloading surface during the plastic flow, the consistency equation is applied to the subloading surface of the eroded soils, as shown:

$$df = \frac{\partial f}{\partial p} dp + \frac{\partial f}{\partial q} dq + \frac{\partial f}{\partial R} dR + \frac{\partial f}{\partial \varepsilon_v^p} d\varepsilon_v^p + \frac{\partial f}{\partial R_{er}} dR_{er} = 0 \tag{5.15}$$

The plastic multiplier can be obtained as:

$$\Lambda = \frac{\frac{\partial f}{\partial p} \cdot K \cdot d\varepsilon_v + \frac{\partial f}{\partial q} \cdot 3G \cdot d\varepsilon_q}{K \cdot \left(\frac{\partial f}{\partial p}\right)^2 + 3G \cdot \left(\frac{\partial f}{\partial q}\right)^2 + H} \tag{5.16}$$

where H is the hardening function and is expressed as:

$$H = -\frac{\partial f}{\partial \boldsymbol{k}} \cdot \frac{\partial \boldsymbol{k}^T}{\partial \varepsilon_{ij}^p} \cdot \frac{\partial f}{\partial \sigma_{ij}} \tag{5.17}$$

where $\boldsymbol{k}$ indicates the hardening parameters in this study, ε_v^p, R, R_{er} respectively.

5.2.3 Stress-strain relation

The elastoplastic equation with the triaxial stress and strain parameters is expressed as:

$$\begin{pmatrix} dp \\ dq \end{pmatrix} = \boldsymbol{D}_{ep} \begin{pmatrix} d\varepsilon_v \\ d\varepsilon_q \end{pmatrix} \tag{5.18}$$

where $\boldsymbol{D_{ep}}$ is the elastoplastic stiffness matrix, $\boldsymbol{D}_{ep} = \boldsymbol{D}_e - \frac{\boldsymbol{D}_e \partial \boldsymbol{f} \partial \boldsymbol{f}^T \boldsymbol{D}_e}{\partial \boldsymbol{f}^T \boldsymbol{D}_e \partial \boldsymbol{f} + H}$, in which $\boldsymbol{D}_e = \begin{bmatrix} K & 0 \\ 0 & 3G \end{bmatrix}$, and $\partial \boldsymbol{f}^T = \begin{Bmatrix} \frac{\partial f}{\partial p} & \frac{\partial f}{\partial q} \end{Bmatrix}$. K and G can be obtained from the equations below:

$$G = G_0 \frac{(2.97 - e)^2}{1 + e} \sqrt{p p_0} \quad , \quad K = G \frac{2(1 + \nu)}{3(1 - 2\nu)} \tag{5.19}$$

5.3 Effects of the erosion on the model parameters

In Chapter 4, the tests done by Ke and Takahashi (2015) are used to examine the relation between the key model parameters and the parameters that represent the state of the soils. In addition to this, the tests by Chen *et al.* (2016) and Li *et al.* (2020), which are introduced in Chapter 3, are used to examine the effects of the erosion on the model parameters

.

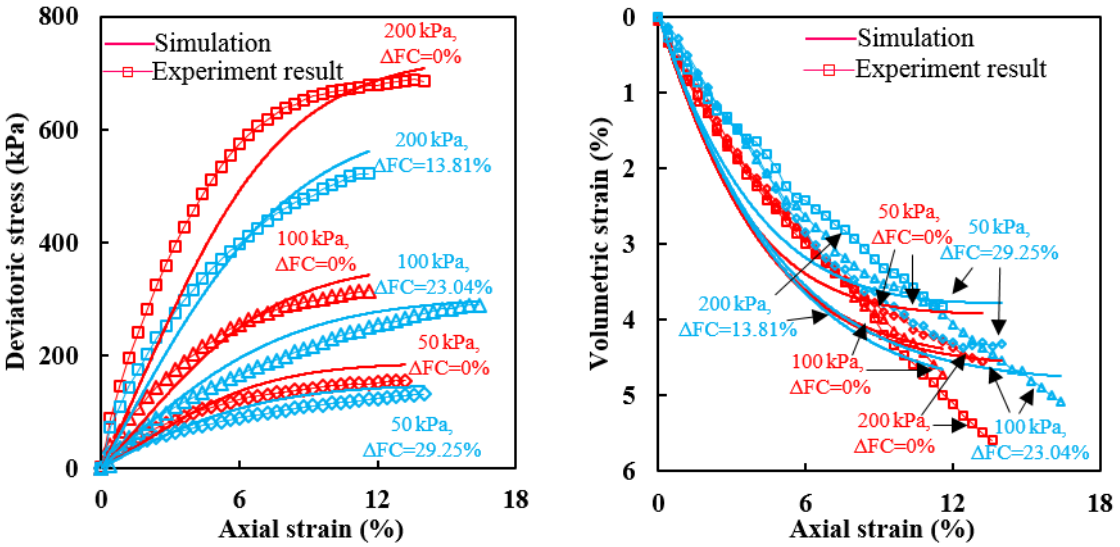

(a)Deviatoric stress-axial strain response (b)Volumetric strain-axial strain response

Figure 5.2 Typical simulation results of drained triaxial shearing through the modified model on loose soils with and without erosion (Experimental data from Ke and Takahashi, 2015)

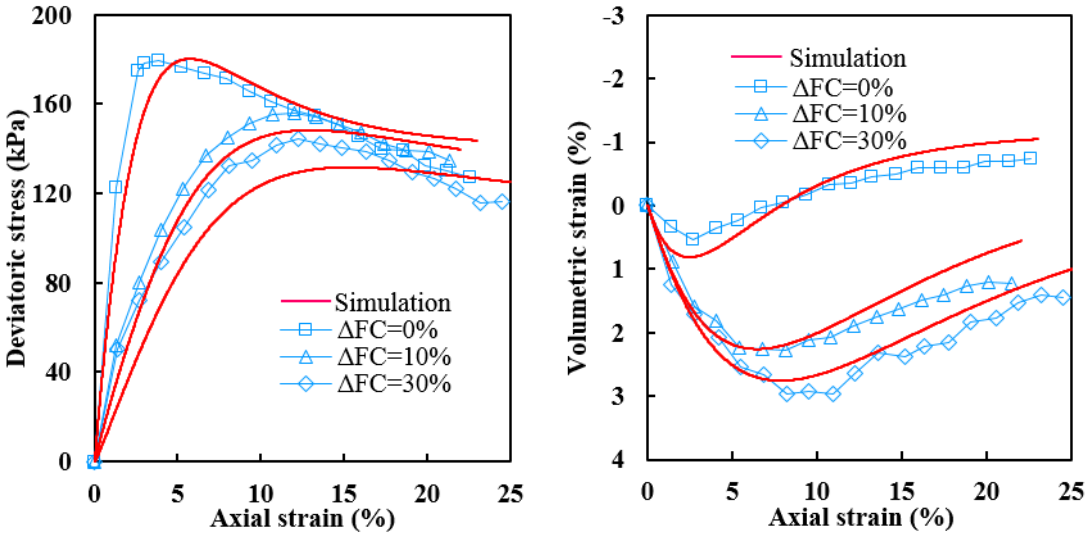

(a)Deviatoric stress-axial strain response (b) Volumetric strain-axial strain response

Figure 5.3 Simulation results of drained triaxial shearing through the modified model on dense soils with and without erosion (Group B, Experimental data from Chen *et al.*, 2016)

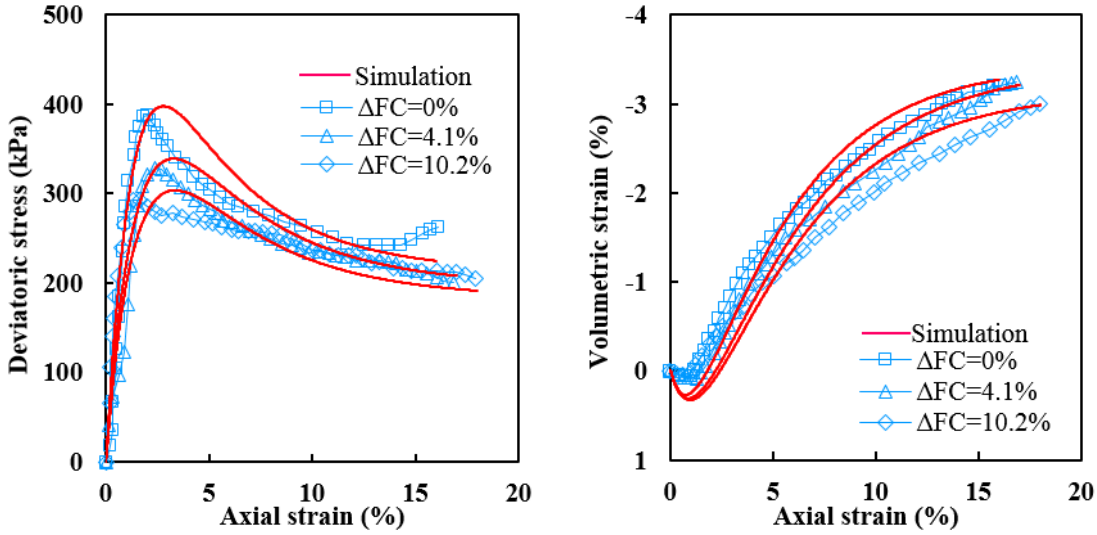

(a)Deviatoric stress-axial strain response (b) Volumetric strain-axial strain response

Figure 5.4 Simulation results of drained triaxial shearing through the modified model on dense soils with and without erosion (Experimental data from Li *et al.*, 2020)

The modified subloading Cam-clay model is used to predict the mechanical behavior of the eroded soils. The stress behavior of both uneroded and eroded loose soils can be predicted. The contractive trend of the volumetric strain for the eroded loose soils under 50 kPa confining pressure can be captured. However, the predicted volumetric strain for both uneroded and eroded loose soils under 100 kPa and 200 kPa confining pressures are similar,

which is due to the underestimation of the volumetric strain of the uneroded loose soils (Fig. 5.2). The modified subloading Cam-clay model can capture the main features of both uneroded and the eroded soils dense soils with different cumulative fines losses (Fig. 5.3 and 5.4). The model parameters from tests and back analysis are summarized in Table 5.1, in which G_0 is considered to be unchanged after erosion, and h_0 is obtained by trial and error to fit the stress-strain response of the experimental results for eroded soils.

Table 5.1 Model parameters used in the modified subloading Cam-clay model

Samples	e_c	ΔFC	λ	κ	M	G_0/MPa	v	R_0	m_R	R_{er}	h_0	References
35E-50	0.55	29.25%	0.072	0.014	1.47	100	0.2	0.71	0.2	1.17	100	Ke and
35E-100	0.56	23.04%	0.069	0.014	1.51	100	0.2	1	0.2	1.11	100	Takahashi
35E-200	0.54	13.81%	0.064	0.014	1.53	100	0.2	1	0.2	1.06	100	(2015)
35E-50	0.377	0%	0.045	0.01	1.45	100	0.3	0.125	0.3	1	100	Group B
35E-50	0.377	10%	0.084	0.01	1.36	100	0.3	0.125	0.3	0.7	100	soils, Chen
35E-50	0.377	30%	0.098	0.01	1.28	100	0.3	0.125	0.3	0.625	100	*et al.* (2016)
32E-50	0.33	0%	0.060	0.02	1.76	150	0.3	0.048	0.5	1	200	Li *et al.*
32E-50	0.33	4.1%	0.065	0.02	1.70	150	0.3	0.048	0.5	0.85	200	(2020)
32E-50	0.33	10.2%	0.068	0.02	1.65	150	0.3	0.048	0.5	0.78	200	

Note: "0.33" is the void ratio after consolidation for the case of 32E-50, which is not given in the original paper and is calculated based on Eqn. (3.6).

5.3.1 Fines content-dependent angle of shearing resistance at the critical state (φ)

The critical stress ratio (M) can be estimated from the critical strength of the stress path. When the fines content is smaller than the threshold fines content, the angle of shearing resistance at critical state ($M = 6\sin\varphi/(3-\sin\varphi)$) increases with the final fines content. The angle of shearing resistance at the critical state is affected by many factors, such as particle shape, fines content, particle size distribution, and so on. The relations between the angle of shearing resistance at the critical state and final fines content for both loose and dense soils are plotted in Fig. 5.5 and are fitted by:

$$\varphi(FC_\infty) = a_3 \cdot FC_\infty + b_3 \tag{5.20}$$

where a_3 is the gradient of the angle of shearing resistance at the critical state, b_3 is the angle of shearing resistance at a critical state for the soils when FC_∞ equals to zero.

Figure 5.5 indicates that the angle of shearing resistance at the critical state increases with the final fines content when the final fines content is smaller than the threshold fines content. Depending on the particle shape and mineral composition, the gradient of the angle of the shearing resistance at the critical state (a_3) and the angle of shearing resistance at critical state for the soils without fines (b_3) are different. The expected curves for uneroded soils are plotted (Ke and Takahashi, 2015; Li *et al*., 2020), and the explanation of the variation is the same as that in Subsection 4.4.1. For the eroded soils after salt dissolution, the effect of heterogeneity of particle size distribution can be ignored. In this case, the expected curve of the uneroded soils might be the same as that of the eroded soils with the same final fines content.

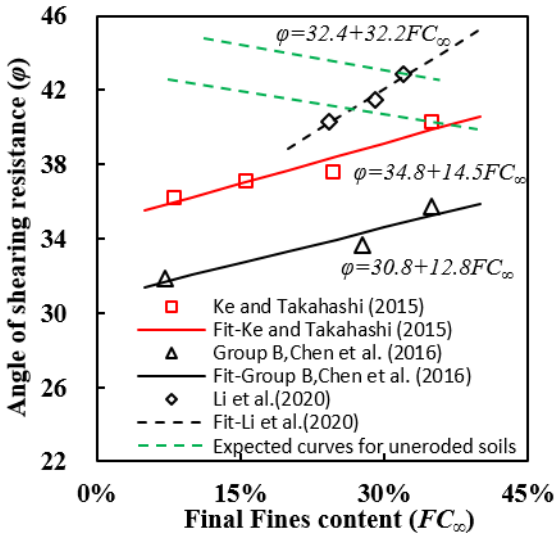

Figure 5.5 Relation between the angle of shearing resistance at the critical state and the final fines content

5.3.2 Initial void ratio before shearing-dependent slope of the normal compression line (λ)

The slope of the normal compression line is normally obtained from the isotropic

compression tests. It is also possible to estimate the slope of the normal compression line from the back analysis. Based on the study in Subsection 4.4.3, it is reasonable to assume that the slope of the normal compression line has a linear relation with the initial void ratio before shearing (Fig. 5.6), as follow:

$$\lambda(e_{bs}) = a_4 \cdot e_{bs} + b_4 \tag{5.21}$$

where a_4 is the gradient of the λ, b_4 is the intercept of the λ-axis, e_{bs} denotes the initial void ratio before shearing.

Figure 5.6 indicates that the slope of the normal compression line increases with the initial void ratio before shearing for all the examined soils. Depending on the initial fines contents and the material compositions, the gradient a_4 and the intercepts b_4 are different for different examined soils.

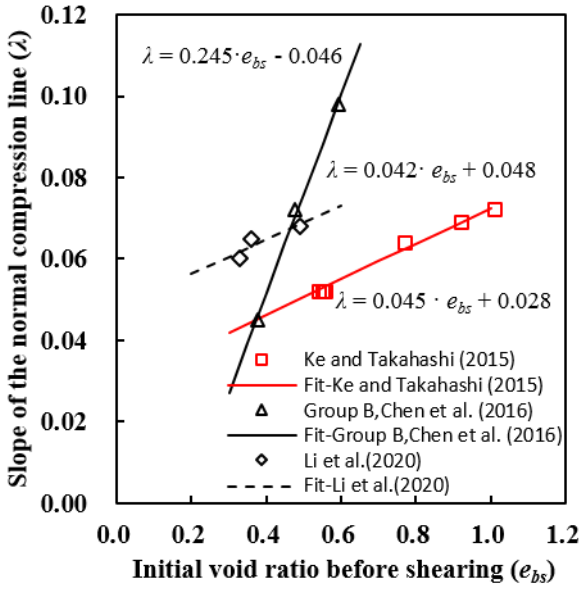

Figure 5.6 Relation between the slope of the normal compression line and the initial void ratio before shearing

5.3.3 Normalized cumulative fines loss-dependent initial similarity ratio

The initial similarity ratio of the eroded soils ($R_{er,0}$) should be determined by the extent of the erosion prior to shearing. The initial similarity ratio $R_{er,0}$ of the eroded soils is expressed by using $\Delta p_{N,0}$ as:

$$R_{er,0} = \frac{p_{N,er0}}{p_{N,0}} = \frac{p_{N,0} + \Delta p_{N,0}}{p_{N,0}} \tag{5.22}$$

where $\Delta p_{N,0}$ is an initial stress parameter that represents the change in the size of the normal yield surface by erosion, $p_{N,0}$ is the initial intersection of the normal yield surface of uneroded soils and the mean effective stress axis (pre-consolidation stress). $\Delta p_{N,0}$ is assumed to be related to both the cumulative fines loss and initial fines content, expressed as:

$$\Delta p_{N,0} = \beta_0 \cdot \left(\frac{\Delta FC}{FC_0}\right)^{\alpha_0} \cdot p_{N,0} \tag{5.23}$$

where α_0 and β_0 are material constants. By substituting Eqn. (5.23) into Eqn. (5.22), we can obtain:

$$R_{er,0} = \frac{p_{N,0} + \beta_0 \cdot \left(\frac{\Delta FC}{FC}\right)^{\alpha_0} \cdot p_{N,0}}{p_{N,0}} = 1 + \beta_0 \cdot \left(\frac{\Delta FC}{FC_0}\right)^{\alpha_0} \tag{5.24}$$

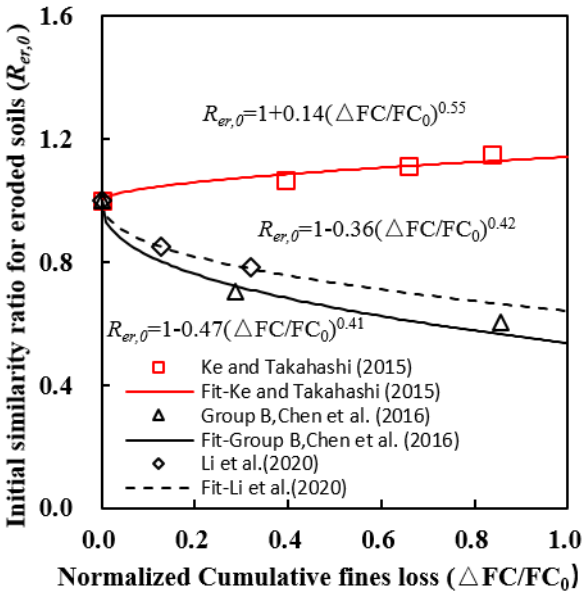

Figure 5.7 Relation between the initial similarity ratio and the normalized cumulative fines content

The initial similarity ratios can be obtained from the back analysis of different series of drained triaxial tests with different cumulative fines loss. The relations between the initial

similarity ratio and normalized cumulative fines loss for both loose and dense soils are plotted in Fig. 5.7. The initial similarity ratio for the dense soils decreases from one with the loss of fines, while the initial similarity ratio for the loose soils slightly increases with the loss of fines.

5.3.4 Determination of initial conditions considering the internal erosion

The shear behavior of soils is affected by the extent of the erosion. The above-mentioned parameters, such as the volumetric strain induced by erosion, the angle of shearing resistance at the critical state, the slope of the normal compression line, and the initial similarity ratio of eroded soils may have a great impact on the soil responses. By using the equations above and those shown in Chapter 3, it is possible to determine the parameters needed for the calculation of the responses of the internally eroded soils, as shown in Fig. 5.8.

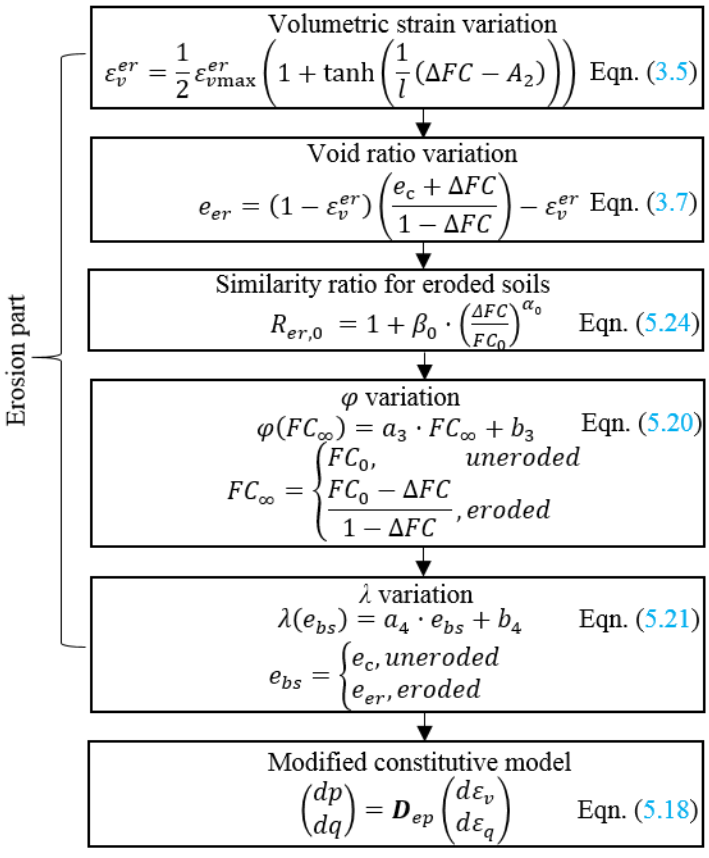

Figure 5.8 Determination of parameters for calculation of the responses of the internally eroded soils

5.4 Summary

Based on the back analysis and the experimental observations on the mechanical behavior of the eroded loose and dense soils, the similarity ratio of the eroded soils that characterizes the normal yield surface of the eroded soils to the normal yield surface of the uneroded soils is introduced to consider the change in the size of the yield surface due to erosion and its decay with the shearing. The concept of the normal yield surface of the eroded soils is implemented into the subloading Cam-clay model.

From the experimental results and back analysis of the experimental results (Ke and Takahashi 2015; Chen *et al.*, 2016; Li *et al.*, 2020), key parameters of the modified model are identified, i.e., the post-erosion void ratio, the slope of normal compression line, the angle of shearing resistance at the critical state, and the similarity ratio for the eroded soils. The effects of the erosion on the modified model parameters are quantified. And the determination method of the erosion-related model parameters is proposed.

[This page intentionally left blank]

CHAPTER 6

PERFORMANCE OF THE MODIFIED SUBLOADING CAM-CLAY MODEL

6.1 Introduction

In this chapter, to evaluate the capability of the modified subloading Cam-clay model, a series of drained triaxial tests by Chen *et al.* (2016) and DEM calculations by Wang and Li (2015) with different cumulative fines losses under the same confining pressure (50 kPa) are simulated. To confirm the capability of the predictive equations of both the fines content and the volumetric strain and the modified subloading Cam-clay models, the laboratory seepage and drained triaxial tests conducted by Ke and Takahashi (2014a) are chosen in this chapter.

6.2 Simulation of drained triaxial tests on the eroded dense soils

The drained triaxial shearing tests (Group A soils, cf. Subsection 3.2.3) conducted by Chen *et al.* (2016), which has not been used in the previous Chapter, are used for the simulation. The poorly graded specimen was prepared by a mixture of the sand having different grain sizes. The drained triaxial shearing tests were conducted with 20% initial fines content under 50kPa confining pressure.

6.2.1 Calibration of the model parameters

The parameters of the modified subloading Cam-clay model can be divided into two parts: 1) the model parameters for the uneroded soil, the slopes of normal compression line and the swelling line in the e-ln p space (λ and κ), which can be obtained from the isotropic compression test. M is the critical stress ratio, which can be obtained from the triaxial shearing test. R_0 is the initial similarity ratio (stress ratio), and m_R is the degradation factor of the stress ratio, which can be obtained from the triaxial shearing tests. ν is Poisson's ratio, which is selected as 0.3. G_0 is a material constant, taken as 100 MPa. 2) the model

parameters for the eroded soil, h_0, α_0, β_0, a_3, a_4 are estimated by the calibration for the Group B soils (Figs. 5.6, 5.7, and 5.8 for Chen *et al*., 2016); A_2, l, $\varepsilon_{v\max}^{er}$ are estimated by the fitting of the erosion-induced volumetric strain against the cumulative fines loss of Group B soils (Fig. 3.22 for Chen *et al.*, 2016). All parameters are summarized in Tables 6.1 and 6.2.

Table 6.1 The material parameters and physical constants of the dense soils for Group A, Chen *et al.* (2016)

Case	Original Model Parameters							
	λ	κ	M	e_c	R_0	m_R	G_0	ν
Group A	0.055	0.01	1.35	0.461	0.12	0.3	100	0.3

Table 6.2 The erosion parameters of the dense soils for Group A, Chen *et al.* (2016)

Case	Erosion Parameters							
	h_0	α_0	β_0	A_2	l	$\varepsilon_{v\max}^{er}$	a_3	a_4
Group A	100	0.41	-0.47	19%	0.095	20%	12.8	0.245

6.2.2 Simulations of the drained triaxial tests on both uneroded and eroded dense soils

Figure 6.1 shows the comparisons between experimental and simulation results of the dense soils (Group A, Chen *et al.*, 2016). The soils were subjected to seepage flow, after which the drained triaxial tests were conducted. The soils have the same initial void ratio of 0.461 before erosion, exhibiting the dilative behavior. The deviatoric stress increases to the peak and then decreases with axial strain for all the cases. However, both peak strength and deviatoric stress at the critical state decrease for the soils with 5% and 15% cumulative fines loss. With the increase of cumulative fines loss, the volumetric strain becomes more contractive.

A good agreement is obtained between the experimental and simulation results. The modified constitutive model can capture the mechanical behavior of the internally eroded

soils at the dense state.

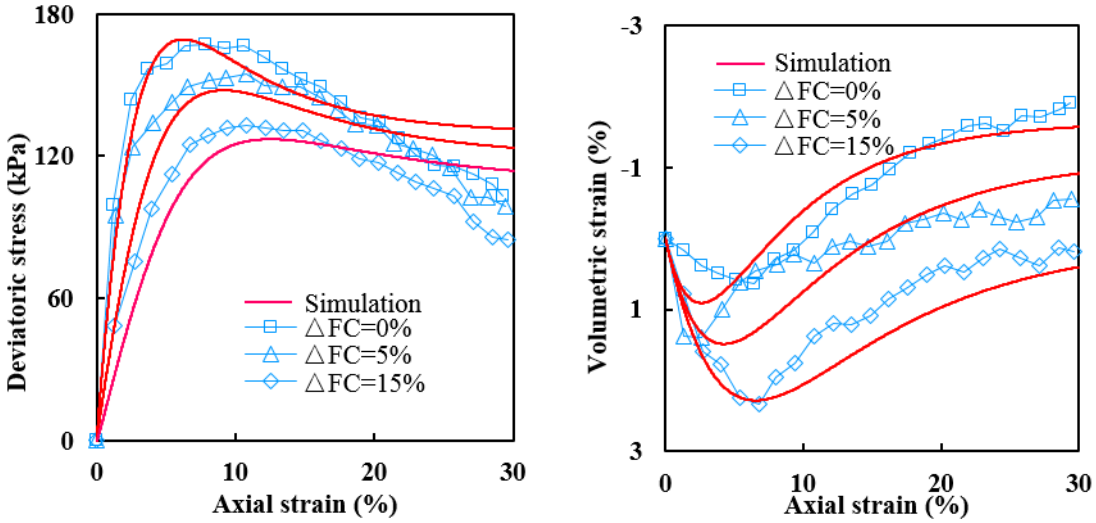

(a)Deviatoric stress-axial strain response (b)Volumetric strain-axial strain response

Figure 6.1 Comparison between experimental and simulation results of drained triaxial shearing on eroded dense soils (Group A, Experimental date from Chen *et al.*, 2016)

6.2.3 Effects of the degradation parameter h_0

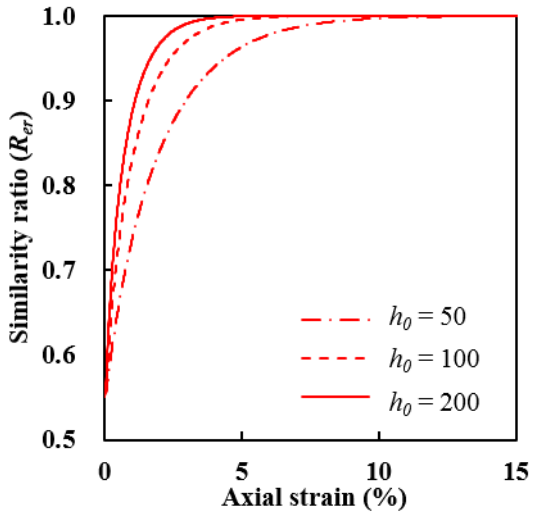

Figure 6.2 Variation of similarity ratio of the dense soils (R_{er}) along with axial strain under different degradation parameters

The parameter h_0 represents the degradation of the similarity ratio (R_{er}). The soils (Group A, Chen *et al.*, 2016) with 15% cumulative fines loss are considered to study the effect of the degradation parameter on the evolution of the similarity ratio for the eroded dense soils. Figure 6.2 shows the variation of the similarity ratio for the eroded dense soils under different

degradation parameters h_0. The similarity ratio for the eroded dense soils increases with shearing, finally reaches one, which indicates that the effect of erosion fades with the continuing shearing. The greater the value of the degradation parameter h_0, the faster the degradation of the erosion effect.

6.3 Comparison between the theoretical analysis and DEM simulation

The DEM model was established by Wang and Li (2015) to investigate the effect of internal erosion on the mechanical behavior of the soils. The specimen was made up of 40000 particles totally, with an initial fines content of 40%. The fines were directly deleted to simulate the process of internal erosion through some subroutines. In this subsection, the mechanical behavior of the soils with different cumulative fines losses (0%, 1%, and 3%) was simulated through the modified subloading Cam-clay model. After confirming that the simulation results through the modified subloading Cam-clay model agreed well with those through DEM simulations, the relations between the modified model parameters (similarity ratio and angle of shearing resistance at the critical state) and the erosion parameters (normalized cumulative fines loss and final fines content) could be obtained. Through these relations, the modified subloading Cam-clay model could predict the mechanical behavior of the soils with other cumulative fines losses (2% and 4%).

6.3.1 Determination of the modified model parameters

The drained triaxial tests on the dense soils with 0%, 1%, and 3% cumulative fines losses were simulated through the DEM simulation. The modified subloading Cam-clay model was employed to predict the mechanical behavior of the internally eroded soils under the 50 kPa confining pressure (Fig. 6.3). The main features of the eroded soils from both the DEM simulation results and the modified subloading Cam-clay model results are shown in Figure 6.3. As the cumulative fines losses are relatively small, deviatoric stress at the critical state after erosion shows a slight decrease. However, a clear reduction of the peak strength can be observed for the internally eroded soils. The specimen with the larger cumulative fines loss

has a larger remarkable reduction. The porosity increases during the triaxial shearing, which tends to the critical state with the shearing. The parameters of the modified model were summarized in Table 6.3.

Table 6.3 Model parameters used in the modified subloading Cam-clay model for Wang and Li (2015)

Samples	e_c	ΔFC	λ	κ	M	G_0/MPa	ν	R	m_R	$R_{er,0}$	h_0
E1	0.377	0%	0.042	0.01	0.73	150	0.2	0.04	1.5	1	-
E2	0.377	1%	0.042	0.01	0.70	150	0.2	0.04	1.5	0.9	200
E3	0.377	3%	0.042	0.01	0.68	150	0.2	0.04	1.5	0.6	200

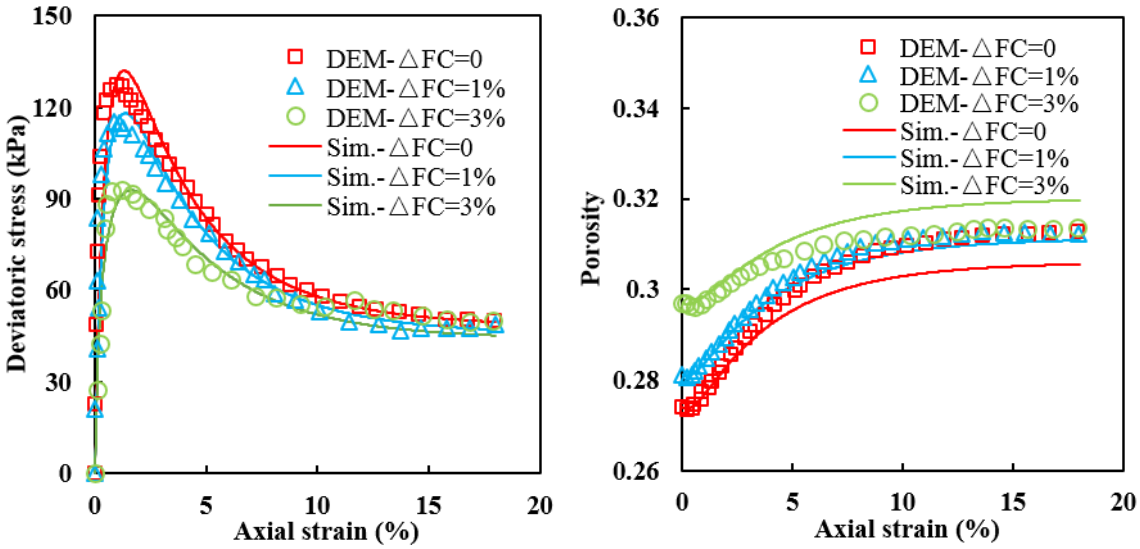

(a)Deviatoric stress-axial strain response (b)Relation between porosity and axial strain

Figure 6.3 Comparison between DEM simulation results and the modified Cam-clay simulation results of drained triaxial shearing on dense soils with 0%, 1%, and 3% cumulative fines losses (DEM simulation data from Wang and Li, 2015)

It was found that the volume did not change when the cumulative fines loss was less than 4%. The post-erosion void ratio can be calculated based on Eqn. (3.6) while ignoring the effect of the volumetric strain. The λ and κ are assumed to be unchanged because the cumulative fines losses are relatively small. The M and $R_{er,0}$ decrease after internal erosion, whose evolution laws with erosion parameters are plotted in Figs.6.4 and 6.5.

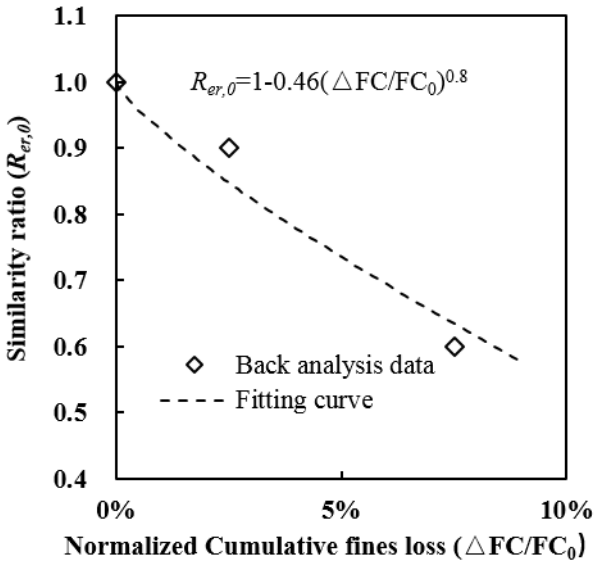

Figure 6.4 Relation between the similarity ratio and the normalized cumulative fines loss for the internally eroded soils with 0%, 1%, and 3% cumulative fines losses (Data from Wang and Li, 2015)

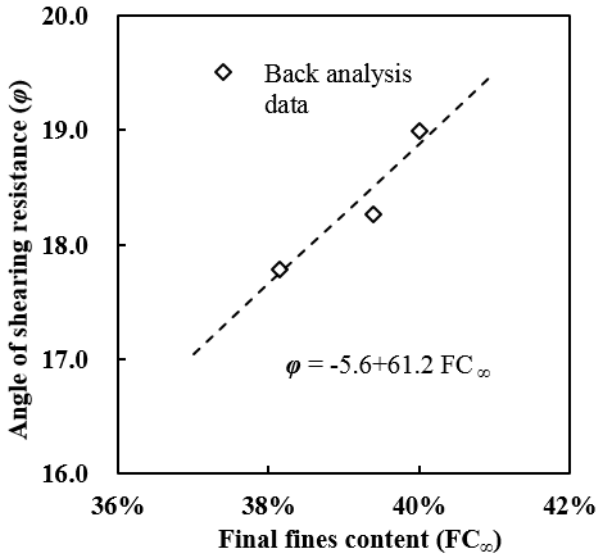

Figure 6.5 Relation between the angle of shearing resistance at the critical state and the final fines content for the internally eroded soils with 0%, 1%, and 3% cumulative fines losses (Data from Wang and Li, 2015)

6.3.2 Comparison between the theoretical results and DEM simulations

Wang and Li (2015) also simulated the drained triaxial tests of the soils under 50 kPa confining pressure with 2% and 4% cumulative fines losses through the DEM approach,

which were used to show the capability of the modified subloading Cam-clay model in this subsection. The parameters of the modified subloading Cam-clay model include two parts: 1) the model parameters for the uneroded soil, λ and κ are considered to be unchanged because of the small cumulative fines loss. M can be calculated based on the fitted equation in Fig. 6.5. R_0, m_R, ν, G_0 are also regarded unchanged after erosion for simplification. 2) the model parameters for the eroded soil, $R_{er,0}$ can be obtained from the fitted equation in Fig. 6.4. The parameters for the modified subloading Cam-clay model are summarized in Table 6.4.

Table 6.4 Model parameters used in the modified subloading Cam-clay model for Wang and Li (2015)

Samples	e_c	ΔFC	λ	κ	M	G_0/MPa	ν	R_0	m_R	$R_{er,0}$	h_0
E4	0.377	2%	0.042	0.01	0.69	150	0.2	0.04	1.5	0.74	200
E5	0.377	4%	0.042	0.01	0.66	150	0.2	0.04	1.5	0.54	200

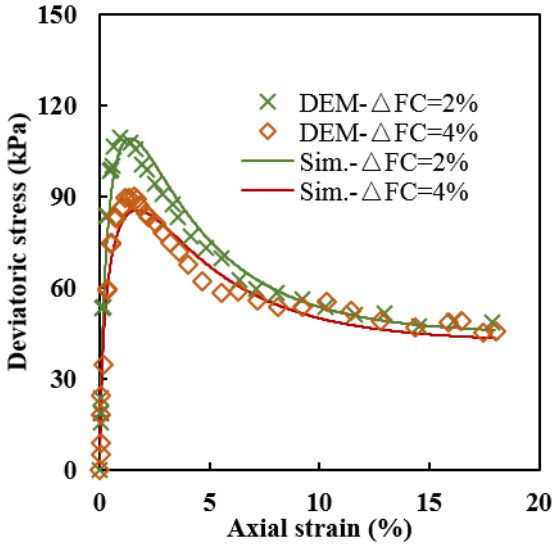

Figure 6.6 Comparison between DEM simulation results and the modified subloading Cam-clay simulation results of drained triaxial shearing on eroded dense soils with 2% and 4% cumulative fines losses (DEM simulation data from Wang and Li, 2015)

Figure 6.6 shows the comparisons between results from the modified subloading Cam-clay model and DEM simulation of the internally eroded soils with 2% and 4% cumulative fines losses. The soils have the same initial void ratios (0.377) before erosion, exhibiting the

dilative behavior. The deviatoric stress increases to the peak and then decreases for these two cases. The peak strength decreases with the increase of cumulative fines loss.

A good agreement is obtained between prediction results from the modified subloading Cam-clay model and DEM simulation. The modified constitutive model can capture the mechanical behavior of the internally eroded soils.

6.4 Model performance in seepage and drained triaxial tests (two-step calculation)

The seepage tests under 50 kPa confining pressure with 15%, 25%, and 35% initial fines contents were conducted by Ke and Takahashi (2014a), after which the drained triaxial tests were conducted on the internally eroded soils. The variation of the internal erosion process and triaxial responses of the soils could be predicted based on the proposed predictive equations of fines contents and volumetric strain, and the modified subloading Cam-clay model.

6.4.1 Estimation in seepage tests part

The specimens, a mixture of silica No.3 and No.8 sands, underwent a constant flow rate of 310 mL/min under the 50 kPa confining pressure. Eqn. (3.2) can be used to predict the final fines contents. The material parameters used in Eqn. (3.2) are the same as those for specimens with 35% initial fines content under different confining pressures 50 kPa, 100 kPa, and 200 kPa respectively. After obtaining the final fines content after the seepage flow, the erosion-induced volumetric strain can be achieved upon knowing the cumulative fines loss through Eqn. (3.5). The parameters used in Eqn. (3.5) can be obtained from Fig. 3.22 for the loose sand.

Finally, we can calculate the post-erosion void ratio through Eqn. (3.7). The estimated parameters of the specimens subjected to internal erosion with different initial fines contents are summarized in Table 6.5.

Table 6.5 Estimated parameters of the internally eroded soils with different initial fines contents for Ke and Takahashi (2014a)

Samples	e_c	FC_0	FC_∞	ΔFC	ε_v^{er}	e_{er}	e_s
15E-50	0.68	15%	3.70%	11.73%	0.73%	0.89	0.96
25E-50	0.57	25%	6.16%	20.08%	3.43%	0.90	1.02
35E-50	0.55	35%	8.63%	28.86%	4.16%	1.01	1.20

6.4.2 Prediction of drained triaxial shearing tests part

The drained triaxial shearing tests were conducted on the eroded specimens under 50kPa confining pressure. The modified subloading Cam-clay model is used to predict the mechanical behavior of the internally eroded soils with different initial fines contents. The model parameters of the uneroded soils contain λ, κ, M, R_0, ν, and G_0. The determination of these parameters has been introduced detailly in Subsection 6.2.1. The model parameters of the internally eroded soils are h_0, α_0, β_0, a_3, and a_4, which can be estimated by the calibration for the soils with 35% initial fines content under different confining pressures (Figs. 5.6, 5.7, and 5.8 for Ke and Takahashi, 2015). The parameters for both uneroded and internally eroded soils are summarized in Tables 6.6 and 6.7.

Table 6.6 Model parameters of the uneroded soils for Ke and Takahashi (2014a)

Samples	e_c	FC_0	λ	κ	M	G_0/MPa	ν	R_0	m_R	e_s
15N-50	0.68	15%	0.058	0.014	1.70	100	0.2	0.71	0.2	0.98
25N-50	0.57	25%	0.058	0.014	1.59	100	0.2	0.71	0.2	1.09
35N-50	0.55	35%	0.056	0.014	1.56	100	0.2	0.71	0.2	1.38

Table 6.7 Estimated parameters for the modified subloading Cam-clay model for Ke and Takahashi (2014a)

Samples	e_{er}	h_0	α_0	β_0	a_3	a_4
15E-50	0.89	100	0.55	0.14	14.5	0.045
25E-50	0.90	100	0.55	0.14	14.5	0.045
35E-50	1.01	100	0.55	0.14	14.5	0.045

Figures 6.7, 6.8, and 6.9 show the comparisons between experimental and simulation results of drained triaxial shearing tests on both uneroded and the internally eroded soils under 50 confining pressure with 15%, 25%, and 35% initial fines contents respectively. The modified subloading Cam-clay model can predict that both uneroded and internally eroded soils with smaller initial fines content have larger deviatoric stress than those with larger initial fines content; the deviatoric stress of the eroded soils is lower than that of the uneroded soils (Figures 6.7a, 6.8a, and 6.9a). However, the deviatoric stresses of both uneroded and internally eroded soils at the smaller strain level are underestimated, especially for the case with 15% initial fines contents. The possible reason may be that the soils prepared with 15% initial fines content have a strong structure, as there are more contacts between coarse particles in the soils with 15% initial fines content.

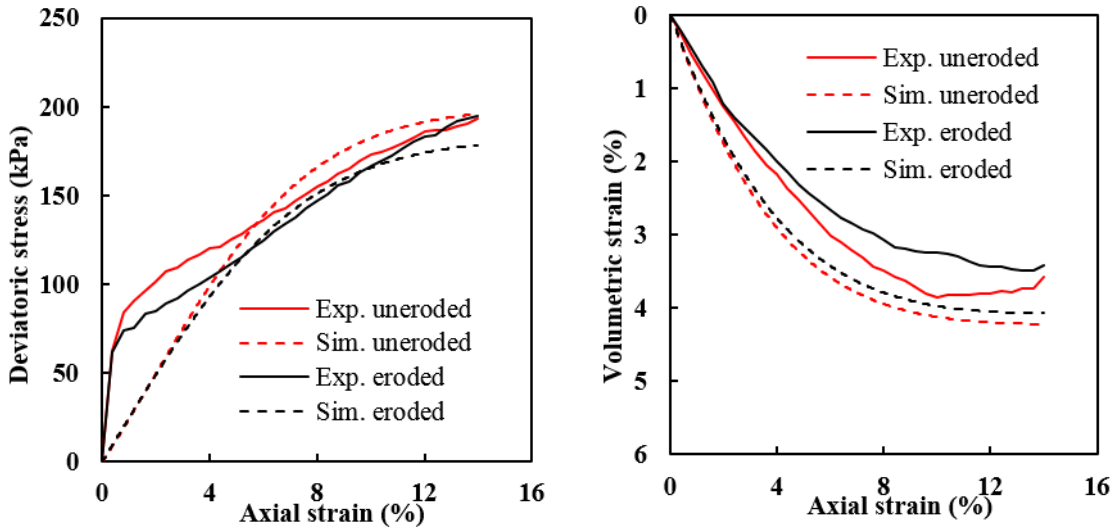

(a)Deviatoric stress-axial strain response (b)Volumetric strain-axial strain response

Figure 6.7 Comparison between experimental and simulation results of drained triaxial shearing tests on both uneroded and internally eroded soils with 15% initial fines content (Experimental data from Ke and Takahashi, 2014a)

The volumetric strains of both the uneroded soils and the internally eroded soils do not show a dramatic variation for the soils with 35% initial fines content (Fig. 6.9b). However, the volumetric strains of the internally eroded soils with 15% and 25% show a minor change and decrease after erosion (Figs. 6.7b and 6.8b). The modified subloading Cam-clay model can capture the feature that the volumetric strains of all internally eroded loose soils decrease

after erosion.

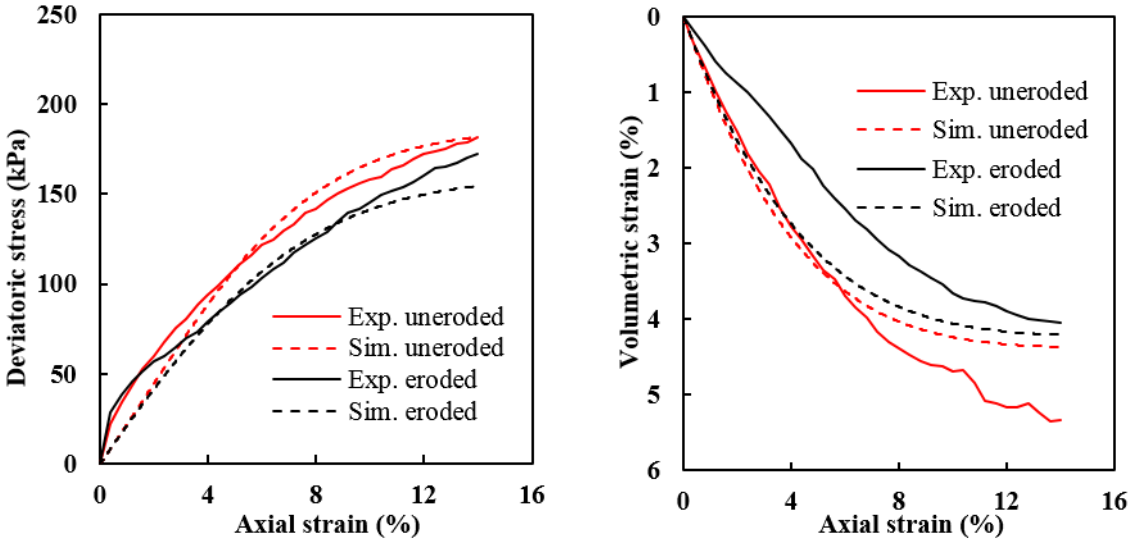

(a)Deviatoric stress-axial strain response (b)Volumetric strain-axial strain response

Figure 6.8 Comparison between experimental and simulation results of drained triaxial shearing tests on both uneroded and internally eroded soils with 25% initial fines contents (Experimental data from Ke and Takahashi, 2014a)

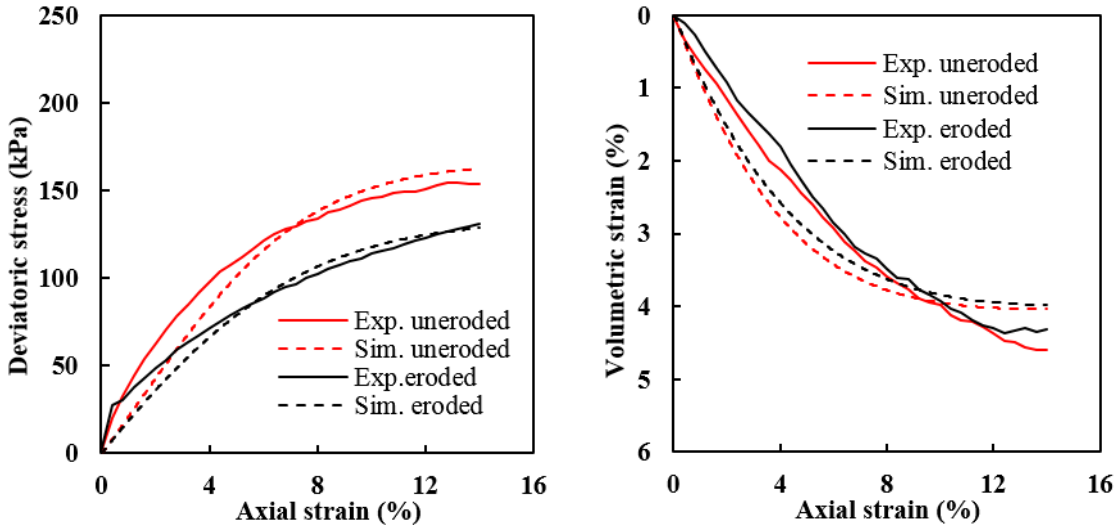

(a)Deviatoric stress-axial strain response (b)Volumetric strain-axial strain response

Figure 6.9 Comparison between experimental and simulation results of drained triaxial shearing tests on both uneroded and internally eroded soils with 35% initial fines content (Experimental data from Ke and Takahashi, 2014a)

Through the proposed predictive equations of fines content and the volumetric strain, the post-erosion void ratios under different initial fines contents are predicted. The mechanical behavior of both uneroded and internally eroded soils obtained through the modified

subloading Cam-clay model agrees reasonably well with the experimental results.

6.5 Applicability of the proposed model for the eroded soils

The predictive equations can be used to estimate the variation of some properties (e.g., fines content, volumetric strain) for the gap graded soils under the seepage flow. The proposed constitutive model can simulate the mechanical behavior of both uneroded and eroded gap graded soils under the drained condition. However, some limitations are existing in the proposed model.

When salt functions as fines under the seepage flow, all salt is dissolved after the seepage flow at a designated hydraulic gradient, which will cause a large volumetric strain (Fig. 6.10). If all the salt is replaced by the fines, fewer fines can be washed out under the seepage flow at the same hydraulic gradient as other factors (e.g., constriction size) can prevent fines from migrating. In this case, both volumetric strain and void ratio of the specimen mixed with fines are smaller than that of the specimen mixed with the salt after erosion. Compared with the mechanical behavior of the eroded specimen mixed with fines under the drain condition, the deviatoric stress of the specimen mixed with the salt under the drain condition becomes smaller and volumetric strain becomes contractive after salt dissolution.

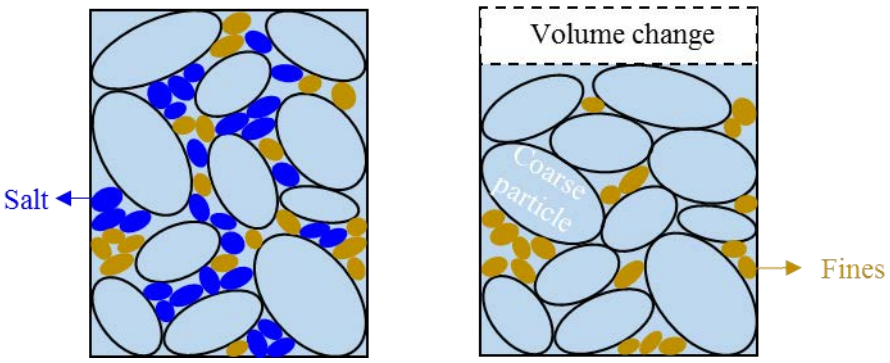

(a)Before dissolution (b)After dissolution

Figure 6.10 Variation of the specimen before and after the salt dissolution

The usage of the salt intends to investigate the variation of the mechanical behavior of the soils with different cumulative fines losses. Eqns. (3.2) and (3.4) for the estimation of the

fines content are not suitable for the specimen after salt dissolution. Eqn. (3.5) and (3.7) for the estimation of the erosion-induced volumetric strain and post-erosion void ratio are suitable for the specimen after salt dissolution. In the selected cases (Chen *et al*., 2016), the drained triaxial tests were conducted on the eroded specimens without any salt, i.e., salt did not participate in the stress transmission during the triaxial shearing. However, dissoluble chemicals, such as salt, take part in the stress transmission in the field. Therefore, the proposed constitutive model cannot simulate the variation of mechanical behavior of the soils suffering the chemical dissolution in the field.

Under the undrained condition, the prediction of the pore water pressure is highly related to the prediction of the volumetric strain under the drained condition. The simulated volumetric strain of the loose sand at the small strain is overestimated (Figs. 5.2 and 6.7), in which case the simulated pore water pressure of the loose sand at the small strain under the undrained condition may also be overestimated.

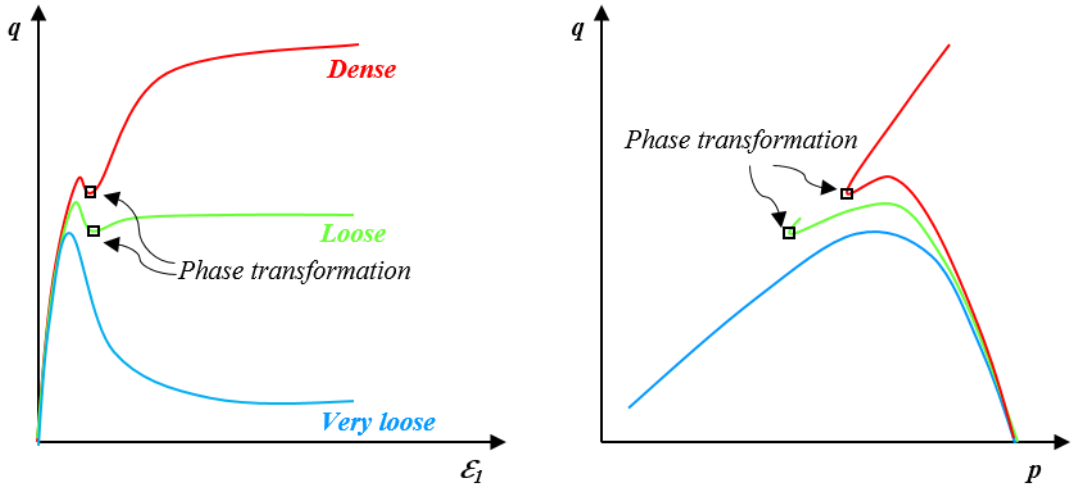

(a)Deviatoric stress-axial strain response (b)Effective stress path

Figure 6.11 Typical mechanical behavior of the sand under the undrained condition and definition of the phase transformation state

The mechanical behavior of the eroded soils under the undrained condition can be classified into no-flow for the dense soils (Fig. 4.5), limited flow for the loose soils (Fig. 4.4), and flow for the very loose soils (Fig. 4.8). The phase transformation is a significant feature for the

undrained mechanical behavior of the soils (Fig. 6.11), which has also been considered in some constitutive models (Li and Dafalias, 2000; Nguyen et al., 2018). At this state, the dilatancy (d) equals zero. The proposed constitutive model may predict the mechanical behavior of the eroded soils under the undrained condition, whose dilatancy ($d = M - \eta$) is the same as that of the original cam clay model. In this case, the phase transformation can be reflected by other parameters (e.g., R, R_{er}) in the proposed constitutive model, not the clear model parameters obtained from the condition that dilatancy (d) equals zero. Therefore, the proposed model cannot simulate the phase transformation state with clear model parameters.

6.6 Summary

By using the proposed modified subloading Cam-clay model, the shearing after the erosion of the dense soils through laboratory tests and DEM simulation can be simulated. The similarity ratio of the eroded dense soils (R_{er}) increases with the continuing shearing and reaches to be one finally. And it increases faster with the larger value of the degradation parameter h_0.

The performance of the predictive equations in the seepage part and the modified subloading Cam-clay model is shown through the simulation of the seepage and drained triaxial shearing tests. The final fines contents of the eroded loose soils with 15%, 25%, and 35% initial fines contents are calculated through the proposed predictive equation. Considering the different cumulative fines losses, the erosion-induced volumetric strains are obtained. And the post-erosion void ratios are calculated by considering the cumulative fines loss and erosion-induced volumetric strain. With the post-erosion void ratios and other estimated model parameters, the modified subloading Cam-clay model can capture the main features of the eroded loose soils with different initial fines contents.

The modified model cannot predict the change in shearing response due to erosion during shearing, which needs further research from the respects of both experiment and theory.

CHAPTER 7

CONCLUSIONS

7.1 Main conclusions

The main goal of this dissertation is to develop a constitutive model of granular materials considering deterioration induced by internal erosion. For this purpose, several series of seepage tests have been recalled firstly. The effects of erosion on soils have been quantified, which are described in Chapter 3 and the conclusions are as follows:

(1) When a large number of fines are washed out, the post-erosion void ratio increases, and the amount of this increase also depends on the confining pressure and the initial fines content.

(2) The post-erosion grading curves shift downward in fines fraction for all erosion tests, the amount of this shifting depends more on the applied confining pressure compared with the effect of initial fines content.

(3) The predictive equation of the fines content after erosion considering the mean effective stress, the initial fines content, and the flow velocity is proposed, which can capture the main features of the variations of the fines content under seepage flow.

(4) Change of the erosion-induced volumetric strain with cumulative fines loss can be expressed by using a hyperbolic tangent function. The post-erosion void ratio can be estimated by considering the cumulative fines content and the volumetric strain.

To investigate the effect of erosion on the mechanical behavior of soils, many experimental studies are elaborated in Chapter 4. The subloading Cam-clay model is employed to predict the mechanical behavior of the original loose soils under the drained condition. After confirming the capability of the subloading Cam-clay model for the original loose soils, it is used to simulate the mechanical behavior of soils with suffosion under the drained condition.

Then, key parameters are identified and quantified. The specific conclusions are as follows:

(1) The mechanical behavior of the eroded soils is largely dependent on the erosion phenomena (suffusion and suffosion), the initial fines content, and the intergranular void ratio.

(2) The slope of the normal compression line (λ) and initial stress ratio (R_0) are identified as the key parameters to characterize the suffosion effects on the mechanical behavior of the gap-graded loose soils.

(3) The slope of the normal compression line of the loose soils has a positive correlation with the initial void ratio before shearing.

(4) The initial stress ratio of the loose soils decreases with the increase of the initial void ratio before shearing, which means that the suffosion makes the over-consolidation ratio larger or makes the soil highly structured condition.

In Chapter 5, the normal yield surface is expected to expand for the eroded loose soils based on the finding in Chapter 4. The normal yield surface is expected to shrink for the eroded dense soils as both peak strength and deviatoric stress at the critical state decrease under the drained condition and the volumetric strain becomes more contractive. The similarity ratio of the eroded soils that characterizes the normal yield surface of the eroded soils to the normal yield surface of the uneroded soils is proposed. The similarity ratio is incorporated into the subloading Cam-clay model. The evolutions of key parameters are obtained through the prediction of the mechanical behavior of the eroded soils under the drained condition. The conclusions are as follows:

(1) The modified subloading Cam-clay model is proposed by incorporating with the similarity ratio for the eroded soils.

(2) The key parameters in the modified subloading Cam-clay model are the post-erosion void ratio, the slope of normal compression line, the angle of shearing resistance at the

critical state, the similarity ratio of the eroded soils.

(3) The determination method of erosion-related parameters, such as the similarity ratio for the eroded soils, is proposed.

In Chapter 6, the capability of the modified subloading Cam-clay model is discussed through the simulation for the drained triaxial tests of the eroded soils from the laboratory tests and DEM approach. The performance of both predictive equations in the seepage part and the modified subloading Cam-clay model is confirmed through the two-step calculation. The conclusions are summarized as follows:

(1) By using the modified subloading Cam-clay model, the shearing after erosion can be simulated for the eroded dense soils under the drained condition. However, the modified subloading Cam-clay model cannot predict the change in shearing response due to erosion during shearing.

(2) The variation of material properties due to erosion and the subsequent variation of the drained mechanical behavior is predicted through the two-step calculation.

7.2 Recommendations for future study

Seepage flow can cause heterogeneity, such as the variation of void ratio, fines contents, particle size distribution of different parts for the soils along the seepage direction. (Li *et al.*, 2020). Subsequently, it affects the mechanical behavior of the internally eroded soils. However, the modified constitutive model considering internal erosion has ignored the effect of heterogeneity. The modified constitutive model considering the heterogeneity would help us to establish a greater degree of accuracy on the prediction of the mechanical behavior of the internally eroded soils.

The mechanical behavior of the internally eroded soils is obtained after finishing the seepage tests in the laboratory. However, the change in mechanical behavior occurs during the erosion process in nature. Therefore, the modified model, predicting the change in

mechanical behavior due to erosion during shearing, can make contributions to the design of earthen structures subjected to internal erosion.

REFERENCES

Al-Khafaji, A. W. N., & Andersland, O. B. (1992). Equations for compression index approximation. *Journal of Geotechnical Engineering*, 118(1), 148-153.

Andrianatrehina, N. L., Souli, H., Rech, J., Fry, J. J., Fleureau, J. M., & Taibi, S. (2016). Influence of the percentage of sand on the behavior of gap-graded cohesionless soils. *Comptes Rendus Mecanique*, 344(8), 539-546.

Arulanandan, K., Loganathan, P., & Krone, R. B. (1975). Pore and eroding fluid influences on surface erosion of soil. *Journal of Geotechnical and Geoenvironmental Engineering*, 100(1), 51-66.

Belkhatir, M., Arab, A., Della, N., Missoum, H., & Schanz, T. (2010). Influence of inter-granular void ratio on monotonic and cyclic undrained shear response of sandy soils. *Comptes Rendus Mecanique*, 338(5), 290-303.

Bendahmane, F., Marot, D., & Alexis, A. (2008). Experimental parametric study of suffusion and backward erosion. *Journal of Geotechnical and Geoenvironmental Engineering*, 134(1), 57-67.

Bonelli, S., & Marot, D. (2011). Micromechanical modeling of internal erosion. *European Journal of Environmental and Civil Engineering*, 15(8), 1207-1224.

Bowman, E., & Hunter, R. P. (2017). Visualisation of seepage induced suffusion and suffosion within internally erodible granular media. *Geotechnique*, 68(10), 918-930.

Caldeira, L. (2019). Internal erosion in dams: studies and rehabilitation. *International Journal of Civil Engineering*, 17(4), 457-471.

Cedergren, H. R. (1997). Seepage, drainage and flow nets (Vol. 16). *John Wiley & Sons*,

New York.

Chang, D. S. (2012). Internal erosion and overtopping erosion of earth dams and landslide dams. *Ph.D. thesis, HKUST*.

Chang, D. S., & Zhang, L. M. (2011). A stress-controlled erosion apparatus for studying internal erosion in soils. *Geotechnical Testing Journal*, 34(6), 579-589.

Chang, D., Zhang, L., & Cheuk, J. (2014). Mechanical consequences of internal soil erosion. *HKIE Transactions*, 21(4), 198-208.

Chapuis, R. P., Contant, A., & Baass, K. (1996). Migration of fines in 0-20 mm crushed base during placement, compaction, and seepage under laboratory conditions. *Canadian Geotechnical Journal*, 33(1), 168-176.

Chareyre, B., Cortis, A., Catalano, E., & Barthélemy, E. (2012). Pore-scale modeling of viscous flow and induced forces in dense sphere packings. *Transport in Porous Media*, 94(2), 595-615.

Chen, C., Zhang, L. M., & Chang, D. S. (2016). Stress-strain behavior of granular soils subjected to internal erosion. *Journal of Geotechnical and Geoenvironmental Engineering*, 142(12), 06016014.

Chien, L. K., Oh, Y. N., & Chang, C. H. (2002). Effects of fines content on liquefaction strength and dynamic settlement of reclaimed soil. *Canadian Geotechnical Journal*, 39(1), 254-265.

Cividini, A., Bonomi, S., Vignati, G.C., and Gioda, G. (2009). Seepage-induced erosion in granular soil and consequent settlements. *International Journal of Geomechanics*, 9(4), 187-194.

Cividini, A., & Gioda, G. (2004). Finite-element approach to the erosion and transport of fine particles in granular soils. *International Journal of Geomechanics*, 4(3), 191-198.

Craig, R. F. (2004). Craig's soil mechanics, eighth ed. *Spon press*, London and New York. 169 pp.

Cundall, P. A., and Strack, O. D. L. (1979). A discrete numerical model for granular assemblies. *Geotechnique*, 29(1), 47-65.

Daouadji, A., Darve, F., Al Gali, H., Hicher, P. Y., Laouafa, F., Lignon, S., ... & Sibille, L. (2011). Diffuse failure in geomaterials: Experiments, theory and modelling. *International Journal for Numerical and Analytical Methods in Geomechanics*, 35(16), 1731-1773.

Fannin, R. J., & Slangen, P. (2014). On the distinct phenomena of suffusion and suffosion. *Geotechnique Letters*, 4(4), 289-294.

Fell, R., Fry, J. J., (2013). State of the art on the likelihood of internal erosion of dams and levees by means of testing. *Erosion in Geomechanics Applied to Dams and Levees*, 1-99.

Ferreira, P. M. V., & Bica, A. V. D. (2006). Problems in identifying the effects of structure and critical state in a soil with a transitional behavior. *Geotechnique*, 56(7), 445-454.

Flores-Berrones, R., Ramírez-Reynaga, M., & Macari, E. J. (2011). Internal erosion and rehabilitation of an earth-rock dam. *Journal of Geotechnical and Geoenvironmental Engineering*, 137(2), 150-160.

Foster, M., Fell, R., & Spannagle, M. (2000). The statistics of embankment dam failures and accidents. *Canadian Geotechnical Journal*, 37(5), 1000-1024.

Gai, X., & Sánchez, M. (2019). An elastoplastic mechanical constitutive model for microbially mediated cemented soils. *Acta Geotechnica*, 14(3), 709-726.

Goldin, A.L., Rasskazov, L.N. (1992) Design of earth dams. *Balkema*, Rotterdam

Goudarzy, M., König, D., & Schanz, T. (2016). Small strain stiffness of granular materials containing fines. *Soils and Foundations*, 56(5), 756-764.

Gregory, A. S., Whalley, W. R., Watts, C. W., Bird, N. R. A., Hallett, P. D., & Whitmore, A. P. (2006). Calculation of the compression index and precompression stress from soil compression test data. *Soil and Tillage Research*, 89(1), 45-57.

Hájek, V., Mašín, D., & Boháč, J. (2009). Capability of constitutive models to simulate soils with different OCR using a single set of parameters. *Computers and Geotechnics*, 36(4), 655-664.

Hanna, A., & Al-Romhein, R. (2008). At-rest earth pressure of overconsolidated cohesionless soil. *Journal of Geotechnical and Geoenvironmental Engineering*, 134(3), 408-412.

Hardin, B. O., & Black, W. L. (1966). Sand stiffness under various triaxial stresses. *Journal of Soil Mechanics & Foundations Div*, 92(3), 27-42.

Hashiguchi, K. (1989). Subloading surface model in unconventional plasticity. *International Journal of Solids and Structures*, 25(8), 917-945.

Hicher, P. Y. (2013). Modelling the impact of particle removal on granular material behavior. *Geotechnique*, 63(2), 118-128.

Hillel, D. (1980). Fundamentals of Soil Physics, *Academic Press*, Inc., San Diego, CA.

Honjo, Y., & Veneziano, D. (1989). Improved filter criterion for cohesionless soils. *Journal*

of Geotechnical Engineering, 115(1), 75-94.

Hosn, R. A., Sibille, L., Benahmed, N., & Chareyre, B. (2016). A discrete numerical description of the mechanical response of soils subjected to degradation by suffusion. *In Scour and Erosion: Proceedings of the 8th International Conference on Scour and Erosion*, Oxford, UK, 12-15 September, Paper ID: 397.

Huang, Q. F., Zhan, M. L., Sheng, J. C., Luo, Y. L., & Su, B. Y. (2014). Investigation of fluid flow-induced particle migration in granular filters using a DEM-CFD method. *Journal of Hydrodynamics, Ser. B*, 26(3), 406-415.

Humes, C. (1996). A new approach to compute the void-size distribution curves of protective filters. *In Proceedings of GeoFilters*, Montreal, Canada, 57-66.

Hu, Z., Zhang, Y., & Yang, Z. (2019). Suffusion-induced deformation and microstructural change of granular soils: a coupled CFD–DEM study. *Acta Geotechnica*, 14(3), 795-814.

Indraratna, B., Raut, A. K., & Khabbaz, H. (2007). Constriction-Based Retention Criterion for Granular Filter Design. *Journal of Geotechnical and Geoenvironmental Engineering*, 133(3), 266-276.

Ishihara, K. (1993). Liquefaction and flow failure during earthquakes. *Geotechnique*, 43(3), 351-451.

Jones, J. A. A. (1981). The nature of soil piping-A review of research. *Norwich: Geo Books*.

Kawano, K., Shire, T., O'Sullivan, C. (2016). Using DEM to assess the influence of stress and fabric inhomogeneity and anisotropy on susceptibility to suffusion. *In Scour and Erosion: Proceedings of the 8th International Conference on Scour and Erosion*, Oxford, UK, 12-15 September, 85-94.

Kawano, K., Shire, T., & Osullivan, C. (2018). Coupled particle-fluid simulations of the initiation of suffusion. *Soils and Foundations*, 58(4), 972-985.

Ke, L., & Takahashi, A. (2012). Strength reduction of cohesionless soil due to internal erosion induced by one-dimensional upward seepage flow. *Soils and Foundations*, 52(4), 698-711.

Ke, L., & Takahashi, A. (2014a). Experimental investigations on suffusion characteristics and its mechanical consequences on saturated cohesionless soil. *Soils and Foundations*, 54(4), 713-730.

Ke, L., & Takahashi, A. (2014b). Triaxial erosion test for evaluation of mechanical consequences of internal erosion. *Geotechnical Testing Journal*, 37(2), 347-364.

Ke, L., & Takahashi, A. (2015). Drained monotonic responses of suffusional cohesionless soils. *Journal of Geotechnical and Geoenvironmental Engineering*, 141(8), 04015033.

Kenney, T. C., Chahal, R., Chiu, E., Ofoegbug., I., Omange, G. N., and Ume, C. A. (1985). Controlling constriction sizes of granular filters. *Canadian Geotechnical Journal*, 22(1), 32-43.

Kenney, T. C., & Lau, D. (1985). Internal stability of granular filters. *Canadian Geotechnical Journal*, 22(2), 215-225.

Kezdi, A. (1979). Soil physics: Selected Topics-Developments in Geotechnical Engineering, *Elsevier Scientific Publishing Co.*, Amsterdam, Netherland.

Koelewijn, A. R., & Bridle, R. (2017). Internal erosion in dams and dikes: a comparison. *In Proceedings of the 25th Meeting European Working Group on Internal Erosion in Embankment Dams & their Foundations*, Delft, Netherlands, 4-7 September, 1-11.

Kohler, H.J. (1993). The Influence of Hydraulic Head and Hydraulic Gradient on the Filtration Process. *Filters in Geotechnical and Hydraulic Engineering*. Balkema, Rotterdam, 225-240.

Kovacs, G. (1981). Seepage hydraulics. *Elsevier Scientific Publishing Company*, Amsterdam, Netherlands.

Ladd, R. S. (1978). Preparing test specimens using undercompaction. *Geotechnical Testing Journal*, 1(1), 16-23.

Lade, P. V., Liggio, C. D., & Yamamuro, J. A. (1998). Effects of non-plastic fines on minimum and maximum void ratios of sand. *Geotechnical Testing Journal*, 21(4), 336-347.

Langroudi, M. F., Soroush, A., & Tabatabaie, P. (2012). Effects of gradation on the internal instability of soils-a micromechanical approach using DEM. *In 5th Asian Particle Technology Symposium*, National University of Singapore, Singapore.

Liu, M. D., & Carter, J. P. (2002). A structured cam clay model. *Canadian Geotechnical Journal*, 39(6), 1313-1332.

Li, S., Russell, A. R., & Wood, D. M. (2017). Stress-strain behavior of soils having undergone different amounts of internal erosion. *In Proceedings of 25th Meeting of European Working Group on Internal Erosion in Embankment Dams & their Foundations*, Delft, Netherlands, 4-7 September, 114-122.

Li, S., Russell, A. R., & Wood, D. M. (2020). The influence of particle size distribution homogeneity on the shearing of soils having been subjected to internal erosion. *Canadian Geotechnical Journal*, 57(11), 1684-1694.

Li, X. S., & Dafalias, Y. F. (2000). Dilatancy for cohesionless soils. Géotechnique, 50(4),

449-460.

Locke, M., Indraratna, B., and Adikari, G. (2001). Time-dependent particle transport through granular filters. *Journal of Geotechnical and Geoenvironmental Engineering*, 127(6), 521-529.

Lominé, F., Scholtes, L., Sibille, L., & Poullain, P. (2013). Modeling of fluid–solid interaction in granular media with coupled lattice Boltzmann/discrete element methods: application to piping erosion. *International Journal for Numerical and Analytical Methods in Geomechanics*, 37(6), 577-596.

Luo, Y. L., Qiao, L., Liu, X. X., Zhan, M. L., & Sheng, J. C. (2013). Hydro-mechanical experiments on suffusion under long-term large hydraulic heads. *Natural hazards*, 65(3), 1361-1377.

Mahmoudi, Y., Cherif Taiba, A., Belkhatir, M., Arab, A., & Schanz, T. (2018). Laboratory study on undrained shear behavior of overconsolidated sand–silt mixtures: effect of the fines content and stress state. *International Journal of Geotechnical Engineering*, 12(2), 118-132.

Marot, D., Rochim, A., Nguyen, H., Bendahmane, F., & Sibille, L. (2016). Assessing the susceptibility of gap-graded soils to internal erosion: proposition of a new experimental methodology. *Natural Hazards*, 83(1), 365-388.

Mehdizadeh, A., Disfani, M. M., Evans, R., & Arulrajah, A. (2017). Progressive Internal Erosion in a Gap-Graded Internally Unstable Soil: Mechanical and Geometrical Effects. *International Journal of Geomechanics*, 18(3), 04017160.

Mehdizadeh, A., Disfani, M. M., Evans, R., & Arulrajah, A. (2019). Impact of suffusion on the cyclic and post-cyclic behavior of an internally unstable soil. *Geotechnique Letters*,

9(3), 218-224.

Muir Wood, D., & Maeda, K. (2007). Changing grading of soil: effect on critical states. *Acta Geotechnica*, 3(1), 3-14.

Muir Wood, D., Maeda, K., & Nukudani, E. (2008). Discrete element modelling of soil erosion. *In 4th International Conference on Scour and Erosion*, Tokyo, Japan, 5-7 November. Paper ID: C-18.

Muir Wood, D., Maeda, K., & Nukudani, E. (2010). Modelling mechanical consequences of erosion. *Geotechnique*, 60(6), 447-457.

Murthy, T. G., Loukidis, D., Carraro, J. A. H., Prezzi, M., & Salgado, R. (2007). Undrained monotonic response of clean and silty sands. *Geotechnique*, 57(3), 273-288.

Naeini, S. A., & Baziar, M. H. (2004). Effect of fines content on steady-state strength of mixed and layered samples of a sand. *Soil Dynamics and Earthquake Engineering*, 24(3), 181-187.

Ng, T. T., Zhou, W., & Chang, X. L. (2017). Effect of particle shape and fine content on the behavior of binary mixture. *Journal of Engineering Mechanics*, 143(1), C4016008.

Nguyen, C. D., Benahmed, N., Andò, E., Sibille, L., & Philippe, P. (2019). Experimental investigation of microstructural changes in soils eroded by suffusion using X-ray tomography. *Acta Geotechnica*, 14(3), 749-765.

Nguyen, H. B. K., Rahman, M. M., & Fourie, A. B. (2018). Characteristic behavior of drained and undrained triaxial compression tests: DEM study. Journal of Geotechnical and Geoenvironmental Engineering, 144(9), 04018060.

Ni, Q., Tan, T. S., Dasari, G. R., & Hight, D. W. (2004). Contribution of fines to the

compressive strength of mixed soils. *Geotechnique*, 54(9), 561-569.

Nova, R. (1989). Sinfonietta classica: an exercise on classical soil modelling. *In International workshop on constitutive equations for granular non-cohesive soils*, Amsterdam, Netherslands, July 22, 501-519.

Odenwald, B., & Ratz, K. (2012). Prevention of internal erosion by cut-off walls in river embankments on the Upper Rhine. *La Houille Blanche*, (4–5), 48-53.

Ouyang, M., & Takahashi, A. (2015). Influence of initial fines content on fabric of soils subjected to internal erosion. *Canadian Geotechnical Journal*, 53(2), 299-313.

Pavlov, A. P. (1898). About relief of plains and its change under the influence of subsurface and surface water. *Geosciences*, 5(34), 91-147.

Pitman, T. D., Robertson, P. K., & Sego, D. C. (1994). Influence of fines on the collapse of loose sands. *Canadian Geotechnical Journal*, 31(5), 728-739.

Prasomsri, J., & Takahashi, A. (2020). The role of fines on internal instability and its impact on undrained mechanical response of gap-graded soils. *Soils and Foundations*. (in press)

Rahman, M. M., Lo, S. R., & Gnanendran, C. T. (2009). Reply to the discussion by Wanatowski and Chu on "On equivalent granular void ratio and steady state behavior of loose sand with fines". *Canadian Geotechnical Journal*, 46(4), 483-486.

Razavi, S. K., Hajialilue Bonab, M., & Dabaghian, A. (2020). Investigation into the internal erosion and local settlement of Esfarayen earth-Fill dam. *Journal of Geotechnical and Geoenvironmental Engineering*, 146(4), 04020006.

Reddi LN, Lee I, Bonala MVS. (2000). Comparison of internal and surface erosion using flow pump test on a sand-kaolinite mixture. *Geotechnical Testing Journal*, 23(1), 116-

122.

Richards, K. S., & Reddy, K. R. (2012). Experimental investigation of initiation of backward erosion piping in soils. *Geotechnique*, 62(10), 933-942.

Richart, F. E., Hall, J. R., & Woods, R. D. (1970). Vibrations of soils and foundations. *Prentice-Hall*, Englewood Cliffs, N.J.

Rousseau, Q., Sciarra, G., Gelet, R., & Marot, D. (2018). Constitutive Modeling of a Suffusive Soil with Porosity-Dependent Plasticity. *In European Working Group on Internal Erosion*, September 10-13, Milan, Italy, 114-122.

Rousseau, Q., Sciarra, G., Gelet, R., & Marot, D. (2020). Modelling the poroelastoplastic behavior of soils subjected to internal erosion by suffusion. *International Journal for Numerical and Analytical Methods in Geomechanics*, 44(1), 117-136.

Sari, H., Chareyre, B., Catalano, E., Philippe, P., & Vincens, E. (2011). Investigation of internal erosion processes using a coupled dem-fluid method. *In Particles 2011 II International Conference on Particle-Based Methods, E. Oate and DRJ Owen (Eds),* Barcelona, Spain, 1-11.

Shibata, T. (1963). On the volume changes of normally consolidated clays. *Annuals, Disaster Prevention Research Institute*, Kyoto University, 6, 128-134. (in Japanese)

Shire, T., and O'Sullivan, C. (2013). Micromechanical assessment of an internal stability criterion. *Acta Geotechnica*, 8(1), 81-90.

Shire, T., Osullivan, C., Hanley, K. J., & Fannin, R. J. (2014). Fabric and effective stress distribution in internally unstable soils. *Journal of Geotechnical and Geoenvironmental Engineering*, 140(12), 04014072.

Sibille, L., Lominé, F., Poullain, P., Sail, Y., & Marot, D. (2015). Internal erosion in granular media: direct numerical simulations and energy interpretation. *Hydrological Processes*, 29(9), 2149-2163.

Skempton, A. W., & Brogan, J. M. (1994). Experiments on piping in sandy gravels. *Geotechnique*, 44(3), 449-460.

Sowers, G. F. (1979). Introductory soil mechanics and foundations. *Geotechnical Engineering*. 92, 114-117.

Stavropoulou, M., Papanastasiou, P., & Vardoulakis, I. (1998). Coupled wellbore erosion and stability analysis. *International Journal for Numerical and Analytical Methods in Geomechanics*, 22(9), 749-769.

Sterpi, D. (2003). Effects of the erosion and transport of fine particles due to seepage flow. *International Journal of Geomechanics*, 3(1), 111-122.

Tao, H., & Tao, J. (2017). Quantitative analysis of piping erosion micro-mechanisms with coupled CFD and DEM method. *Acta Geotechnica*, 12(3), 573-592.

Tavarez, F. A., & Plesha, M. E. (2007). Discrete element method for modelling solid and particulate materials. *International Journal for Numerical Methods in Engineering*, 70(4), 379-404.

Terzaghi, K. (1925). Erdbaumechanik auf bodenphysikalischer grundlage, *F. Deuticke*, Vienna, Austria.

Terzaghi, K., and Peck, R. B. (1948). Soil mechanics in engineering practice. *John Wiley and Sons*, INC.

Thevanayagam, S., Ravishankar, K., & Mohan, S. (1997). Effects of fines on monotonic

undrained shear strength of sandy soils. *Geotechnical Testing Journal*, 20(4), 394-406.

Thongthamchart, C., & Brohmsubha, P. (2014). The Safety Criteria for Geotechnical Instruments on the Internal Erosion in Embankment Dams. *In International Symposium on DAMS in a Global Environmental Challenges*. Bali, Indonesia, 1-6 June, Paper ID: 519.

Thevanayagam, S., Shenthan, T., Mohan, S., & Liang, J. (2002). Undrained fragility of clean sands, silty sands, and sandy silts. *Journal of Geotechnical and Geoenvironmental Engineering*, 128(10), 849-859.

Tomlinson, S. S., & Vaid, Y. P. (2000). Seepage forces and confining pressure effects on piping erosion. *Canadian Geotechnical Journal*, 37(1), 1-13.

Tsuji, Y., Tanaka, T., & Ishida, T. (1992). Lagrangian numerical simulation of plug flow of cohesionless particles in a horizontal pipe. *Powder Technology*, 71(3), 239-250.

Uzuoka, R., Ichiyama, T., Mori, T., & Kazama, M. (2012). Hydro-mechanical analysis of internal erosion with mass exchange between solid and water. *In Scour and Erosion: Proceedings of the 6th International Conference on Scour and Erosion*, Paris, France, 27-31 August, 655-662.

Vandenboer, K., van Beek, V., & Bezuijen, A. (2014). 3D finite element method (FEM) simulation of groundwater flow during backward erosion piping. *Frontiers of Structural and Civil Engineering*, 8(2), 160-166.

Vanmarcke, E. H., and Honjo, Y. (1985). Probabilistic description of the void phase of soil with reference to assessing risk of internal erosion. *In Structural Safety and Reliability: Proceedings of the 4th International Coference on Structure Safety and Reliability*, Kobe, Japan, 27-29 May, 321-330.

Wan, C. F., & Fell, R. (2004). Laboratory tests on the rate of piping erosion of soils in embankment dams. *Geotechnical Testing Journal*, 27(3), 295-303.

Wan, C. F., & Fell, R. (2008). Assessing the Potential of Internal Instability and Suffusion in Embankment Dams and Their Foundations. *Journal of Geotechnical and Geoenvironmental Engineering*, 134(3), 401-407.

Wang, H. L., Cui, Y. J., Lamas-Lopez, F., Calon, N., Saussine, G., Dupla, J. C., ... & Chen, R. P. (2018). Investigation on the mechanical behavior of track-bed materials at various contents of coarse grains. *Construction and Building Materials*, 164, 228-237.

Wang, M., Feng, Y. T., Pande, G. N., Chan, A. H. C., & Zuo, W. X. (2017). Numerical modelling of fluid-induced soil erosion in granular filters using a coupled bonded particle lattice Boltzmann method. *Computers and Geotechnics*, 82, 134-143.

Wang, X., & Li, J. (2015). On the degradation of granular materials due to internal erosion. *Acta Mechanica Sinica*, 31(5), 685-697.

Wautier, A., Bonelli, S., & Nicot, F. (2019). DEM investigations of internal erosion: Grain transport in the light of micromechanics. *International Journal for Numerical and Analytical Methods in Geomechanics*, 43(1), 339-352.

Wilson, G. V., Wells, R., Kuhnle, R., Fox, G., & Nieber, J. (2018). Sediment detachment and transport processes associated with internal erosion of soil pipes. *Earth Surface Processes and Landforms*, 43(1), 45-63.

Xiao, M., & Shwiyhat, N. (2012). Experimental investigation of the effects of suffusion on physical and geomechanic characteristics of sandy soils. *Geotechnical Testing Journal*, 35(6), 890-900.

Yang, J., Yin, Z. Y., Laouafa, F., & Hicher, P. Y. (2019). Internal erosion in dike-on-

foundation modeled by a coupled hydromechanical approach. *International Journal for Numerical and Analytical Methods in Geomechanics*, 43(3), 663-683.

Yang, J., Yin, Z. Y., Laouafa, F., & Hicher, P. Y. (2020). Three-dimensional hydromechanical modeling of internal erosion in dike-on-foundation. *International Journal for Numerical and Analytical Methods in Geomechanics*, 44(8), 1200-1218.

Yang, S., Lacasse, S., & Sandven, R. (2005). Determination of the transitional fines content of mixtures of sand and non-plastic fines. *Geotechnical Testing Journal*, 29(2), 102-107.

Yin, J. H. (1999). Properties and behavior of Hong Kong marine deposits with different clay contents. *Canadian Geotechnical Journal*, 36(6), 1085-1095.

Yin, Z. Y., Zhao, J., & Hicher, P. Y. (2014). A micromechanics-based model for sand-silt mixtures. *International Journal of Solids and Structures*, 51(6), 1350-1363.

Zhang, F., Li, M., Peng, M., Chen, C., & Zhang, L. (2019). Three-dimensional DEM modeling of the stress–strain behavior for the gap-graded soils subjected to internal erosion. *Acta Geotechnica*, 14(2), 487-503.

Zhang, S., Leng, W., Zhang, F., & Xiong, Y. (2012). A simple thermo-elastoplastic model for geomaterials. *International Journal of Plasticity*, 34, 93-113.

Zhang, Y., & Chen, Y. (2017). A constitutive relationship for gravelly soil considering fine particle suffusion. *Materials*, 10(10), 1217.

Zhu, H., Ye, B., Cai, Y., & Zhang, F. (2013). An elasto-viscoplastic model for soft rock around tunnels considering overconsolidation and structure effects. *Computers and Geotechnics*, 50, 6-16.

Zuo, L., & Baudet, B. A. (2015). Determination of the transitional fines content of sand-non plastic fines mixtures. *Soils and Foundations*, 55(1), 213-219.